The background of the entire page is a complex contour plot. It features a dense network of thin, black contour lines that form irregular, interconnected shapes. The color palette is a gradient from dark purple and blue to bright yellow and green, with the yellow and green areas representing higher values or peaks in the data being visualized. The overall effect is a textured, organic pattern that resembles a topographic map or a scientific visualization of a field.

Enhanced characterization of tow gaps in fiber steered laminates

Advanced specimen design
for better representation of defects in structures

Master's Thesis
László Dávid Czél

Enhanced characterization of tow gaps in fiber steered laminates

Advanced specimen design
for better representation of defects in structures

by

László Dávid Czél

Student Name	Student Number
László Czél	5703077

Supervisors: Dr. Daniël M.J. Peeters
Dr.-Ing. Saullo G.P. Castro
Project Duration: September, 2023 - March, 2024
Faculty: Faculty of Aerospace Engineering, Delft

Cover: Digital image correlation plot from the thesis research work under
CC BY-NC 2.0 (Modified)

Preface

This document marks the end of my six year long university studies. I started my studies at the Technical University of Budapest on the Mechanical Engineering BSc program. Here I acquired the fundamentals of the engineering profession. My friends and the Formula Student team I worked in made these years amazing, despite the endless line of exams (at that time it seemed endless), assignments or even a global pandemic. Towards the end of those years, I felt like I could push my limits further and I liked the idea of some adventurous years abroad. This brought me to Delft University of Technology. And I am glad it did.

In my two years in Delft, I became a far better engineer, and learned a wide range of new skills. I am grateful for my local friends, as they made this time a complete blast. And of course, I would like to thank my family the support and encouragement through the highs and lows of the past six years. Without them, I could not have done it.

This research was written as a first shot in the dark of the research problem, attempting to make a foundation for further work. Thus, I wish this document will help future students and researchers in their work. I wish all readers joy in reading.

*László Dávid Czél
Delft, March 2024*

Summary

The novel method of 'Variable Stiffness' laminates offers the ultimate exploitation of the mechanical performance of fiber-reinforced composites. It does so by aligning the admirable axial strength and stiffness of composite tapes with the optimal orientations over the laminate field. This process, also called 'Fiber Steering', uses the Automated Fiber Placement method for manufacturing. The method features a robotic arm with a deploying head, which starts, feeds, compacts, and terminates the used material. The material in this case comes in the form of a 'tow', a narrow tape if you will. These tows are deformed to the desired curvatures upon the lamination process. However, there are limits to the material's ability to deform - which is the source of the research problem. Over the whole product geometry, there are points where the tows cannot be aligned with each other because the material cannot be deformed to the needed level. At this point, the choice arises - one could either leave a gap between the material strips or add more material to the troubling zone. This is the origin of manufacturing-induced defects, gaps, and overlaps. Since the thesis has limited time, gaps were chosen as the defect to investigate.

Many researchers worked on the problem over the years but mostly with lower-level experimental methods, and some numerical tools. Some shortcomings were pointed out about the methods, mostly connected to the used coupon specimens. A few publications also emphasized the need for enhanced characterization of the problem with advanced specimens. This became the topic of this master's thesis.

Using a testing method one step higher than coupon samples, element-level testing was chosen for the analysis. Against a favorable specimen, requirements were set based on the idea of representing an important structural zone. With the requirements, the main hypothesis about the failure of laminates with gaps was also stated. In detail, it was that 'gaps negatively affect the off-axis tows, thus introducing failure/strength knockdown'. In other words, gaps are imposing a matrix failure on local material.

A promising design was created in an iterative process based on the stated requirements. The development tool was a Finite Element Model, with simplifications and neglects. The major simplification was the omission of post-curing deformations, reducing the complex geometries to straight plies. Above this, delamination was not accounted for, mainly because of the lack of input data. These were done because the lack of input data, and to speed up the design work in order to have time for testing in real life. The initial concepts revolved around the usage of steering of tows, which met several shortcomings. The improved concept focused on the homogeneous characterization of the research problem, where the specimen failure could be directly correlated to the manufacturing defects. Load introduction of the testing samples received increased focus, by means of common engineering practices and a dedicated simulation.

The designed specimens were manufactured with the help of Sam XL. The procedure featured a combination of hand lamination and an AFP robot. Upon testing, despite the extra efforts, some specimens failed at the load introduction area. The problem was found to be a result of the simulation model's applied boundary conditions. Fortunately, the load level was enough to start microcracks in the samples. The cracks were not solely and evidently initiated at locations anticipated by the simulation, therefore not proving the main hypothesis. However, several other observations were proved to be valuable. Microscopical images displayed a strong tendency for void formation at gap locations and presented ply deformations caused by the curing process. Digital Image Correlation was used through the experimental work, which showed valuable insights into the deformations and behavior of the laminate. The equipment proved an affection of gaps in the response of the laminates, in the form of deformation peaks. These peaks, depending on which strain component, were either at gap locations, or inside zones bordered by gaps. The simulation outcome proved a poor correlation with the experimental counterparts. The comparison of the simulation method and the Digital Image Correlation observations pointed to the origin of the inaccurate predictions. This was thought to be coming from the major geometrical neglect of post-curing laminate deformations. Using realistic cross-sectional parameters, a numerical tool was suggested for further work on the complete characterization of the problem. The envisioned research should feature preceding studies for a more comprehensive understanding of post-curing properties and also imperfect laminate responses.

Acknowledgement

First and foremost, I would like to express my gratitude towards my supervisors, Dr. ir. Daniël Peeters and to Dr.-Ing. Saullo Castro. Throughout the months of thesis work, their supervision pushed my research work to higher levels, while I also became a more skilled engineer. I also appreciate the friendly atmosphere and laughs during the regular meetings.

I would like to thank SAM XL company for the opportunity to manufacture my specimens with their equipment. I greatly appreciate the help of André Florindo, who did an excellent work with the programming and operating of the AFP machine. From the faculty lab, Victor Horbowiec gave me great tips along the production phase.

Testing work couldn't have been done without the help of Dave Ruijtenbeek and Chantal de Zeeuw. For the microscopical part, I would like to thank Emma Chiavelli and Pietro Marchese.

I appreciate the help of Yi-Hsiu Wu in software problems and in using the high performance cluster. I want to thank the general help of my favourite Canadians. Dante Raso and Nico Renauld helped me through the concept phase with valuable recommendations, and they improved my writing by an order of magnitude.

Lastly, but most importantly, I would like to express my gratitude towards my family, who supported me along the whole process. Their encouragement helped me to overcome any hurdles along the way.

Contents

Preface	i
Summary	ii
Acknowledgement	iii
Nomenclature	vi
1 Introduction	1
2 Literature study	3
2.1 Fundamentals of Fracture Mechanics	3
2.1.1 Strain Energy Release Approach	3
2.1.2 SERR approach for delamination	5
2.1.3 Strength of materials approach	10
2.2 Ply failure	11
2.3 Manufacturing induced defects of AFP	14
2.4 Strength characterization of gaps	15
2.5 Summary of Literature Study	23
3 Specimen requirements	24
3.1 Sample size and layout	24
3.1.1 Case study - business jet fuselage section	26
3.2 Loading condition and stress state	27
3.3 Specimen Lay-up	29
3.3.1 Failure mode hypothesis of variable stiffness laminates containing gaps	31
3.4 Manufacturing	32
3.5 Realistic defects	32
3.6 Failure mode	33
3.7 Test output	34
3.8 Summary of Requirements	35
4 Design of specimen	36
4.1 Used failure criteria	36
4.1.1 Matrix cracking	36
4.1.2 Fiber kinking and fiber splitting	37
4.1.3 Fiber tension	38
4.2 Material input	38
4.3 Applied simulation model	39
4.4 Initial concept	42
4.5 Final concept	46
4.5.1 Load introduction and tabbing	50
4.6 Simulation of grip zones	52
4.7 Testing methods	53
4.8 Design summary	54
5 Manufacturing, experimental work	55
5.1 Specimen manufacturing	55
5.2 Testing	63
5.2.1 General testing outcomes	63
5.2.2 DIC measurements and results	66
5.3 Microscopical observations	73
5.4 Chapter summary	73

6 Discussion	75
6.1 Answering the research questions	75
6.1.1 Specimen requirements	75
6.1.2 Optimal design	76
6.1.3 Modeling of VS laminates	78
6.1.4 Testing observations	80
6.1.5 Answering the main research question	82
6.2 Future recommendations	83
7 Conclusion	85
References	87
A Mesh convergence study	93
B Adhesive failure calculation	95
C Frictional force calculation for clamping plates	96
D DIC plots not discussed in main text	97

Nomenclature

Abbreviations

Abbreviation	Definition
AFP	Automated Fiber Placement
ASTM	American Society for Testing and Materials
BK	Benzeggagh and Kenane
CBM	Crack Band Method
CDM	Continuum Damage Model
CFRP	Carbon Fiber Reinforced Composite
CLT	Classical Laminated Plate Theory
CTE	Coefficient of Thermal Expansion
CZM	Cohesive Zone Model
DASML	Delft Aerospace Structures and Materials Laboratory
DCB	Double Cantilever Beam
DIC	Digital Image Correlation
DoF	Degrees of Freedom
EASA	European Union Aviation Safety Agency
ECT	Edge Crack Torsion
ENF	End Notched Flexure
FAA	Federal Aviation Administration
FEM	Finite Element Method
FPF	First Ply Failure
FS	Fiber Steering
GFRP	Glass Fiber Reinforced Polymer
MCDM	Multiscale Continuum Damage and Failure Model
PEEK	Polyether-etherketone
QI	Quasi-isotropic
SamXL	Smart Advanced Manufacturing XL
SCB	Split Cantilever Beam
SERR	Strain Energy Release Rate
TP	Thermoplastic
TS	Thermoset
UD	Unidirectional
UMAT	User-defined Mechanical Material Behavior
VS	Variable Stiffness
WWFE-II	Second World-Wide Failure Exercise
XFEM	Extended Finite Element Method

Symbols

Symbol	Definition	Unit
a	Crack length	[m]
A	Surface area	[m ²]
b	Tapering of one layer in the out-of-plane direction	[m]
E	Young's modulus	[Pa]
F_x	Failure index for 'x' criteria	[-]
FoS	Factor of safety	[-]
G	Shear modulus	[Pa]
G_n	Strain energy release rate for mode 'n'	[J/m ²]
M_i	Applied moment in 'i' direction	[N]
M_{xy}	Applied torsional moment load	[N]
N_i	Applied membrane line load in 'i' direction	[N/m]
N_{xy}	Applied shear line load	[N/m]
r	Polar coordinate in fracture mechanics	[m]
S	Shear strength	[m]
S_{ij}	Interlaminar stress limit in 'ij' orthogonal direction	[m]
t	Ply thickness	[m]
u	Displacement in x direction	[m]
v	Displacement in y direction	[m]
X^c	Axial compressive strength	[Pa]
X^t	Axial tensile strength	[Pa]
Y^c	Transversal compressive strength	[Pa]
Y^t	Transversal tensile strength	[Pa]
z	Object distance from optical equipment	[m]
x_{avg}	Characteristic distance in strength of material approach	[m]
α	Crack propagation direction angle	[°]
α_0	Fracture surface angle in pure compression case	[°]
ϵ	Longitudinal strain	[-]
η_L	Longitudinal friction coefficient	[-]
η_T	Transversal friction coefficient	[-]
γ	Shear strain	[-]
κ	Laminate curvature	[1/m]
μ	Shear modulus in isotropic media	[-]
ν_{ij}	Poisson ratio	[-]
ϕ_0	Local fiber misalignment or fiber waviness	[°]
ψ	Orientation mismatch between adjacent layers	[°]
σ	Stress	[Pa]
τ	Shear stress	[Pa]
θ	Ply orientation angle	[°]

*...He deals the cards to find the answer
The sacred geometry of chance
The hidden law of a probable outcome
The numbers lead a dance..."*

Sting

Introduction

Background

Current composite materials offer outstanding performances in several fields, owing to a synergistic pairing of its constituents. The joining of such materials results in a unique combination of properties, which can not be surpassed nor even equaled for traditional monolithic metals, ceramics, or polymer materials [1].

The common polymer composites usually feature two distinct components - a matrix phase and a reinforcement phase. The matrix phase surrounds and protects the reinforcement phase, gives a solid shape to the product, but most important of all, conveys the loads to it. These are polymer materials of either thermoplastic or thermoset origin. Thermoset matrices are more common in the industry because of their earlier appearance, although they are envisioned to be overtaken in the future, because of sustainability aspects. Reinforcement phases are usually in fiber form and generally are from carbon, aramid, or glass materials. The stiff and strong reinforcement takes up the loads in the system. With their fiber form, these reinforcements can be oriented such that the fibers lie in the load path of the structure, resulting in an optimal use of the component. This tailoring of the material further enhances the potential of the composites [1].

Polymer composites stand out even from composites, with their prime stiffness and strength, all while offering it at a low density to name a few advantageous features. Thus, these are the top contenders for structural applications, especially where weight plays a role. One such industry is the aerospace field, where the usage of composites has grown. This tendency is illustrated on Figure 1.1 [2].

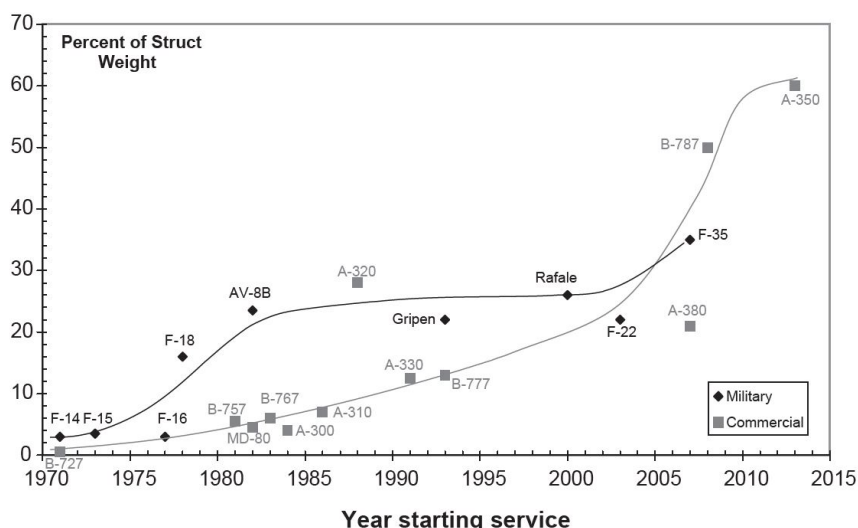


Figure 1.1: Quantity of composite materials in aircraft structures [2]

The superb performance of polymer composite materials comes with a cost, namely complexity. To aid manufacturing, the fibers are ordered in reinforcement plies (or 'lamina'), which are eventually

stacked together in the final part ('laminates'). The stacking process is called 'lamination'. The reinforcement form results in high anisotropy, meaning that the physical properties are dependent on directions. The anisotropic behaviour makes it much harder to predict the structural responses and decide on an optimum design, especially in hyper-static structures that offer multiple load paths.

The challenges to design anisotropic structures enabled by polymer composites have been successfully addressed in academia and industry, given the increasing adoption of these materials in novel designs. The stiffness (or 'constitutive') behavior of polymer composites can be quite accurately characterized and predicted based on current methodologies. However, the load-bearing capability of these systems is much harder to forecast, even for materials evaluated under their pristine condition. This being said, structural engineering still requires both aspects to be accounted for, in order to have high performance and sufficient safety. Especially in the aerospace sector, where certification in airworthiness is a major hurdle for novel designs to reach operation. For this thesis research, the mechanical performance prediction of materials was chosen for its great challenge.

Variable stiffness laminates

For decades the only form of reinforcement was the plies pre-processed (e.g. trimmed for shape) for lamination, which were of either unidirectional (only parallel fibers) or woven nature. Still to this day, these fabrics build up the vast majority of composite structures. These fabrics or tapes have constant orientation angles throughout the layer, which means the stiffness properties are also constant in the zone they are laid to. This limits the ultimate tailoring of the fibers to the load paths, as there is an ever-changing optimal direction over the field. However, there is one method that offers even greater tailoring of the base material - Fiber Steering (FS). In this process, an automated robotic arm deploys a narrow tape (the step known as 'Automated Fiber Placement' - AFP), but in any trajectory it is desired. This results in a variable stiffness ('VS') laminate, fully exploiting the material's capabilities [3]. One such fiber laying machine is presented on Figure 1.2.

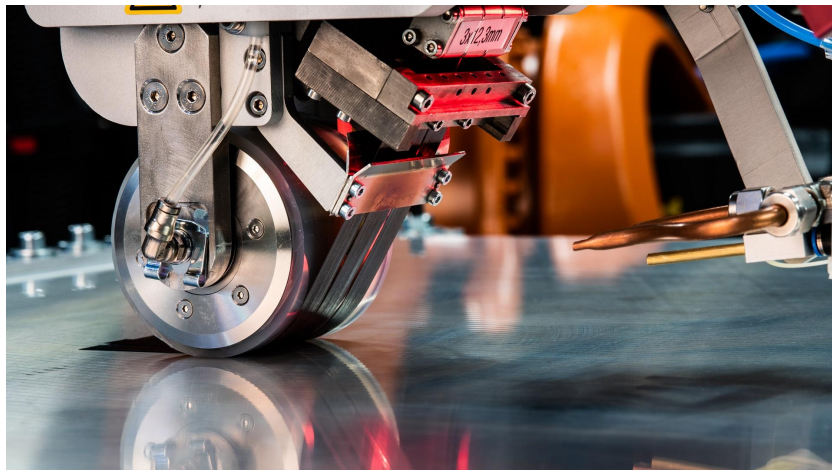


Figure 1.2: Tape laying machine in action [4]

The process uses narrower tapes of materials, called 'tows'. These tows suffer a deformation during the lamination process because the originally straight strip of material is forced to curve in intricate patterns. As one can imagine, there is a limit to these materials' deformability too - they cannot take too sharp corners. This is the primary source of the problem. There can be situations in a product surface, where tows cannot be stacked nicely next to each other because the material doesn't allow so. Thus, engineers have two choices, to leave gaps between the tows, or add overlapping material as a 'band-aid' to the problem. Thus, the primal problem of the research was born. These manufacturing defects, gaps and overlaps, are known to the scientific community, but the understanding of the imposed effects on mechanical performance is close to minimal. This topic was chosen to be the focus of this research.

2

Literature study

The literature study chapter summarizes the scientific background, upon which the research questions are founded, and which guides to subsequent solution. The chapter starts with a brief introduction to fracture mechanics and delamination in composite laminates. Subsequently, ply failure and manufacturing-induced defects are presented. Thus, the major failure modes are put into context, which influenced the tools and methodology used. The chapter ends with state-of-the-art characterization research on gap defects and a brief summary.

2.1. Fundamentals of Fracture Mechanics

Fracture mechanics in the context of composite delaminations have two distinct ways of dealing with crack propagation. One is the 'Strain Energy Release Approach' and the other is the 'Strength of Materials Approach'. These are discussed in detail in the next sections.

2.1.1. Strain Energy Release Approach

Aeronautical engineering structures have been dominated by metallic materials until recently. The revolution peaked around the 2010s when even the major airliner companies (Boeing, Airbus) released their new flagships with composite fuselage and wings, resulting in the Boeing 787 Dreamliner and the Airbus A350. Both feature more than 50% composite materials with respect to structural weight [2]. As the new materials evolved and surpassed common monolithic (e.g. metallic alloys) materials, scientific knowledge of the new field was built using the existing isotropic knowledge. Thus, an introduction to composite fracture mechanics should start from the basics, the simple isotropic media with a sharp crack. Such a case is represented on Figure 2.1.

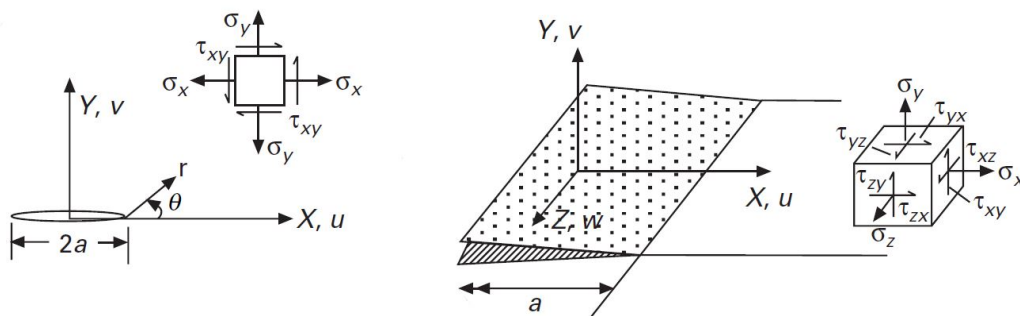


Figure 2.1: Axonometric representation of a crack in an isotropic media [5]

A crack tip, or in a more precise term, the crack front is under a complex 3D stress state, which varies along the crack and also in the close vicinity of the tip [5]. It is well-known that any complex loading, and therefore the resulting deformation can be described using the three major cases, the

so-called "fracture modes". These are the opening (Mode I), the sliding (Mode II), and tearing (Mode III) modes, which are represented on Figure 2.2.

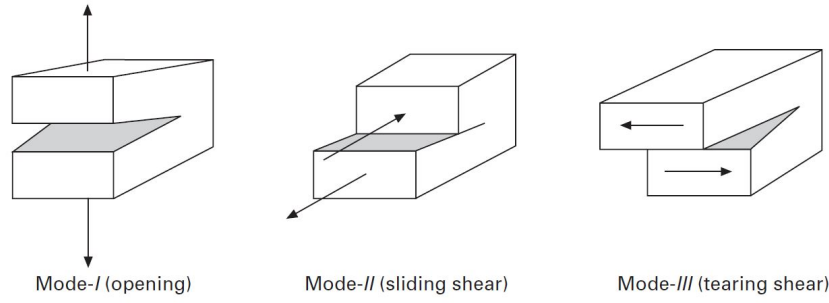


Figure 2.2: The three fracture modes of crack propagation [5]

The function which describes the stress field in the Y direction (following the notation of Figure 2.1) and the corresponding displacement (v) are detailed in Equation 2.1 and Equation 2.2 [5].

$$\sigma_y = \frac{K_I}{\sqrt{2\pi r}} \cos\left(\frac{\theta}{2}\right) \left[1 + \sin\left(\frac{\theta}{2}\right) \sin\left(\frac{3\theta}{2}\right)\right] + \frac{K_{II}}{\sqrt{2\pi r}} \sin\left(\frac{\theta}{2}\right) \cos\left(\frac{\theta}{2}\right) \cos\left(\frac{3\theta}{2}\right) \quad (2.1)$$

$$v = \frac{K_I}{2\mu} \sqrt{\frac{r}{2\pi}} \sin\left(\frac{\theta}{2}\right) \left[\kappa + 1 - 2\cos^2\left(\frac{\theta}{2}\right)\right] - \frac{K_{II}}{2\mu} \sqrt{\frac{r}{2\pi}} \cos\left(\frac{\theta}{2}\right) \left[\kappa - 1 - 2\sin^2\left(\frac{\theta}{2}\right)\right] \quad (2.2)$$

In the equations, θ and r represent the polar coordinates with respect to the crack tip, μ is the shear modulus, in case of plane stress condition $\kappa = (3 - \nu)/(1 + \nu)$, where ν is the Poisson ratio. K_I , K_{II} (and the not presented K_{III}) are called stress intensity factors for the respective modes. These factors are commonly used for fatigue in isotropic cases. Upon closer inspection, the stress function shows a singularity at the crack tip, with stresses tending to infinity. This, of course, is not realistic, as the finite strength of the material leads to failure along the points with exceeding loading. In other words, the crack steps further.

Irwin [6] introduced the term strain energy release rate ('SERR') upon the described functions. His hypothesis relies on the idea that the loss of elastic energy (enforced externally to the system) upon crack propagation is used up for the creation of new surfaces. This hypothesis holds well for brittle materials, where there is no significant yielding of the material during failure. Thus, extending a crack - through failure - of length a by Δa takes up the same amount of energy as if one simply closes a crack from $a + \Delta a$ to a . This crack-closing energy is expressed in Equation 2.3.

$$W = \frac{1}{2} \int_0^{\Delta a} \sigma_y(\Delta a - r) \cdot v(r) dr \quad (2.3)$$

The known work function was used to introduce the strain energy release rate definition, which mathematically means (Equation 2.4):

$$G = \lim_{\Delta a \rightarrow 0} \frac{W}{\Delta a} = \lim_{\Delta a \rightarrow 0} \frac{1}{2\Delta a} \int_0^{\Delta a} \sigma_y(\Delta a - r) \cdot v(r) dr \quad (2.4)$$

The final expression for isotropic materials thus becomes:

$$G = G_I + G_{II} + G_{III} = \frac{K_I^2}{E'} + \frac{K_{II}^2}{E'} + (1 + \nu) \frac{K_{III}^2}{E} \quad (2.5)$$

where G_I , G_{II} and G_{III} are the strain energy release rates for their respective modes, G is the total strain energy release rate. In plane-stress condition, E' equals to E , where E denotes Young's modulus of the material. Note that, the expression only holds for isotropic materials in this form. With a known quantity for crack propagation, the damage onset and the process itself can be characterized. A homogeneous material has three critical SERR values, G_{Ic} , G_{IIc} , and G_{IIIc} , for the three modes.

In a simple case of pure mode loading, crack propagation will occur if the applied SERR equals the corresponding critical value. Mathematically:

$$G_i \geq G_{ic}, i = 1, 2, 3 \quad (2.6)$$

here, G_i denotes the applied SERR, while the right side represents the critical value. Pure mode loadings are seldom found in real-life applications, thus there is a need for mixed-mode criteria. One of the initial solutions for this was the power-law criterion by Wu and Reuter [7], presented in Equation 2.7. The exponents $m, n,$ and p are empirically determined coefficients. Interestingly, this criterion was developed already on composite materials, in 1965.

$$\left(\frac{G_I}{G_{Ic}}\right)^m + \left(\frac{G_{II}}{G_{IIc}}\right)^n + \left(\frac{G_{III}}{G_{IIIc}}\right)^p \geq 1, i = I, II, III \quad (2.7)$$

Recently, the criterion of Benzeggagh and Kenane [8] became more widely used ("BK criterion"). Their original work (Equation 2.8) holds for 2D problems only, without Mode III loading, although Reeder [9] extended it for complex 3D case (Equation 2.9). The latter is commonly referred to as the BK method too since it is a direct extension of the original one.

$$\frac{G_I + G_{II}}{G_{Ic} + (G_{IIc} - G_{Ic}) \left[\frac{G_{II}}{G_I + G_{II}}\right]^m} \geq 1 \quad (2.8)$$

$$\frac{G_I + G_{II} + G_{III}}{G_{Ic} + \left(\frac{G_{II}(G_{IIc} - G_{Ic}) + G_{III}(G_{IIIc} - G_{Ic})}{G_I + G_{II} + G_{III}}\right) \left[\frac{G_{II} + G_{III}}{G_I + G_{II} + G_{III}}\right]^{m-1}} \geq 1 \quad (2.9)$$

2.1.2. SERR approach for delamination

As discussed before, delamination is the failure of the integrity of plies [5]. The SERR approach with the presented criteria are the primary method to model delaminations in composites. Williams [10] studied the issue of a fracture at the boundary (interface) of two different isotropic materials and found that the stresses in the close proximities of crack tips show oscillatory character. The relation mathematically is detailed in Equation 2.10.

$$\sigma \sim r^{\frac{1}{2} \pm i\gamma} \quad (2.10)$$

The expression contains the imaginary unit i , and γ , which is a complex term involving the shear moduli and poisson ratios of the two adjacent layers. This expression indicates well how much the anisotropy complicates the mechanics of materials. To complicate matters further, the real plies are built up of separate phases with separate material properties and load-bearing capabilities. Under pure opening, shearing, or furthermore, under mixed mode interlaminar stresses, the pristine interply media's microcracks were proven to develop at an inclined angle compared to the laminate plane (Greenhalgh [11]). The reason is simple, the interply stress state can be transformed into a 'resolved' principal stress state by rotation, which has only a normal (opening) stress. The microcracks are driven to grow to the edges of the interply region, where they coalesce into one larger crack surface. Thus, the spread of damage will happen along the ply boundaries (Figure 2.3).

Based on the idea of the matrix phase conveying the loads to the fibres, it feels evident that the matrix around the fibers is bearing a concentrated higher load. Knowing the crack propagates where a stress state is most prominent, engineering intuition can rightfully say the failure can choose the ply over the interface. This occurrence is well represented visually in the micromechanical FEA simulations of Varandas et al. [12] (Figure 2.4). If the initial microcrack angle points directly between fibers (for instance, into a 90° ply, see Figure 2.4), the phenomenon has a high chance of occurring.

In the event that the crack switches from its original interface to an adjacent interface by destroying the ply along the way, the phenomenon is called "crack jumping" or "crack migration" [13]. Numerous studies present the frequent occurrence of crack migration, which happens even in cases where the crack is forced to grow along one interface by premade cracks and controlled loading condition [14–20]. The occurrence or even further, the point of crack migration should be influenced by numerous stochastic effects, such as the presence of voids, debris, manufacturing defects, or the random distribution of fibers to name a few. Thus it is founded to conclude that, modeling delamination propagation

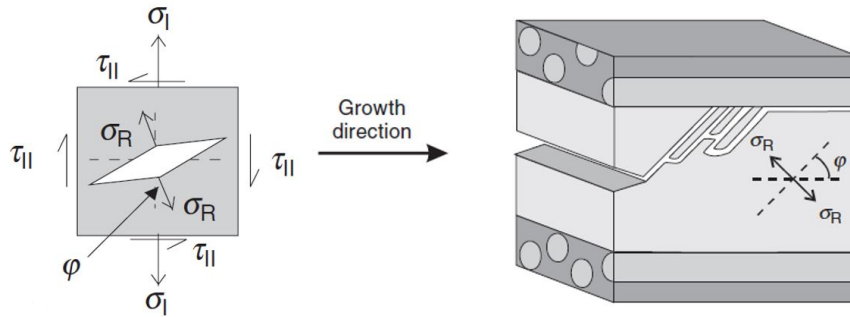


Figure 2.3: Failure development of interply media [11]

only between plies could well overlook the real case, where the initiation and area of influence can be at vastly different points. Nevertheless, a good prediction of the initiation and early life of the crack is still a valuable tool for the industry.

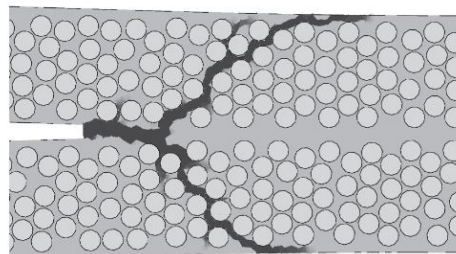


Figure 2.4: Micromechanical simulation of crack propagation in fiber reinforced composites [12]

Apart from crack jumping, the R-curve effect has been known for a while (Irwin, 1958 [21]), impacting even isotropic systems under plane stress conditions [22]. The curve describes how during damage growth, the material's crack growth resistance increases with crack extension. This curve for composites is usually very pronounced. Presenting steady-state resistance to be twice the initial resistance is not uncommon. Especially in opening mode loading, one can observe fibers connecting the fracture surfaces in interaction. These fibers, in the wake of the cracked front, alleviate the opening at the tip, imposing an increased apparent resistance. This is the so-called "fiber bridging" phenomenon (Figure 2.5 left) [22]. Other noteworthy parameters of the R-curve effect include friction between mating surfaces or crack closure [23]. A typical R-curve is presented on Figure 2.5 (right).

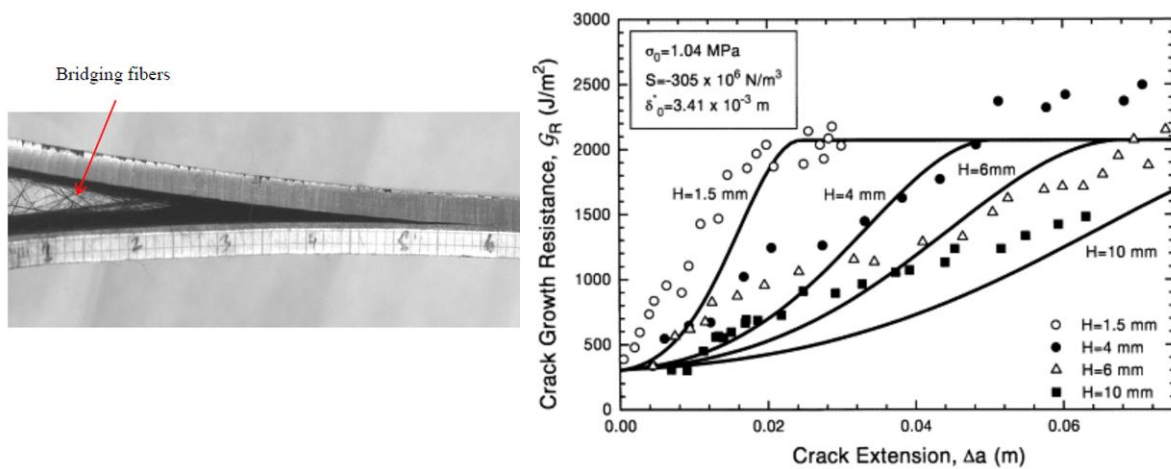


Figure 2.5: Fiber bridging of a specimen (left, [23]) and typical R-curve plot (right, [24])

The previously mentioned prediction of delamination initiation using the SERR approach still bears some concerns. Although there are working initiation criteria, the critical SERR values (or sometimes "fracture toughness") to use are not straightforward. The article of Anderson and König gathered experimental G_c variations of all modes with respect to two parameters [25]. The first is the difference in fiber orientation of neighbouring plies of crack surfaces, and the other is the crack propagation direction with respect to ply orientations. To effectively merge the large literature data set, they introduced a notation for the two parameters as it is presented on Figure 2.6. The dashed lines represent the ply orientations, and the ψ fiber orientation (mismatch) angle is measured from the bisection axis of the adjacent orientations. Crack propagation angle α is measured between the bisection axis and the vector of the crack propagation direction. With both angles varying from 0° to 90° , all possible cases could be defined. Their work processed more than 60 research articles from the related field.

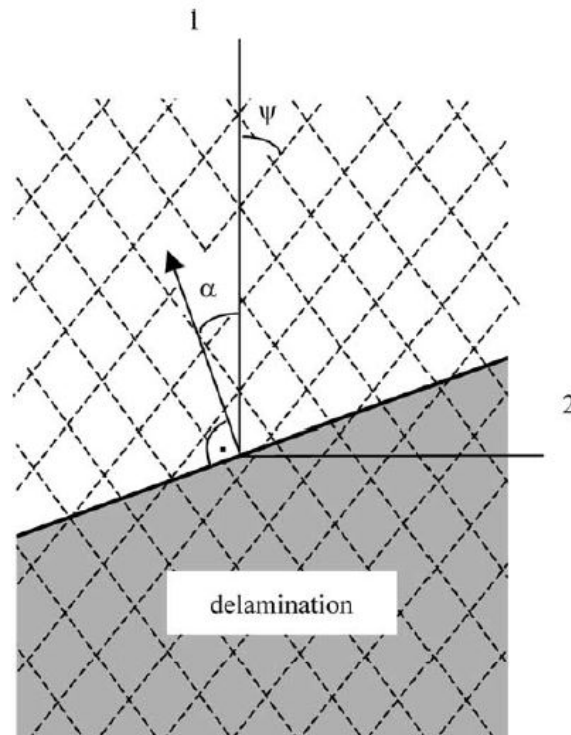


Figure 2.6: Notation to the parameter study. ψ as the ply orientation difference, α as the crack propagation direction. [25]

Obtaining fracture toughness values

The G_c values in the discussion are exclusively from standard measurements, solely from standards of the American Society for Testing and Materials (ASTM). For Mode I values, the corresponding standard is ASTM D5528/D5528M [26], the common Double Cantilever Beam (DCB). For Mode II, the standard is the ASTM D7905/D7905M, known as the End Notched Flexure (ENF) test [27]. Mode III testing involves the Split Cantilever Beam (SCB) test, which has been reported to impose significant Mode II effects onto the crack, questioning the validity of data [25]. In addition to this method, Edge Crack Torsion (ECT) tests are getting increasingly popular, though it is not a standard as of today.

Mode I variation with crack propagation direction

The discussion of Mode I fracture toughness variation starts with crack propagation direction dependence in unidirectional laminates ($\psi = 0^\circ$). For $\alpha = 0^\circ$ and $\alpha = 90^\circ$, about identical (around maximum 10% deviation) values were found by Russell and Street [28] and Trakas and Kortschot [29]. This has been supported by Jordan's work [30] also. For glass fiber reinforced polymers (GFRP), Laksimi et al. [31] found no pronounced dependence between $\alpha = 0^\circ \dots 60^\circ$. Hwang et al.'s research [32] confirms no clear variation as well between $\alpha = 0^\circ \dots 45^\circ$ due to large scatter.

Opposite to these observations, Mode I fracture toughness has been reported to increase with an increasing α in numerous other publications. Robinson and Song [17] found 35% larger values for 45°

compared to axial loading. Lakshimi et al. [33] reported a 26% increase in G_{Ic} at 90° , contrary to their previous work [31]. Schön [15] initially found 50% higher toughness for $\alpha = 90^\circ$ compared to the classic unidirectional sample ($\alpha = 0^\circ$), although the measurement is questionable since cracks migrated to adjacent $0^\circ/90^\circ$ interfaces through plies. The same phenomena occurred with Fish and Malaznik [18] and Chou et al. [19] [20] at $\alpha = 90^\circ$. This is a good representation of the crack's tendency to penetrate adjacent lateral fiber plies. Probably the most convincing data obtained is by Lucas [34]. He reported a clean increase across the whole spectrum. This being said the magnitudes of the increase do not fully align with the previously mentioned outcomes, and a clear tendency is hard to find.

There is a third group of results, which reported decreasing values. Chou et al. [20] found smaller values for a $\pm 45^\circ$ than axial loading. Polaha et al. [14] measured $\alpha = 0^\circ, 15^\circ, 30^\circ$ and found a decreasing tendency. This measurement was discussed to be questionable by the authors since fibers from the adjacent plies probably migrated to each other, resulting in corrugated fracture surface and fiber bridging.

Mode I variation with interface orientation mismatch

For the G_{Ic} variation with respect to interface orientation mismatch, the agreement is even less than it was with the crack propagation direction. Russell and Street [28] observed somewhat lower toughness for $\psi = 45^\circ$ when compared to UD specimens. Polaha et al. [14] found decreasing values through $\psi = 0^\circ \dots 30^\circ$, although the data scatter is large enough to question the tendency. Tohgo et al. [35] measured carbon fiber embedded in thermoplastic (TP) polyamide matrix, and at $\psi = 0^\circ, 30^\circ, 60^\circ$ interface mismatches. Their measurements also observed a decrease in the values, although there are some concerns stated by the authors. Namely, the standard measurement requires an insert (an inert release film between the layers of interest to initiate the crack at the desired location), which creates a resin-rich pocket at the edge. Therefore, the first crack initiation could indicate more favourable properties, inclining to a non-conservative side. This is a concern for all measurements presented, although some publications used pre-cracked specimens (first crack propagation is discarded, and measurement starts at the second increment). This phenomenon is also known for the standards, which allow for both methods. Ozdil and Carlsson [36] found a decrease to an angle of $\psi = 45^\circ$, but in their other work [37], they investigated larger angles for a different material (e.g. $\psi = 30^\circ$ and 55°) and found an increasing tendency.

Robinson and Song [17] made the same comparison as Russell and Street [28], and found the exact opposite tendency (24% increase for $\psi = 45^\circ$). Lachaud et al. [38] sampled $\psi = 0^\circ, 22.5^\circ, 45^\circ$, not just for the common thermoset (TS) carbon fiber reinforced polymers (CFRP), but also for thermoplastic matrix (polyether-etherketone, PEEK). The article presents a clear and monotonic increasing tendency, which becomes also very significant for the larger mismatch (more than 50% for both matrices). Allix et al. [39] published only the steady state values (the plateau value of R-curves). The results show a 70% increase for larger orientation mismatch.

A stronger difference was observed by Nicholls and Gallagher [40] between UD and angle ply specimens (75% larger value for angle ply stackups), although the variation between angles is negligible. Chou et al. [19] [20] found a negligible increase (maximum of 12%) for larger angles, but the difference is not comparable to the large scatter bands. Hwu et al [41] measured GFRP specimens for a wide range of values (up to $\psi = 60^\circ$ in 15° increments), and found no systematic trend. Small or negligible variation was found by Davies and Rannou [42], Jordan [30], and Trakas and Kortschot's [29] data bears too large scatter to bear any consequences.

Mode II variation with crack propagation direction

Decreasing Mode II values were found mostly with respect to increased crack propagation direction. Trakas and Kortschot [29] obtained 40% lower G_{IIc} values for $\alpha = 90^\circ$ compared to $\alpha = 0^\circ$ case. Hwang et al. [32] corroborated the latter and found a decreasing tendency in the $\alpha = 0^\circ \dots 45^\circ$ interval. Monotonic reduction with angle difference was the outcome of Lakshimi et al. [43].

Polaha et al. [14] did not find significant difference between $\alpha = 0^\circ, 15^\circ, 30^\circ$. Schön et al. [16] experienced troubles with severe crack migration in obtaining founded results.

Mode II variation with interface orientation mismatch

A more broad study field in Mode II values is considering the orientation mismatch for the sensitivity study. Allix et al. [39] measured $\psi = 0^\circ, 22.5^\circ, 45^\circ$, with steady-state toughness values being larger

for the latter case by a huge margin (90% increase, no initial toughness values reported). The same interval was measured by Lachaud et al. [38] for both TS and TP matrices. The brittle TS matrix proved a substantial increasing tendency, while the tough TP matrix did not show any strong sensitivity (although, contrary to TS, a 12% decrease). Shi et al. [44] measured a wide range of angle mismatches for both tougher GFRP and brittle CFRP systems. While the former showed a somewhat constant nature, an increasing trend was the latter's outcome. Ascending averaged values are presented by Rubbrecht and Verpoest [45] but upon a closer look, one could completely deny the validity of the trend based on the immense scatter bands. Chai [46] studied TS and TP systems, while TP systems remained constant, larger mismatch TS interfaces were shown to be stronger than UD counterparts. For $\psi = 45^\circ$, initiation toughness was found to be 45% higher than a pure 0° stackup for Choi et al. [47]. Ozdil et al. [37] [48] came to the same conclusion.

In contrast to the previously mentioned publications, UD interface was reported to be 30% stronger by Chou et al. [19] compared to UD specimens. The decreasing tendency was found especially in cases where one of the plies was parallel to the crack propagation direction, mathematically referring to $\psi = \alpha$. Trakas and Kortschot [29] experienced a 20% smaller value for angle plies, which is in good agreement with the results of Russell and Street [28]. Tao and Sun [49], and Yang and Sun [50] investigated the same material, in quite fine mismatch increments. While the previous reported a monotonic decrease, the latter found about constant values, contrarily, UD being the lowest value for the latter. Hwang [32] agrees with the 'lower toughness for angle plies' line of publications, obtaining 25% and 30% lower values accordingly. His work also bears non-negligible scatter.

Polaha et al. [14] reported no dependency in the interval of 0° to 30° . The same nature was experienced by Hwu et al. [41] between $\psi = 0^\circ$ and $\psi = 60^\circ$ in 15° increments.

Mode III variation

Significantly fewer studies focused on Mode III delamination. As it is much harder to impose onto a specimen in a pure form, all measurements bear extra (mostly Mode II) loading modes. Donaldson [51] found no general tendency for Mode III fracture toughness since $\psi = 15^\circ$ and $\psi = 75^\circ$ interfaces were stronger than UD counterparts, however, $\psi = 45^\circ$ fall short of even the latter specimens. Chai [46] measured 60% higher initiation values for angle ply interfaces in the case of TS, and 15% higher for TP matrix systems. Liao and Sun [52] tested on torsional specimens, and obtained 20% higher values for cross-ply specimens. Liao and Donaldson tested the same material with different methods and found them to deviate by a factor of 2. Solely the measurement setup change caused a significant deviation, which shows how not only does the material cause scatter of random nature, but quantifying pure mode values is also immensely hard. Trakas and Kortschot [29] had a contradictory result, having the highest values for UD specimens.

Discussion of critical value variations

To summarize the presented review of a large batch of measurements on fracture toughness values, it is safe to say there is no agreement in any mode loading tendency with respect to interface angle mismatch or crack propagation direction. Moreover, measurements most of the time are not comprehensive on the entire angle range. The data scatter often is so considerable, that drawing any conclusion becomes unfounded. Figure 2.7 presents the results of two discussed papers. On the left, the significant increase in fracture toughness is represented through a Mode I R-curve. One can see, take the $0^\circ/90^\circ$ interface, for instance, the measured values are almost homogeneous over a domain. Because of this, crack propagation predictions in progressive damage analysis must be taken as a rough estimation of reality, especially in more developed phases of the process.

In the case of onset predictions, the use of measured values can also mislead an analysis. The diagram on the right of Figure 2.7 presents a measurement from the work of Hwang et al. [32]. The substantial variation in the measured values of initiation fracture toughness values also conveys some uncertainty. Therefore, based on the presented literature, the usage of the strain energy release rate approach to model delamination should be rather focused on the onset stage, with values corresponding to actual interface parameters and crack propagation directions. If one uses constant SERR values, the results should be treated with caution, as it could only capture major tendencies during failures.

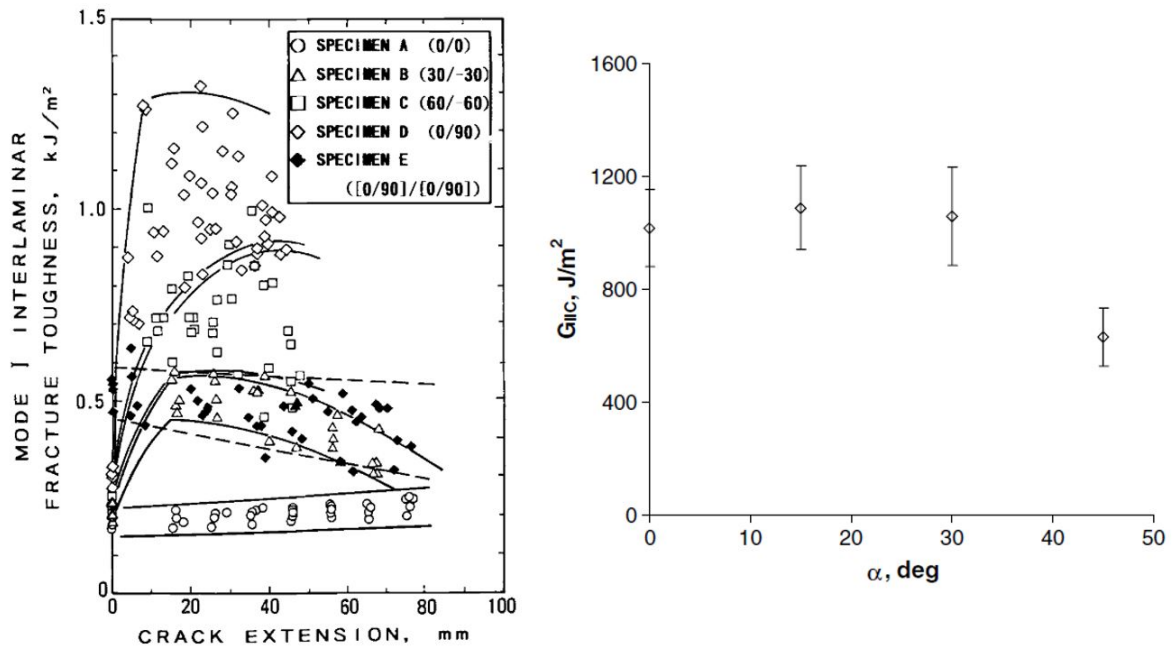


Figure 2.7: Mode I R-curves for different interfaces (left, [19]), and Mode II measurements with usual size scatter (right, [25] based on the values of [32])

2.1.3. Strength of materials approach

If only the onset of delamination is of interest, the "strength of materials" approach can also be sufficient, without the need to analyze damage progression. Even though one can think the process would simplify, other issues arise with the second method. Composite laminates are generally simplified to in-plane properties, as the usual form of products fall into the category of thin shells. However, in this case, out-of-plane interlaminar stresses must be known as the input to the analysis of onset, which is a strong demand even with FEA tools. The nature of stress singularity at crack tips has been previously presented, therefore it seems to be a dead end to create propagation criterion based on stresses. This is exacerbated by at free edges, anisotropy produces singularities too, as was presented by Wang and Choi [53] during the early days of composites. To counter this, Kim and Soni introduced the idea of utilizing an 'average' stress. The average stress criteria predict failure when the average value of stress, $\bar{\sigma}$ over a set distance x_{avg} meets interlaminar tensile strength ahead of the free edge. As an expression for an arbitrary stress component, this is:

$$\bar{\sigma} = \frac{1}{x_{avg}} \int_0^{x_{avg}} \sigma(x) dx \quad (2.11)$$

These stress components are a function of the averaging distance, often referred to as characteristic length. Thus, this represents a major limitation of the approach, as it has to be determined through testing, moreover, it is only "hypothesized to be material system properties" [54], little is known about other factors influencing this. Previously the variation of SERR values with respect to interface orientation was discussed. Considering the SERR and strength of materials approaches describe the same phenomena, variations can be expected for the interlaminar stress limits for different interfaces as well. This field, probably because of the limited nature of onset, is less researched. One outstanding work is the one of Zhang et al. [55], the result of which is presented on Figure 2.8.

The data was obtained through an impressive batch of 665 double-notched specimens (ASTM Standard D 3846). The data deviation bands are significant, as it was in the case of SERR values. The authors experienced crack jumping, in-ply cracking, fiber bridging, and supporting ply fiber breakages too throughout the measurements. The publication contains the probability density functions for each orientation dataset (Figure 2.9). The diagram on the left, corresponding to 0° orientation, presents the values for a UD specimen, which should be a relatively stable measurement. However, 24 of the 35 specimens exhibited some crack migration, which resulted in a large uncertainty in the measured strength, as shown on the graph. The same applies to other interfaces, for example, the 40° case

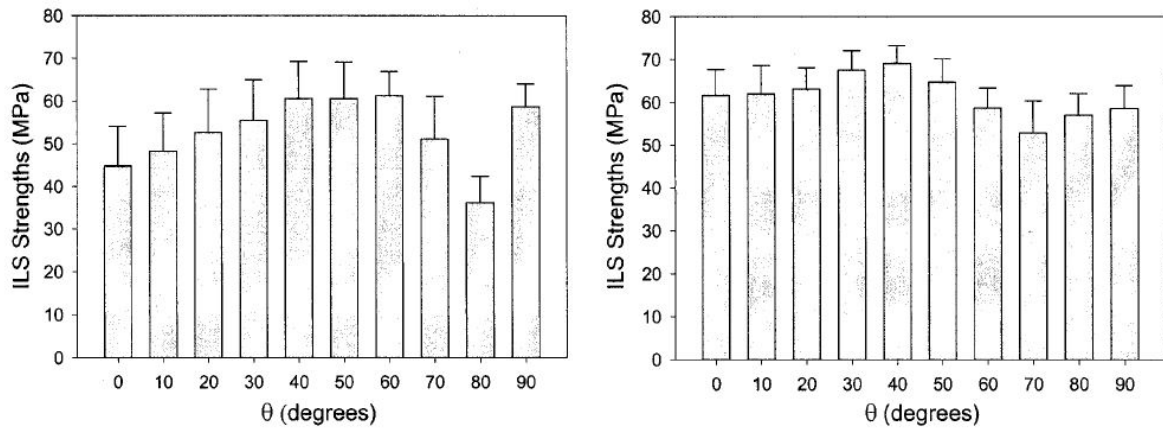


Figure 2.8: S_{13} (left), and S_{23} (right) strength value dependence on orientation mismatch [55]

(Figure 2.9 right). The probability density function is almost a plateau between 45 and 75 MPa values, meaning that using a simple average value could lead to an unconservative solution with about 20-25% error.

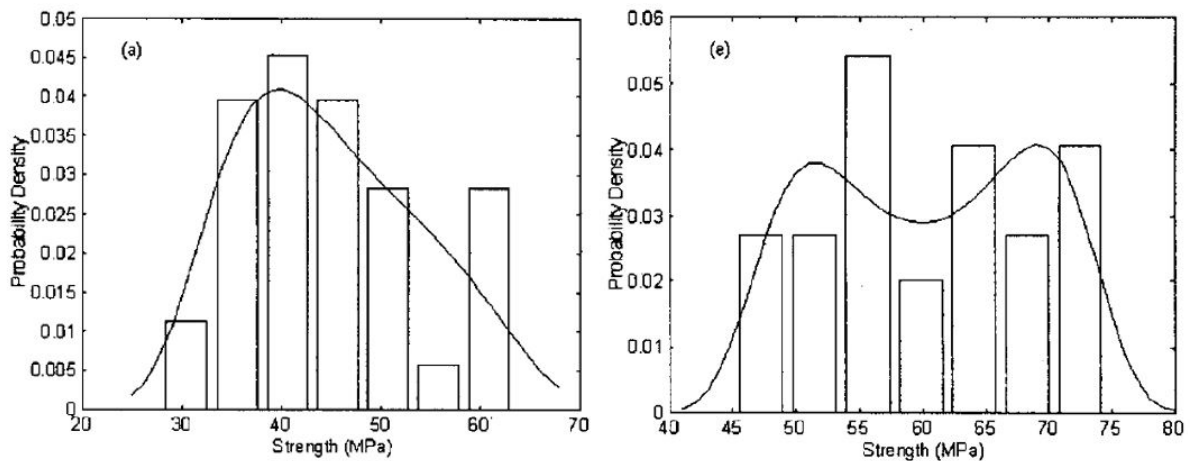


Figure 2.9: Probability density functions of S_{13} for angles 0° (left) and 40° (right) [55]

To summarize, the strength of the materials approach has an inherent limitation to onset only, needs out-of-plane stresses that are hard to obtain, depends on values that are only hypothesized to be material constants, and moreover shows a very large uncertainty in measured values. Thus, this approach can be an inferior method to the SERR approach and bears immense uncertainties upon usage.

2.2. Ply failure

While interply failure has been discussed as being difficult to capture, the case is better with intraply failure. The general approach to analyze a laminate for failure is based on the homogenous treatment of plies, without treating matrix and fiber separately for calculations. This means a homogeneous ply is considered to be loaded with stresses/strains in the 3D space (orthogonal stresses/strains). Altogether, this translates into 3 normal and 3 shear stresses, commonly used in solid mechanics. Note that, the failure modes for the respective constituents are individually recognized though. For UD ply (and therefore for AFP tows as well), these are namely [2] [56]:

- **Fiber failure**

- **In tension**

The desired failure mode of a composite laminate, since the reinforcing material is fully exploited for strength. Upon axial overloading of a ply, the reinforcing fibers cannot bear any more load and suffer a simultaneous transverse fracture. This failure mode offers outstanding performance, but sudden and catastrophic failure, and is governed by the axial tensile strength of the material, X^t .

- **In compression**

In the case of dominant axial compression, usually fibers suffer from so-called "kinking" or "micro-buckling". During micro-buckling, a larger bundle of fibers buckles under the compressive load, resulting in a transverse discontinuity. Fiber kinking happens on a smaller scale when some local areas suffer under transversal loads, which exceed the matrix material's strength. A localized band forms (essentially through fiber rupture) with a different orientation, while on both sides of the band, the orientation remains the same. The phenomenon looks similar to twinning in crystalline structures. This failure mode happens at significantly lower loads than in tension and is governed by the axial compressive strength X^c of a ply.

- **Matrix failure**

- **In tension**

Although fiber fracture is the desired mode, most of the time the failure originates from matrix cracks along fibers, and plies. In transverse loading, the response of a lamina is governed by the matrix phase, rather than the reinforcement. If this transverse load is tensile, the environment is set for microcrack initiation, which eventually leads to total cross-sectional rupture or initiates delamination on the ply interface. A major failure mode, governed by transverse tensile strength Y^t .

- **In compression**

Compressive loads do not initiate perfectly perpendicular crack surfaces as in a tensile case but have an inclined fracture angle, common with brittle materials like cast iron too. Compressive fracture has a stronger interaction with in-plane shear loads, as Puck's work [56] presents in detail. The compressive transverse load is somewhat more favorable, as the transverse compressive strength Y^c is commonly larger than its tensile counterpart.

- **Pure shear failure**

During dominant shear failure, the resultant fracture surface has perpendicular matrix failure along the fibers, similar to the transverse tension instance. Strength is usually denoted with a simple S .

The mentioned load limits or strength values are obtained for materials through testing and are considered material constants. Using Classical Laminated Plate Theory (CLPT) or the computationally expensive 3D mechanics of anisotropic materials, the stress and strain values of plies can be calculated (or simulated through Finite Element Method) individually. In continuum mechanics, the scientific expression or theory that describes the failure of a material is called a failure criterion. For isotropic media, the well-known von Mises criterion has proven to be a useful and accurate method for analyzing material yielding since the early 1900's. For composite materials, the scientific area is more recent, and there are many more criteria in use - as Figure 2.10 represents the main development. The main task for these criteria is to accurately capture the interaction of loads through anisotropy. For example, transverse stress could be worsened by additional in-plane shear load, leading to failure even if the individual load components remain below the respective strengths. The opposite of this, when the stress state is better than the individual load components, is for example a biaxial compression state as the fiber buckling phenomenon is damped. Figure 2.10 represents the level of scientific foundation on the vertical axis for each criterion and time on the horizontal axis. Throughout time, the approaches got more founded on scientific background, and less on statistical data, as a general tendency.

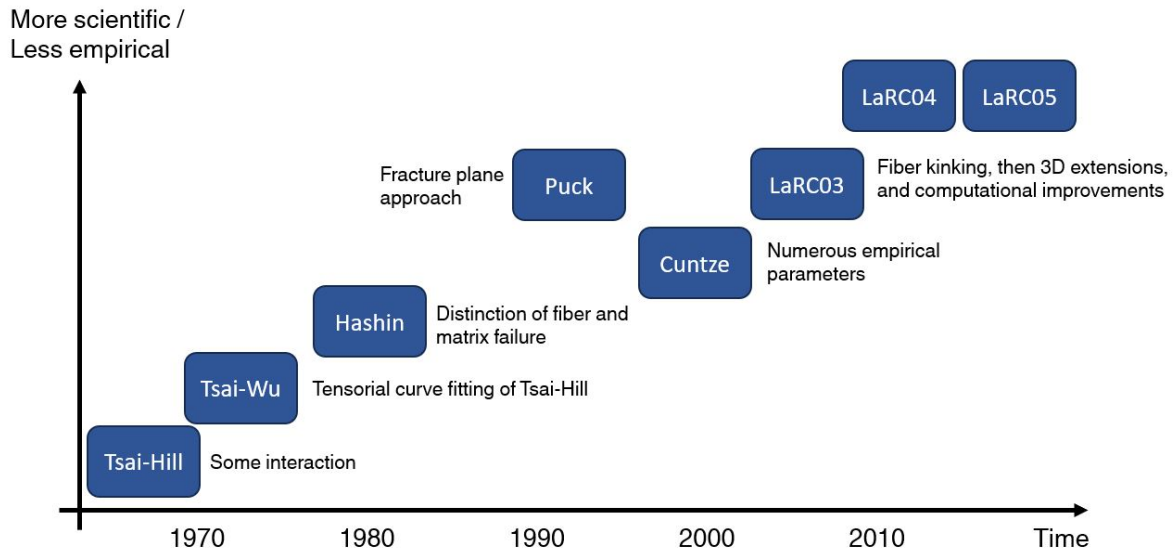


Figure 2.10: Failure criteria going through development over time

The simplest criteria are the "Max stress" and "Max strain" theories, which simply compare individual loads or strains to the corresponding strength or critical strains. Obviously, these are not interaction criteria and are far from accurate. A large step in material strength characterization came around 1970 with the Tsai-Hill and the improved version, the Tsai-Wu criterion. The former augmented the von Mises yield criterion to the anisotropic strength, but just until a given level. Namely, in pure axial, transverse, or shear loading, the equation reduces to a simple max stress criterion, otherwise it has a polynomial mathematical form. Tsai-Wu was a step towards a 3D state. In essence, it was a curve fit of the former criteria in 3D using tensors in vector space. Tsai-Wu is the industrial standard for woven fabric analysis up to this day. Until this point, no criterion considers fiber or matrix failure. This leap happened with the Hashin criterion, and subsequently with the Puck criterion, which calculates fracture planes from transverse and shear loads. Cuntze introduced numerous empirical parameters for his invariant-based criterion, which is rather a step toward statistical approaches. The recent family of LaRC criteria (named after NASA's Langley Research Centre), made by NASA, diverged to the fracture mechanics way with SERR considerations. The criterion gradually improved on modeling of featuring phenomena like fiber kinking and advanced further in computational efficiency [2] [56] [57].

These works were developed for straight fiber laminates. Research makes extensive use of these criteria for variable angle laminates to account for ply failures too, although fewer articles are available that compare it to experimental data. Lopes et al. [58] made Finite Element Method (FEM) simulations with progressive damage analysis for post-buckling cases, where the damage analysis was based on LaRC04 failure criteria. The research tool was tested for an experimental setup, where specimens with open holes were loaded until failure in the post-buckling regime. Specimen versions included straight fiber laminate, and variable orientation ones with tow-drops and tow-overlaps also. In the case of the straight fiber version, the failure load was 1.7% off from the simulated case, for the tow-drop case it was 1.4%, and for overlaps it was 8.2%. Important to note that the simulation utilized shell models without edge effects around gaps and overlaps. Even with these neglects, the accuracy is remarkable. Through FEM discretization, variable tows are approximated with small elements, in which fibers are assumed straight. The use of straight fiber failure criteria could be justified if one investigates the variation of fiber angle in one element. For a curve radius of 400 millimeters, which is barely a lower limit value even for narrower tows (e.g. 1/8 inch), the fiber orientation variation is plotted against element size on Figure 2.11.

Considering even a coarse mesh of 5 mm element size, the orientation mismatch stays under one degree. This amount of error between reality and simulation could happen in straight fiber laminates too, if they were manufactured by manual lamination. Thus, the error for usage of such failure criteria does not hold considerable error for variable angle layups. The foundation of such usage lies in the

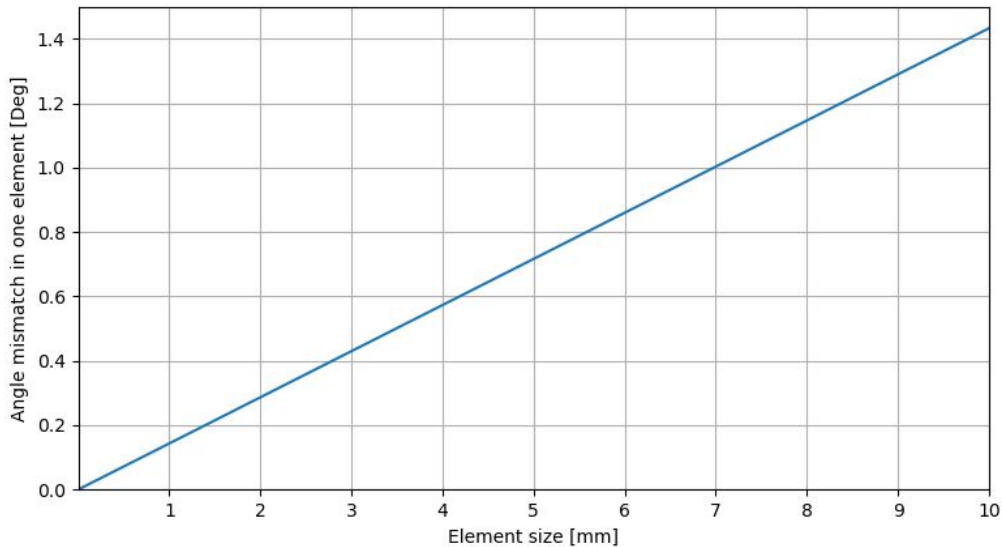


Figure 2.11: Angular mismatch in one element as a function of element size (radius = 400 mm)

manufacturing constraint of minimal radius, which rarely could go under 300 millimeters, reducing the orientation error in meshes.

2.3. Manufacturing induced defects of AFP

Automated fiber placement offers several advantages, such as fiber steering in a tailored path, good repeatability, fast lamination, and controlled quality to name a few. However, there are some manufacturing induced defects. Apart from the air pockets, foreign bodies, in-plane fiber waviness, and tow/ply defects, which also appear in other manufacturing cases, there are some that are typical for this type of method. These are summarized by the work of Heinecke and Willberg [59], notable ones include:

- **Tow Gaps:** Terminating of a tow placement is done automatically by an AFP head mounted onto a gantry or a robotic arm. The head, however, can only cut the tow perpendicular to the fiber direction, leaving a clean cut. Though this may be faster for manufacturing, it leads to gaps in certain smaller areas. Such an area appears where there is an orientation shift between zones (Figure 2.12 right) or when curves are shifted by a translational value, while the orientations remain the same in the translating direction (Figure 2.12 left). Henceforth, the former will be referred to as triangular gaps, the latter as translational gaps. Multilayered laminates exhibit waviness in the out-of-plane direction as a result of these gaps and overlaps. Overall, the defect induces stress concentrations and lowers strength.

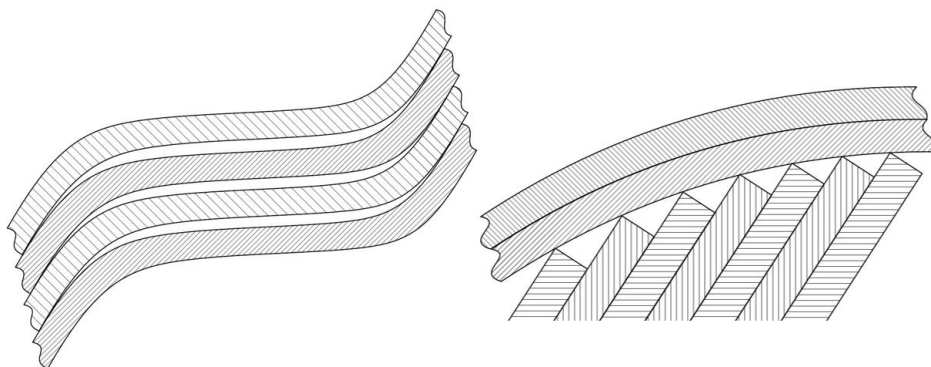


Figure 2.12: Translational gaps and triangular gaps occurring with AFP manufacturing technologies

- **Tow Overlaps:** The fundamental reason for overlaps is the same as with gaps, the tow can not be cut in angles, but this time the tow has overrun the edges, thus covering all of the areas. This method induces out-of-plane waviness, just like the gap version, and under the overarching tow, a resin-rich pocket, essentially a wedge is formed. This also results in stress concentrations, lowering strength. Typical overlaps are presented on Figure 2.13.

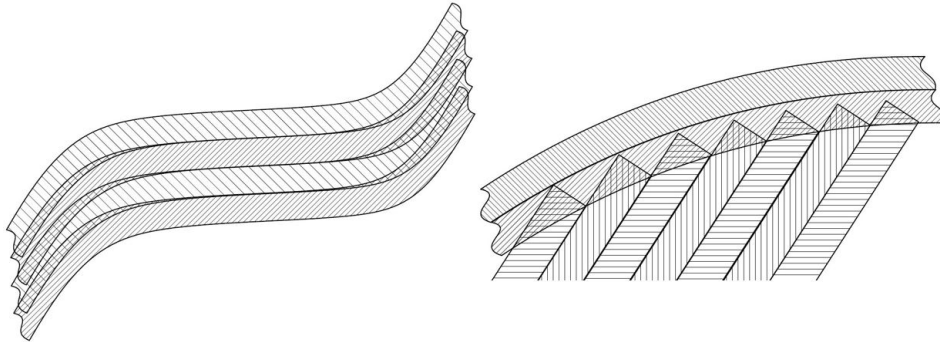


Figure 2.13: Translational overlaps and triangular overlaps occurring with AFP manufacturing technologies

- **Twisted tows:** As the laminating head moves around, the tow can be twisted throughout the motion path if it is not accounted for. More typical for fiber steering parts. The manufacturing error leaves gaps and waviness at the defect location.

These defects lower the load-bearing capabilities of VS structures, which in the strict field of the aerospace industry, must be accounted for. More accurate strength characterization of such defects improves safety and/or reduces the over-conservatism in future structures, making it more efficient. Therefore the goal of this thesis is to characterize manufacturing-induced defects in AFP manufacturing methods. To quote the prominent researchers in the field, Lopes et al. [60] stated:

"The knowledge about the fiber-steered configurations that lead to the highest first-ply failure loads is still rather limited. Furthermore, the full details about the mechanisms that lead to failure of variable-stiffness panels are not known yet, particularly the influence of local effects resulting from the manufacturing of these composites." (p.1761)

Since this quote (2010), there has been newer research in the area, which will be covered and discussed in the next section. Since not all problems can be fixed in a single work, it is chosen to first focus on gaps, for two reasons. On one hand, because the tow overlap case bears much more complexity in 3D space, suggesting it should be a second step after a well-founded first step. On the other hand, gaps are reported to have a more severe effect, opposite to the overlap case where the value can even be increased with the additional material [61, 62] for both strength and stiffness.

2.4. Strength characterization of gaps

The remainder of the literature study focuses on the AFP induced gap characterization with respect to the strength of the structure. This includes the summaries and discussions of significant publications in literature until this point, in chronological order.

The work of Blom et al. [63] from 2009 presents a shell FEM simulation for a variable stiffness panel under compression, which panel contains gaps due to translational method for simultaneous and parallel tow lamination. After deriving a function to determine the location of triangular gaps in space, panels were loaded in compression, with buckling prevented artificially with constraints. The authors themselves reflect on this choice, saying in reality, buckling can not be suppressed for such thin laminates. Thus, future studies should focus on tensile loading or it should include buckling phenomenon. The simulation featured a self-developed material model for progressive damage modeling. Failure criteria in use was LaRC04, delamination was not dealt with. The gradual failure was simulated with a Continuum Damage Model (CDM). Staggering the defects in space (preventing the pile-up of defects on top of each other by shifting tow drop areas on the plane of the laminate) was investigated, and proven to be beneficial in terms of strength, even for this lower fidelity model. Gradual failure propagated from the defects, proving the importance of the subject. Increased tow drop percentage

resulted in increased strength reduction, which was between 5%-15% for various VS layups. The FEM tool doesn't calculate with edge effects or resin-rich pockets, which raises questions about the accuracy of the outcomes. The large size of the analyzed panel makes it possible to have large orientation differences and provides a realistic case with gaps and lower-level gap interaction.

Croft et al. [62] did a comprehensive test on the gap, overlap, half gap/overlap, and twisted tow effects on both lamina and laminate scale. Testing was carried out according to ASTM standards on tension, compression, and in-plane shear, with the addition of open-hole tension and compression specimens. This means all specimens were developed for straight fiber laminates. The defects were one tow wide (around 3 millimeters - which is a really thin tow width) and two tows thick. Their justification for this choice is to capture the variability between defects, since, quote, "it is assumed that one tow defect generates a small effect on a structure because usually, the material used in the AFP process is thin and tough" (p.485). Following the statement, the author of the thesis questions the validity of any drawn consequences for real-life applications. Further deviating from VS laminates, the defects were enclosed in a straight fiber, symmetric, and balanced laminate. The tensile test showed little difference when compared to the baseline (pristine condition laminate) tests. Compression tests presented a larger scatter, and no difference between defects, except for the overlap case, which, through the increased thickness, stood out from the rest. In-plane shear tests exhibited a larger scatter, showing stronger variation with defects. The defects ran to the edges of all coupons, meaning free-edge effect probably influenced the measurements. The overall conclusion from the authors was that defects show negligible effect on strength. Considering the following publications, it is a controversial statement.

Falcó et al. [64] carried out tensile tests for un-notched and open-hole specimens containing triangular gaps or overlaps. The specimens were simple rectangular coupon types, with lengths of 310 millimeters and a width of 32 millimeters (see Figure 2.14). Upon investigating the maximum tow-angle mismatch between zones in VS panels, the critical angle was found to be 13° . The specimens had straight fibers, with the reasoning that in this small specimen size, the orientation variance is negligible. In the middle of the specimen, the triangular gaps or overlaps were placed between 51° and 39° zones, backed up by quasi-isotropic (QI) plies on each side of the laminate. The zone orientation difference is the derived critical/maximum angle difference. In one batch of specimens, the defects were placed on top of each other, while a third batch featured staggering of the gaps. The testing featured microscopic investigation and uniaxial tensile test with Digital Image Correlation (DIC). The DIC images showed good insight into the main tendencies of the damage mechanics and showed the anticipated high concentration of strains in the defect vicinity. Strength reduction was 10.7% and 20.1% for overlaps and gaps respectively, though staggering reduced this effect to 8.6%. Delamination was observed in most cases, fiber pullout was also common. Interlaminar damage always occurred in the same pattern, which was explained to be the result of the layup configuration. Although the work presents an outstanding insight into the problem, the specimens' representative nature to fiber-steered laminates was somewhat limited since gaps were placed to the edge of the coupons. DIC data also shows the large concentration of loads at the edges, rather than the inner points. Moreover, excessive delamination was proven by the edge photographs. This possibly led to an influence on the results, as in reality, these gaps are usually not facing any free edges on the laminate level.

Lan et al. [65] studied the influence of a caul plate on the mechanical performance of laminates with defects through experimental work. Caul plates are used to squeeze the laminate opposite to the tooling side. Instead of a vacuum bag, which exerts more local forces and worse surface roughness, a caul plate presses the laminate to have a uniform thickness over the whole product. One batch of specimens had 5 transversal defects stacked on top of each other, while the other batch had defects in only one ply. The defect types were the same for one specimen, including gaps with different sizes, and one overlap. Notable, the authors admit the five defects stacked together are highly unlikely in real life. As one anticipates, the gaps stacked onto each other result in a much thinner local cross-section, mainly consisting of the adjacent 0° plies and some resin pockets. In the case of one defect, the thickness reduction is less pronounced. Upon tensile loading of the multi-defect specimens, thanks to the mainly zero local layups, the apparent strength and stiffness increase in the defect area, but overall, the total specimen load-bearing capability is significantly reduced (by around 30% in most cases). This phenomenon is greatly alleviated by the use of a caul plate, thanks to the enforced global uniform thickness, and no fiber waviness. For one-layer defects, the deviations from the pristine condition specimen are negligible. The specimens were pretty small coupon types with larger defects, and cross-ply layups, which might not represent the fiber-steered structures well. A similar study was performed by the same

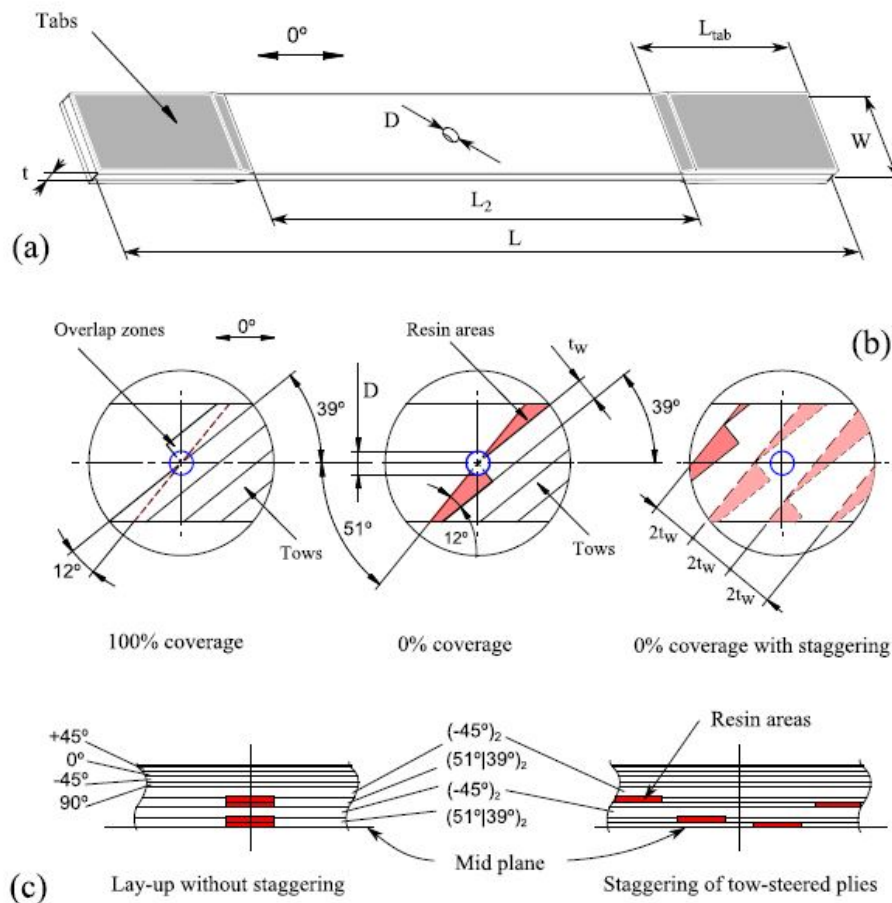


Figure 2.14: Specimen of Falcó et al. [64], with defect and layup visualized

group one year later [66], which presents more nice, realistic (one-layer defects in multidirectional laminates) cross-sectional images. Those images represent more common views of the problem and are represented on Figure 2.15.

The mentioned follow-up [66] of the authors includes in-plane shear loading (tensile loading on 45° rotated laminates), and compression loading (on cross-ply specimens). Two defects were stacked upon each other in the middle of the layups, reasoned to have a more articulated effect. Noteworthy, for the $\pm 45^\circ$ laminates, is the mentioned stacking of the defects results in a cross-shape, as opposed to the double transversal gaps with rectangular shapes. The occurrence of gaps in this configuration can be observed in real fiber steered laminates. For the mentioned laminates, extensive delamination was observed for all cases. Local stiffness reduction was 5-10%, while for strength the magnitude was 15% without the caul plate. In the case of the compression test, the defects were placed on both sides of the laminate, and in all four plies respectively. This is again, a massive difference from real-life laminates. The exaggerated nature is addressed by the authors, claiming that extreme cases result in more pronounced effects. In the middle of the specimens, 0° plies were placed (27% of the total number of plies), which could govern the whole response, based on the large modulus and strength difference. For overlaps, local modulus and strength were reduced significantly (for strength, it was 55%). Small gaps performed the same way as the reference specimen, thanks to the healing through curing - under pressure, these gaps are eliminated even without the use of a caul plate. Larger gaps induced a 12% drop in local strength values. Overall, shear tests presented a representative, smaller impact on performance, while compression test results are rather questionable. If thickness increases with doubling the local number of 90° plies resulting in half of the apparent strength, the response might be governed by the inner 0° plies after all. Caul plates damped the effects for both compression and shear tests, an effect also observed in the authors' previous work for tensile cases. To further discuss the work, local stresses are heavily impacted by thickness variations, and they do not give a

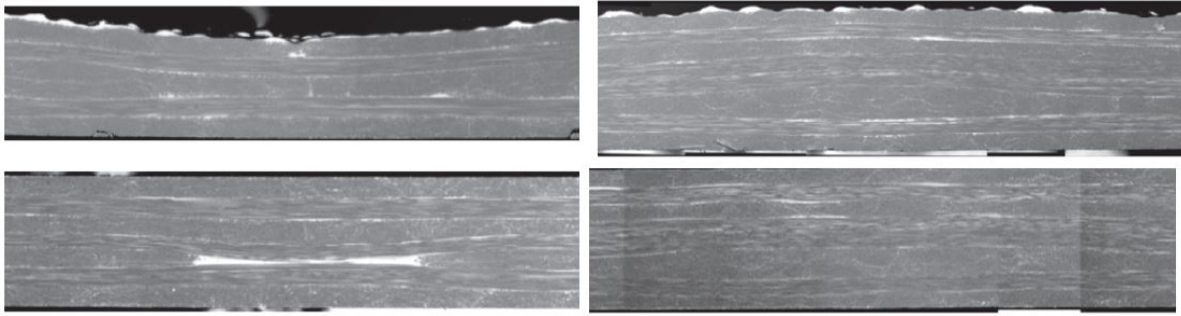


Figure 2.15: Usual cross-section of gaps (left) and overlaps (right) without (top) and with (bottom) caul plates [66]

clear conclusion about the whole system. In other words, the total specimen load-bearing capability, included in the previous tensile work, conveys more information for structural-level application than the mentioned local stresses.

Heinecke et al. [67] took a similar approach to Croft et al. [62], namely, with the use of coupon specimens containing transversal gaps or longitudinal gaps. One major difference is Heinecke et al. used numerical modeling instead of measurements. The other difference is in connection with the gaps, in detail, they used small longitudinal line defects in combination with small transversal gaps, resulting in a grid-like pattern. This type of specimen was simulated next to simple transversal wide-gap ones. Their "virtual test" simulation features a progressive damage model and a cohesive zone approach to account for both ply and interply failure. Gaps are divided into two groups, a long wide gap (larger than 10% of a tow width) and a long narrow gap (smaller gaps than 10% tow width). A debatable aspect in this instance is the usage of resin-filled gaps as a rectangular cross-section. In real tow gaps, the plies are squeezed under several bars of pressure, pressing the plies adjacent to the gaps together. Such a real gap is represented on Figure 2.15 (top left). If a caul plate is used, the approach could be seen as a good approximation (Figure 2.15 bottom left). However, in AFP parts, using a second tool to sandwich the laminate under curing is rare. The smaller gaps (less than 1 mm) in the case of the grid pattern also could be argued to be nonexistent in laminates after the curing process. The material damage model and cohesive zone model used is a similar approach to Blom et al. [63]. The long narrow gaps introduced larger knockdown (10–20%), than the long wide gaps (10%), however, the authors mention their uncertainty of the former outcome inherited by questionable input values (such as the interface stiffness for cohesive zones). Overlaps were also reported to introduce a 20% knockdown. Altogether, the weaker points of the article are the gap modeling, lack of out-of-plane ply waviness, and gap locations.

The experimental work of Falcó et al. [64] was discussed to be a great insight into the triangular gap problem. Their subsequent work [68] created a meso-scale, high-fidelity FEM simulation, which was validated by their previous experimental work. Their X-ray computer tomography (XCT) scans exceptionally present the triangular gaps with resin-rich pockets (wedges) and fiber waviness, in real form (Figure 2.16). Their model does not account for out-of-plane waviness nor tow thickness variations, which eventually proved to be acceptable assumptions based on the outcomes. The finite element model featured a continuum damage model for the plies, and a cohesive zone model to account for delamination between layers. The triangular gaps were treated as "resin wedges", homogeneous, isotropic solid material with plasticity and damage model. The magnitude of complexity is reflected by the five-hour computing time, on a cutting-edge workstation.

The results are impressive, to say the least. The un-notched simulation was observed to deviate 8% from the experimental baseline value and is well within the experimental scatter. The same applies to the more important case of specimen with gap configuration, where 6% was the deviation. For open-hole specimens, the respective values were 2.8% and 7.2%. Moreover, the tool captured minor tendencies, like matrix cracks and their locations, even the delamination from the mentioned damage. Just as with the experiments, the failure was initiated at free edges, hypothesized by the author of the thesis to be an influence of the specimen design to a certain degree. The final failure for the whole cross-section was observed to happen at the defect boundary. In the simulation case, the strength knockdown was in the order of 20% for un-notched specimens, agreeing with the experimental outcome. Since the out-of-plane waviness was neglected, the resin-filled gap area was 60% larger, however, the accuracy

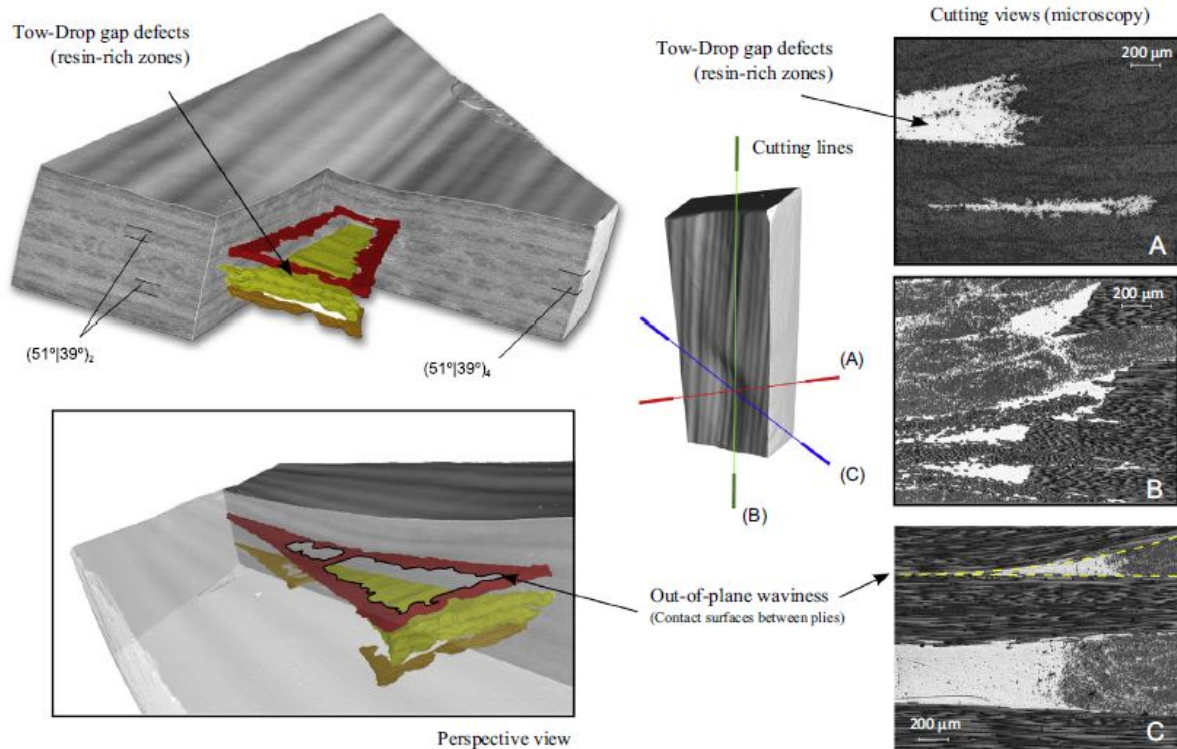


Figure 2.16: XCT imaging of triangular gaps [68]

suggests this approach is acceptable, especially considering the efforts spared in modeling. The authors also reflect on the mentioned argument on specimen design, quote [68]: *“the physical/virtual coupon testing approach show limitations in the analysis of the influence of the tow-drops on laminate response, despite the fact that the coupons are representative of a sub-domain of a large variable-stiffness plate. This is because the specimens free edges also influence the damage mechanisms, mainly delamination, and the influence of the defects is not isolated completely. Hence, future analyses on VSP should take into account the occurrence of delamination without the influence of outside conditions.”* (p.70.).

Lucas et al. [69] took a different approach when they developed a novel method to determine the strength and stiffness of VS panels based on a density functional. A base nonlinear FEA was enriched to incorporate a density functional to account for manufacturing defects, all based on the local densities being a mixture/function of tows and tow gaps. Their work needs more validation, preferably through tests to draw any major consequence about the accuracy. This is noted by the authors too.

Woigk et al. [70] carried out extensive experimental work for symmetric, QI layups with embedded defects. Load cases for small coupon specimens were tension and compression. Defect sizes were 2 mm wide, meaning the outcomes are more suitable to characterize misalignment during AFP manufacturing than the gaps associated with fiber steering laminates. Every layer was doubled/blocked together, to have a more pronounced effect, as done by others. Defects were placed in adjacent layers (through 3 orientations, altogether 6 nominal plies), though the QI layup oriented these defects in a cross or star shape. Baseline (pristine) specimens showed the lowest tensile modulus, attributed to manufacturing mistakes. Gaps had the highest modulus, which is not straightforward either. The largest strength knockdown was observed for “gaps and overlaps” specimens, namely 7.4%. Overlaps were reported to be 3% stronger, while simple gaps and staggered gaps had negligible reductions. Free edge delaminations were noted for all specimens, further reinforcing the hypothesized tendency of small coupon tests influencing failure mode. For compressive specimens, the baseline batch exhibited the lowest average strength, although displayed the highest compressive modulus also. Overlaps were once again proven to be advantageous in compression, however, all defects proved to be somewhat better than “perfect” specimens. Therefore, drawing any conclusions is limited between defect types. “Gaps and overlaps” had large variance, and had significantly lower values than any other batches. Final failures were exclusively fiber breakages in the 0° plies.

Guin et al. [71], based on their experience, found a 0.05" (1.27 mm) gap to be a conservative upper value to represent tow to tow gaps in AFP laminates. Their work, as the previously discussed paper, investigates periodically occurring gaps in the laminates, which for example, could come from incorrect manufacturing setup. This gap size was reasoned to be the smallest gap that could be noticed by visual inspection after lamination. The measurements featured usual tension, compression, and open-hole compression, the former two were done according to the respective ASTM standards, and the latter one was augmented to the standard un-notched ASTM compression test. Thus, the specimens were standard coupon specimens, again with QI specimens. In tension tests, compared to baseline values, gaps in 90° plies resulted in a roughly 4% increase in strength, while gaps in all plies showed a severe 23% loss. The compression test showed a similar tendency, but the 90° ply gap configuration this time did not alter from the pristine condition, though the ones with gaps in all plies were weaker by 14%. In all testing cases, stiffness values were affected less than strength values. The effects of gaps were concluded to be inherited from the occurring fiber waviness at gap locations. The authors stated this amount of gaps is unlikely to happen in an ordered fashion, rather these gaps should be incidental mistakes in manufacturing. Therefore, in real applications, where the machine is set to correct values, these occasional defects do not affect mechanical performance.

Del Rossi's Master's thesis [72] focuses on the so-called "side-to-side gaps/overlaps". This type of defect occurs if one tow is locally misaligned, similar to a "bus stop" shape. The defect leaves a gap on one side, and an overlap on the opposite side of the placed tow. The author expresses the inaccuracies of specimens in existing publications and proceeds to manufacture specimens with better representation. The work features a discussion on free edge effects, and considering it for specimen design - defect edges are a minimum of 6.4 mm away from free edges. The specimens feature a QI layup, and it is a coupon-like geometry, though wider than usual. It is interesting to note that, the specimens feature a woven fabric at laminate surfaces, and defects are placed in several configurations for different specimen types. The offset of a defect (therefore a gap and overlap width) is 1.27 or 2.54 mm. Tensile test results show no significant effect, if defects are aligned with the load, otherwise, a knockdown between 0 and 5% is observed on most specimens. Usual observations were excessive delamination between the innermost plies. A FEM model was created with a progressive damage model and geometric simplification, which could not capture tendencies accurately, relative differences are around 5% for most cases. This would be a good accuracy in most cases, but since the testing showed small knockdowns, the simulated knockdown could be twice the experimental one. The author also mentions a refinement could be in order, to have a correlation between tendencies. From the same university, Cadran's Master's thesis [73] features almost the same setup, but also has compression tests. Here, the knockdowns go between 15-30%, which is significantly more than in the tensile case. However, these were observed for specimens with numerous defects stacked upon each other.

Zenker et al. [74] did testing on carbon fiber composite, with thermoplastic matrix. The defect sizes were 7.35 mm and 2.5 mm for gaps, and 7.35 mm and 1 mm for overlaps, which values were based on aerospace requirements. The specimens had a 16-ply QI layup, where defects were introduced in two plies, in several configurations. The publication follows the trend, it had a standard, narrow coupon specimen, for both tensile and compression tests. The experimental work compared variothermal pressing, autoclave, and isothermal stamping curing processes, which happened after an AFP lamination. Here, only the autoclave results will be discussed, for the sake of uniformity with the previous articles. Only long gaps were observed in the 90° layers and showed 16% and 25% strength reduction for distributed and agglomerated defects respectively. The negative effect is more pronounced in compression loading, with values reaching 33% and 23%. DIC images indicated a strain concentration in the vicinity of the defects, as anticipated.

The work of Nguyen et al. [75] investigated the problem from the experimental side, with a similar setup. Gaps were introduced in 0° and 90° plies in a QI stack-up, in different sizes from 0.8 mm (1/32") to 12.7 mm (1/2"). Therefore, this configuration also rather represents AFP manufacturing inaccuracies, rather than typical gaps from fiber-steered designs. Again, overlaps, gaps, and combinations were tested for tension and compression. The stiffness and strength reductions were found to correlate with gap sizes, as increasing the defect resulted in a larger reduction of mechanical performance. 0° gaps were found to be the most severe case, as the load-bearing layer amount is smaller than in pristine condition. Smaller gaps showed strength reductions between 0-20%, while extreme cases exhibited a 55% knockdown. For compression, the usual values were rather in the 30-40% range. As observed by others, staggering defects were proven to be effective. Generally, for overlaps, an increase in strength

due to additional material was noted.

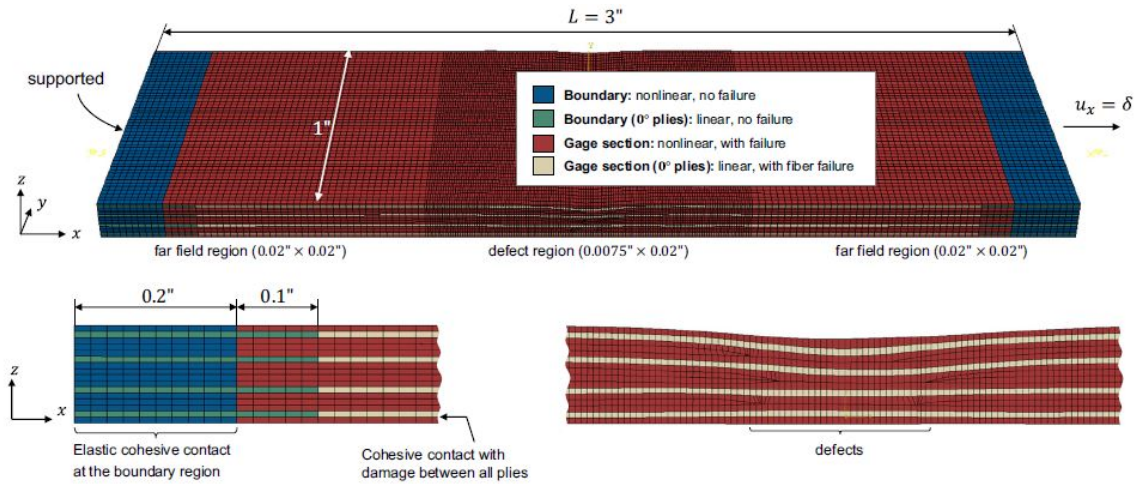


Figure 2.17: High fidelity model to simulate tow gaps by Nguyen et al. [76]

A follow-up on this work by the authors [76] focused on developing a high-fidelity FEM model and comparing it to the experimental data (see Figure 2.17). The material model was based on a multiscale continuum damage and failure model (MCDM). The model is capable of capturing pre-peak nonlinearity, failure initiation (through failure criteria), and post-peak degradation response. The implemented failure criteria was a simple max stress, with the 3 principal directions in consideration. After failure initiation, the crack band method (CBM) gradually degrades the stiffness properties of the anisotropic element. Delamination was covered with cohesive contacts between plies. To accurately model gap and overlap areas, microscopic cross-section images were processed manually, and through curve fit interpolation, realistic layers were created in FEM software. Using 72 CPUs, the simulations were reported to run for 2.5 hours, with 200 000 elements. The virtual tensile tests showed good agreement with the experimental results. Several macroscopic failure processes, like splitting and delaminations were captured. The loading curves showed correct initial stiffness, though, before the ultimate loads, slight deviations were observed. In more detail, the experimental data had a mostly linear nature, while the FEM results displayed a softening tendency at the latter stages of the test. For $\frac{1}{2}$ " gap size, the model overpredicted the final load, while for $\frac{1}{4}$ " defect size, the tool calculated a slightly lower strength. The error values for the steps from $\frac{1}{16}$ " to $\frac{1}{2}$ " for gap specimens were 0.2%, -3.4%, -5.5%, and 13%. The same for overlap configuration was 3.1%, -11%, 0%, and -2.1%. Tendencies with defect sizes were quite similar, considering the significant scatter for experimental data.

Böckl et al. [77] investigated tensile, flexural, and shear strength of AFP laminates containing gaps and overlaps. A novelty in their work lies in the connection between strength results and measured laminate quality by optical means. Again, standard QI (or $\pm 45^\circ$ for shear) specimens were used in testing. which as discussed, is somewhat unrealistic for real-life applications. In order to capture more pronounced effects, the plies are doubled in all directions, essentially forming layers with double thickness. The reasoning for this is, quote: *"This stacking sequence was chosen in order to achieve delamination dominated failure since the ply thickness has a substantial influence on the failure mode of the material."* (Böckl et al. [77], p.5). Then, again, a step from the real-life scenario ends up in the characterization of a quite extreme case. The mentioned aspects are further worsened when the gaps are introduced by either removing or adding a complete tape, moreover, these are aggregated in some instances in four neighboring plies. This raises questions about the practicality of outcomes on the industrial side. This was noted by the authors as well. A novel 3D scanner unit processed the laminate topography through the AFP manufacturing process. Overall, the defects that affect one or two plies were said to not lead to significant differences compared to the idealistic case, otherwise, aggregated gaps introduced 12% and 20% strength decrease in tension. In bending, these values changed to 11% and 29%, while overlaps enhanced the performance. The same tendency, although on a smaller case, was experienced in shear testing, where gaps presented a 5% reduction, contrary to the increase of 6% with overlaps. Defect volume, obtained from the laminate scanning showed correlation with strength reductions.

To end the scientific work in the field of gap strength characterization, the recent (2023) work of

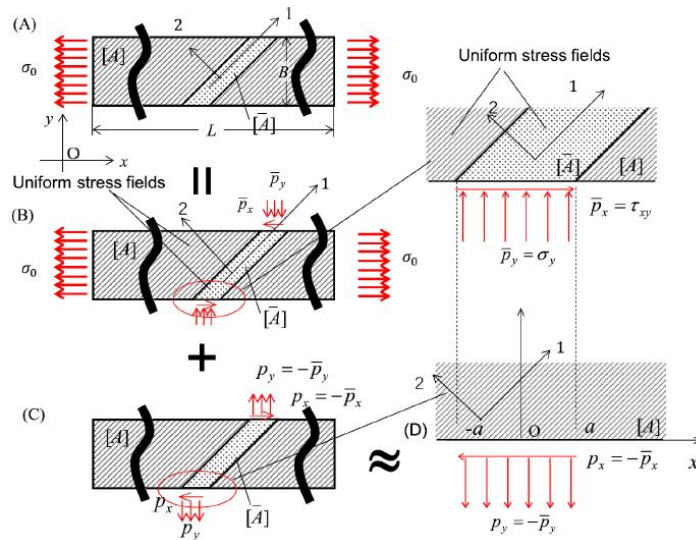


Figure 2.18: Representation of distributed loads acting on free edge to create homogeneous stress field in gap area[78]

Suemasu et al. [78] is considered. His work joins the line of coupon specimen publications consisting of QI laminates. This work differs in that the gap locations are introduced in the $+45^\circ$ and -45° plies. The gaps had different configurations for specimens, depending on where the defects lay in the specimen plane. In case a specimen had defects that did not have an overlapping zone, or in other words, were further apart, mechanical performance was close to a pristine condition specimen. If the linear defects met at the free edge, or in the case where gaps were running parallel, the strength reduction was the largest, namely 16.6%. In other words, the interaction of defects is detected. The authors discuss the loading case and its relation with a gap under a homogeneous stress field. It is noted, under an application environment, gaps do not face free edges, and are under a complex stress state, assumed to be homogeneous along the area (see Figure 2.18). Following this thought, the authors derive the expression for a stress field for the gap's free edges, which satisfies the mentioned homogeneous field across the whole of the defect. Using a FEM simulation with solid elements, it has been proven that defects along free edges suffer under substantial stress peaks. This naturally starts failure sooner than enclosed defects in general. The simulated stress increments are plotted on a graph, presented on Figure 2.19 (left). The notation (right side of same figure) is as follows: a - half gap length, x - axial direction of the specimen, b - tapering of one layer in the out-of-plane direction, $\Delta\sigma_x$ stress increase, σ_0 applied far-field stress. The authors mention a conclusion regarding the specimen size, quote [78]: "...the effect of the size of the specimens must be determined carefully so that the defects are represented suitably in the measurement of properties."

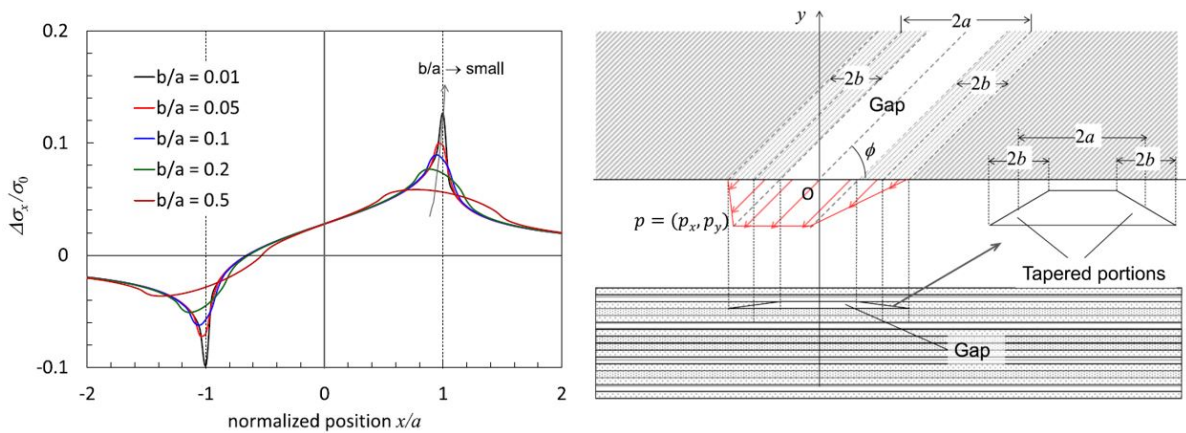


Figure 2.19: Normalized stress increase along normalized gap position, and notation system diagram [78]

2.5. Summary of Literature Study

The chapter introduced the two main fracture mechanics approaches suitable to model delaminations in composite laminates. These were the Strain Energy Release Approach and the Strength of Materials Approach. Both were discussed to be dependent on layer orientation mismatch, crack propagation direction, loading mode, and material parameters amongst others. Dependencies between variables are unclear as there is no agreement between scientific results. The case is worsened as measuring a pure mode value is virtually impossible. The last, and probably the largest hurdle in solving this problem is the frequent crack-jumping between interfaces, through plies. This means, in reality, the failure process could happen at a completely different spatial location with a different environment, compared to the initially predicted scenario. Thus, the remainder of the research excludes delamination concerns for strength characterization. The existing ply failure criterion, however, seems to be a well-established way suitable for analyzing fiber-steered laminates too. The chapter also presents the most common defects of the automated fiber placement manufacturing method. Since the Master's thesis is limited in time, the research is focused on the tow gap defects, as this seems to have a larger negative impact on laminate performance. This thought is confirmed by the state-of-the-art research done in the field of gap and overlap characterization, making up the last part of the literature study. The publications and the author of the thesis discussed a way to enhance the characterization of the mentioned defects. Based on these observations, the next chapters present an improved methodology to solve the main research problem.

Research questions

The following research questions are wished to be answered during the thesis work.

Main question: **Assuming that gaps are manufacturing features that drive the properties being characterized, how can the effects of gaps be generally characterized?**

Subquestions:

1. What are the requirements for a specimen to realistically represent fiber-steered structures?
2. What is an optimal design for an AFP specimen, based on the requirements discussed?
3. How can a specimen like this be modeled?
4. What are the observations in real-life tests? How does the model correlate with test data?

3

Specimen requirements

In the literature study chapter, some debatable aspects were discussed regarding the specimens used in the state-of-the-art research. To name a few, these were specimen size, gaps at free edges, and unrealistic defects. This section elaborates further on the requirements for a specimen that could offer enhanced characterization with respect to gaps in fiber-steered laminates. The main points of these requirements are:

- Sample size and layout
- Loading condition and stress state
- Specimen lay-up
- Manufacturing method
- Realistic defects
- Failure mode
- Test output

3.1. Sample size and layout

The *'testing pyramid'* (Figure 3.1) is a well-known concept amongst developers and researchers in the areas of structures and airworthiness [79]. It represents the levels of testing ordered according to complexity and gained structural information. The lowest level in is the coupon level. These kinds of simple specimens are commonly used in both academic research and industrial work and serve as the founding stone of material characterization. The research on fiber steering and/or AFP defects is still at an early stage. This should be the reason why we only find simple coupon specimens in the research topic - it always serves as a first and easy step. The main advantages of these tests are the ease of use, lower costs, higher number of samples, and good repeatability. It is mainly used at the macro level and for the measurement of material properties and material models.

The second level of the pyramid is the element level. On the element level, smaller components or assemblies are tested, like a bolted joint or a stringer in itself. Thus, after the material characterization step, element-specific features can be added as a matter of influence on the results. An example of this can be the effects of bolts or element manufacturing specific features, like composite draping in a part. Draping is the distortion process of composite fabric architecture over curves. E.g., the phonemon happens when a plain weave cloth, with an original 90° angle between fibers, distorts to sharper angles to take up a complex geometry. This example nicely presents the difference between the mentioned levels of testing - the draping phenomenon is element-specific, and simple rectangular coupons cannot predict the performance knockdown caused by the jump in complexity.

Probably the main questionable point about the state of the art is the usage of coupon-level specimens [62, 64–67, 70–74, 77, 78, 80]. Even some of the authors discussed themselves that an element level testing should be in order [68, 78]. The author of this thesis believes that gaps are not material, but structural features. One can see it as a joining method of the base material in some way. This means, there is a need to step forward from a small coupon specimen, as it restricts the scientific exploitation of

gap effects. This is the major conclusion from the literature study and the most important requirement out of all.

Above element testing, there are detail and sub-component level testings. An example of these tests could be a stiffened panel buckling test. These samples consist of several individual parts that are joined representative of the final structure, and the testing usually carries out a larger number of information, and even more useful ones in the context of the final structure. Component and full structure testing lies at the top of the testing pyramid. These tests are usually certification tests, which are presented to aviation authorities like the FAA (Federal Aviation Administration, the governing authority of the U.S.) or EASA (European Union Aviation Safety Agency, the European counterpart). The costs of these tests are immense, and usually, all the lower-level tests are needed to efficiently and successfully design a feasible structure passing the top-tier test.

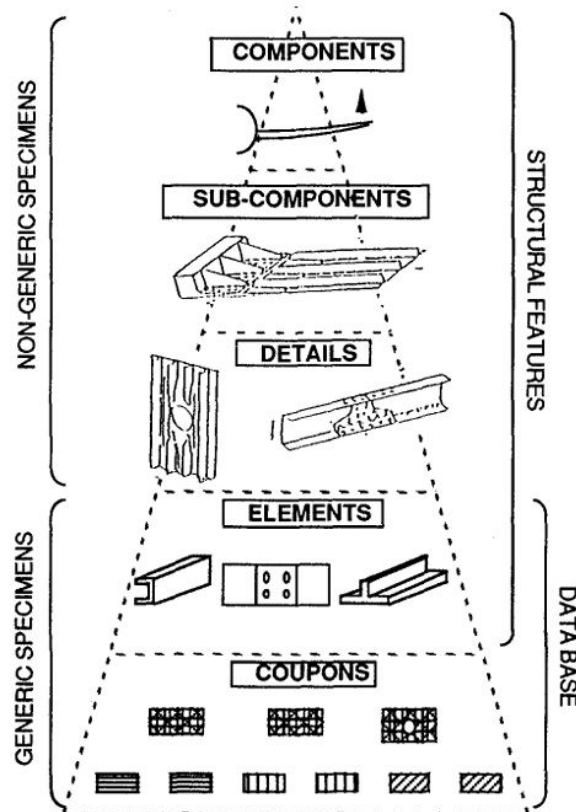


Figure 3.1: Testing pyramid - ordered representation of structural tests [79]

As Figure 3.1 shows, the lower one or two levels are usually generic specimens, while all higher-level tests, which contain structural features, are augmented to the ultimate design objective. Next to this observation, we can also state the complexity and value of output increases towards the top of the pyramid. Complexity here is a general term with several aspects. The first aspect discussed here shall be size. The coupon size problem has already been discussed. On the other end of the scale, with increasing size, the complexity in general increases. Larger structures require special or stronger testing equipment. The Delft Aerospace Structures and Materials Laboratory (DASML) has universal testing machines with maximum force loads of 10, 20, 60, 250, and 3500 kN. While the former three have large limitations in terms of element specimen size - as specimen size is in direct correlation with ultimate load - the latter machine is exponentially more expensive and time-consuming to test on. The 250 kN was chosen to be a limit for this research, but it must be noted that subsequent research in the area could exploit some higher-quality feedback on structural performance if larger machines were used. The 250 kN limit also tends to be a guideline to stay on element-level testing, and not go further into details or sub-components level.

The reactions of materials to gaps should be different, just as strength values also differ between

one material to the other. This should also be one reason for different knockdowns experienced in literature. Thus, knockdowns should be characterized for every material in use preferably. This way, just using one figure from literature could lead either to over-conservatism or to a sacrifice of safety in order to cut down costs. A complete characterization of a material has a significant cost, which could be reduced through smaller specimens. Therefore, size is also important in the economics of the research.

Closely connected to this is the manufacturing and handling of the element. Larger specimens impose troubles with manufacturing, as in general, preprocessing a large specimen could require larger machines, such as a larger autoclave or a large gantry CNC machine for trimming. Testing methods, similarly, might inherit problems, take a load introduction as an example. Introducing loads to a coupon specimen is already somewhat challenging since failure at the clamping region is a known and common phenomenon. Through the installation procedure, just one small hit is enough for a panel to initiate a delamination. Using this thought, a more complex part is more vulnerable to external effects.

Sample layout is also a topic to cover. This concept is more connected to the real-life usage of fiber steering for structures. Suemasu et al. [78] already raised awareness towards the influence of free edges in gap characterization. Free edges for composite laminates bear the so-called 'edge effect', inherited from the anisotropic nature. For a short distance near edges, interlaminar stresses develop to significant magnitudes. This means, that at edges, failure (especially delamination) can be initiated even when far-field stresses are under failure limits. For smaller coupon specimens, this zone, though usually under the millimeter scale, is believed to be too large on a relative scale. The results are believed to be influenced over the acceptable limit, as Falcó et al. [68] summarized in their already discussed work (see chapter 2). Overall structures should also bear this type of phenomenon, however, the sheer size of structures could dampen the effects. Nevertheless, the inclusion or omission of the dampened edge effects on the element level is not entirely intuitive. This shall be put into context using tailored laminates already published.

3.1.1. Case study - business jet fuselage section

Samuel Jsselmuiden [81] elaborated on the optimization of variable stiffness composite structures in his PhD research. His work also featured a case study on a business jet window-belt section (Figure 3.2, left). Windows in aircraft represent a common cutout in fuselage sections, although there are larger (passenger exits or service doors) and smaller (general holes for part attachments) instances as well. All discontinuities force structural problems onto the engineers, as these act as weak points and must be dealt with with more care. The optimization was carried out on a representative specimen geometry. The specimen's overall dimensions were developed by Dassault Aviation, which included a central hole representing the window, and a waisted shape (Figure 3.2, right). This waist shape was tailored in such a way as to mimic the effect of neighboring windows, thus obtaining a representative stress field. The panel should be loaded in tension, as the fuselages experience tensile membrane stresses due to pressurization. The specimen geometry is a great representation of the sub-component level specimens, as it has a simplification from the overall structure, but is designed to have enhanced representation.

Through the optimization for strength and some other constraints (like manufacturability), the presented (Figure 3.2, right) fiber path was obtained. Compared to a QI layup, the load-bearing capability was increased by more than 50%. The algorithm optimized a softer zone above and below the cutout while increasing stiffness in the ligaments next to it. This aligns with the 'engineering common sense' of load paths. The stiffer bands not only featured more axial fibers but also larger thicknesses/more layers. Thus, we can say agglomeration of tows is more likely to happen away from cutouts. Gaps develop where adjacent tows deviate from each other. This could be at sharper orientation changes. The idea of gaps occurring more where there is a large variation in orientation - more gaps might be observed in the soft zone, judging by the results. These two ideas are contradictory, where to inspect gaps. Wherever they might be, a no-free edge specimen could characterize both stiff and soft zones, solving the problem. Still, another question arises - is it more important to characterize at cutouts or in the (edge-less) structure area? For the whole structure, researching gap effects without free edges might be of slightly higher importance, as out of the two, that zone conveys the loads. Hence, it might be more likely to initiate damage, but definitely impacts load carrying overall in a more critical way. This is the reason why it is chosen as an emphasized requirement. Gaps at free edges are not an unjustified area to research, if not encouraged, but at element-level testing or higher order, and recommended as

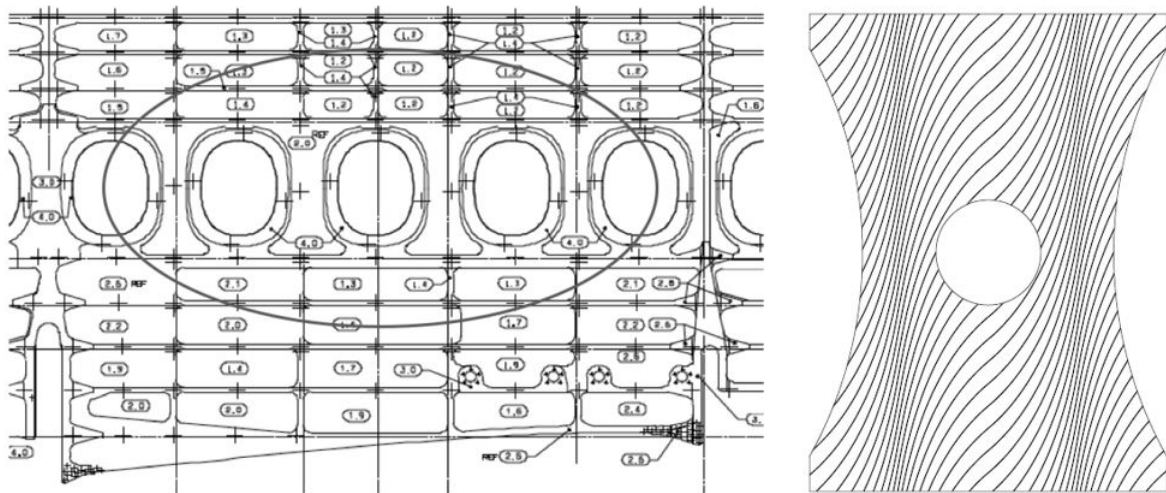


Figure 3.2: Drawing of a Jet fuselage window section (left, from Dassault Aviation) and representative specimen with optimized fiber paths visualized [81]

a further research topic. To summarize, extrapolating knockdowns for both free edge and edge-less areas with the small coupon specimens should fall short of satisfactory accuracy. On element-level testing, edge-less specimens are thought to be of higher importance and, therefore chosen for the thesis research. Nevertheless, subsequent work is encouraged to open up for edge effect, mimicking cutout areas.

3.2. Loading condition and stress state

Loading the tows and tow gaps is also an important aspect. To go deeper into this, the basics of Classical/Composite Laminate Theory (CLT) must be mentioned briefly (following [2]). For referencing the calculations, we distinguish local and global coordinate systems, noted with 1, 2, 3 and with x, y, z respectively. The global coordinate system can be arbitrarily chosen, the local coordinate system, however, varies for every ply. The local system for a ply aligns axis '1' with the fiber direction and axis '2' aligns with the transverse direction. Note, that axes 'z' and '3' coincide, as both mark the 'thickness' or 'out-of-plane' direction. The angle mismatch between axis 'x' and '1' is the ply orientation angle, denoted by θ . The coordinate system convention is represented on Figure 3.3 (left).

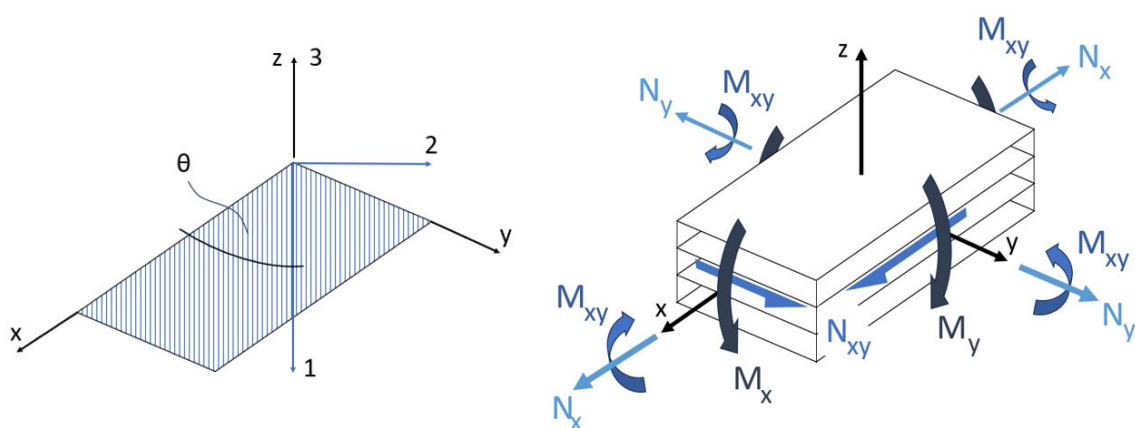


Figure 3.3: Composite Laminate theory coordinate systems convention (left), and CLT loads acting on an arbitrary plate (right)

A composite ply and a laminate built up by these plies are both isotropic, as discussed previously, meaning that in every direction, the responses are different. These responses are characterized by the respective engineering constants, like E_i modulus, G_i shear modulus, or ν_{ij} Poisson ratio. The

responses can be described by stresses or strains, these are:

$$\begin{bmatrix} \sigma_x, \sigma_y, \sigma_z, \tau_{xy}, \tau_{xz}, \tau_{yz} \\ \epsilon_x, \epsilon_y, \epsilon_z, \gamma_{xy}, \gamma_{xz}, \gamma_{yz} \end{bmatrix}$$

Amongst composite laminates, thin shells are dominant, which means usually the thickness of the laminates is much smaller than the other two dimensions. This implies that the out-of-plane stresses are neglectable compared to the in-plane stresses:

$$\sigma_z \approx \tau_{xz} \approx \tau_{yz} \approx 0$$

Leaving the dominant stresses and strains to be the respective three:

$$\begin{bmatrix} \sigma_x, \sigma_y, \tau_{xy} \\ \epsilon_x, \epsilon_y, \gamma_{xy} \end{bmatrix}$$

The expressions are defined in global coordinates, but the same values and neglections are applicable to the local systems, for each ply respectively. Therefore, one ply in an arbitrarily loaded laminate suffers under the following stresses:

$$[\sigma_1, \sigma_2, \tau_{12}]$$

These stresses not only depend on the loading condition but also on the ply orientation and ply position in the laminate amongst other parameters. A question may arise about what stress state a gap 'sees', or what stress should it be described with in characterization. The answer is up to interpretation. In this research, the gap state is referred to as the stress state of the adjacent tows, or in other words, the stress state of defining tows. This can also be put into perspective through the relevant work of Fayazbakhsh et al. [82], namely the 'defect layer method'. Their work is based on modified stiffness and thickness properties of a FEM element, which modification is applied through a knockdown. The knockdown is based on the gap area within one element area. This way, the mesh does not need to be refined to capture a complete gap or overlap, it could remain relatively coarse. The element knockdown process proved to be accurate in a subsequent work (Ghayour et al. [83]) when it was compared to the experimental work of Nguyen et al. [75]. Consequently, the layer nature of the gaps is also an aspect to look at the problem.

A gap/tow, therefore, has 3 main 'variables' for an arbitrary stress state (based on the commonly used CLT). As one can imagine, these three variables exponentially increase the required amount of testing, as most of the combinations of loads should be inspected for gap response. This amount of testing and design work requires an extensive amount of resources, which forced the scope of the present thesis to pre-define one fixed direction. Gaps running parallel to the load mean the gaps are in a fiber-loaded state. In this state, gaps reduce the amount of fiber participating in the structure, leaving a large impact, when normalized to a full layer (see Nguyen et al. [75]). However, when one normalizes to amount of material added - which might be a 'more aerospace' conception - it is hypothesized to have less impact, than in off-axis cases. Some might even go with no impact at all, considering two cases - one nominal ply with gaps and one no-gap layer with the same amount of fibers as the first case, just with a smaller thickness. A fiber-dominated failure must fracture the same amount of fibers in both cases, implying sensitivity concerning weight normalization, and insensitivity concerning cross-section normalization. Thus, the axial knockdown is hypothesized to be easily predictable using the thought of reduced amount of fibers or density.

Contrarily to the mentioned, for all other load cases, the matrix plays a significant role, even though it is not the major load-bearing element in the system. As seen in the Literature Study chapter (chapter 2), translation or triangular gaps often become resin-rich pockets after the curing step of the manufacturing process. These gaps, to put it differently, are discontinuities in reinforcing fibers, which impose the great task of transferring high loads onto the weaker matrix. As a conclusion, it is hypothesized, that the gap effect in laminates is matrix-dominated. As a result of the discussion, gap knockdowns should be dependent on both added fiber weight and also cross-section or distribution of fibers. All in all, an axial case should only contain a significant σ_1 component. The problem with a 90° gap is analogous, only having a significant σ_2 state. Considering all of the mentioned thoughts, arbitrarily a 45° gap

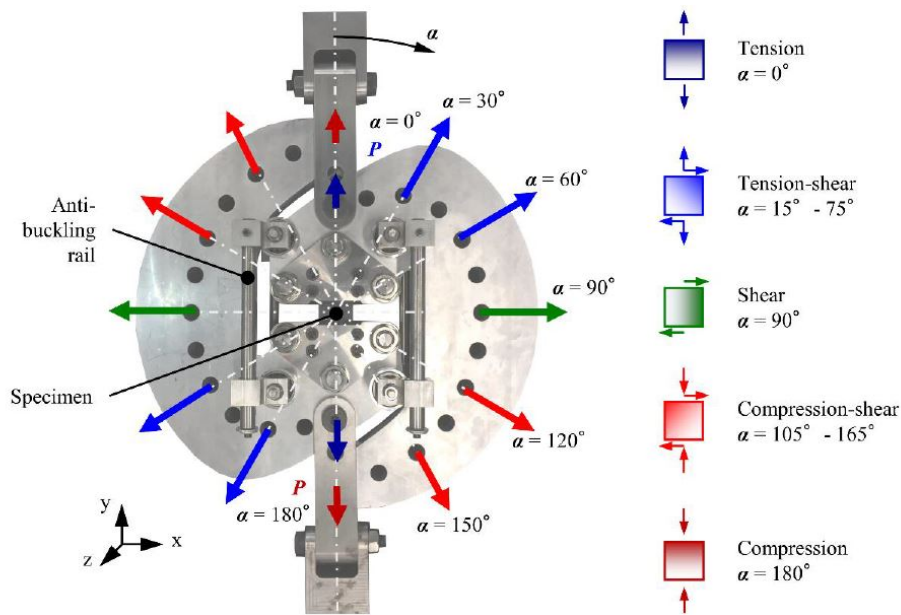


Figure 3.4: Modified Arcan fixture developed by Laux [84]

angle is chosen as a first step in a future full-sweep study. This state is well-representative of matrix sub-component participation, as it has significant σ_1 , σ_2 and τ_{12} as well.

To give an outline to further research, multidirectional loading can be achieved through a so-called Arcan fixture. Figure 3.4 presents a modified version of it, designed by Laux [84]. By changing the loading holes of the fixture, a universal tensile tester machine could introduce pure tension, compression, tension-shear, or compression-shear load state. The presented figure explains the different load cases with their corresponding loading holes. With this device, a deeper understanding could be achieved in the topic.

Next to the stress state, its distribution is also a key aspect. Homogeneous loading is strongly desired across the specimen, giving all parts equal environments and states. However, this is only restricted to the gauge section. For example, ideally, the grip section should be less loaded, see the subsequent chapter on failure mode. If the area of characterization suffers under inhomogeneous loading, the characterization could lead to biased results and misleading consequences.

An arbitrary laminate could be loaded in multiple ways, as represented on Figure 3.3 (right). For the thesis research, in our case, a simple tensile test will be presented. This load case is representative of fuselage skins, or lower skins of aircraft wings to name a few. The reason behind it is simplicity, as in compression, buckling is predominant for thin composite shells. The well-known structural phenomenon complicates matters further, as post-buckling failure is still a developing area of research.

3.3. Specimen Lay-up

The specimen layup was observed to be a detail of conception - different researchers used different layups, which does not help in finding a clear tendency. Hence, a discussion of representative laminate is in order. The variables are total thickness and ply orientations, which shall be discussed in the subsequent paragraphs.

Total thickness can be approached by two sides - one is the representative structural number and the other is the handling minimum for the specimen. Structurally, a fuselage section was mentioned, as the tensile loading can be representative of that. Following this concept, a representative thickness of a fuselage should be sampled. Manufacturers try to hide the parameters of their products to counter industrial espionage. The (non-scientific) article of Werfelman [85] on a Boeing 757 rapid decompression accident contains a value for its aluminium skin thickness, namely 0.99 millimeters. This type of aircraft can be a good baseline, as with a passenger capacity of around 250, it sits in the mid-range of airliners. An important parameter is the mentioned workhorse of the aerospace industry - aluminium. For composites, an equivalent thickness is somewhat larger, as a laminate should contain several di-

rections so as not to be vulnerable to premature matrix failures in secondary loading. This reduces the overall advantage of large stiffness in the axial direction (usually around 135 GPa) compared to the isotropic counterpart (70 GPa). The consequence here is that the laminate should have at least 1-1.25 millimeters of overall thickness, in order to be representative of common structural laminates.

From the handling side, a sub 1 mm laminate also bears some difficulty. Those laminates are so thin, that during handling, the probability of pre-testing damage is thought to be significantly higher. On the other side of the scale, above 2 millimeters, the loads are linearly increasing. This limits a specimen width through the maximum capacity of the tensile testing machine to be used. Maximizing width should be a design objective, as the information gained is increased with specimen width (see. subsequent sections). A solid feedback on the thoughts comes from the ISO standard for the determination of tensile properties of unidirectional FRP composites (ISO 527-5:1997 [86]). The standard determines two types of specimens, one with 1 millimeters of thickness, and one with 2 millimeters.

Orientation-wise, quasi-isotropic layups were used on a larger scale in the state-of-the-art research. The author of the thesis discusses this to be un-representative of real-life fiber steering applications. A well-designed fiber steered/variable stiffness structure has all kinds of layups but a QI one. The workflow of a variable stiffness design starts with a numerical optimization, which outputs intricate spline trajectories for every layer. One such case is presented on Figure 3.5.

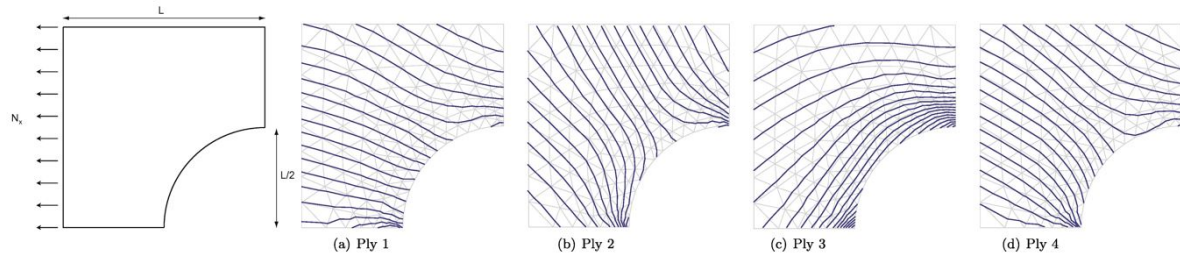


Figure 3.5: Original plate dimension and optimized trajectories for the layer from the work of Khani et al. [87]

The shown work of Khani et al. [87] conveyed a solution for a panel with a central hole under uniaxial tension. The total laminate consisted of 16 plies, assembled from 4 types of layer paths. As a whole, the laminate was governed to be balanced and symmetric over the domain. Judging by the output paths, we can state that an optimal design features pronounced anisotropy in all areas, a feature inherited from the complete exploitation of axial stiffnesses. To rephrase it, quasi-isotropic laminates oppose an optimal layup. Therefore, a representative variable stiffness specimen should feature strong anisotropy, which aligns with the previously discussed idea of investigating at primary load path (3.1).

Some additional thought shall be added to the overall layup. Figure 3.3 (right) has presented the CLT loads of an arbitrary laminate. The well-known ABD matrix connects these loads to the laminate response of membrane strains and curvatures (latter marked with κ).

$$\begin{bmatrix} N_x \\ N_y \\ N_{xy} \\ M_x \\ M_y \\ M_{xy} \end{bmatrix} = \begin{bmatrix} A_{11} & A_{12} & A_{16} & B_{11} & B_{12} & B_{16} \\ A_{12} & A_{22} & A_{26} & B_{12} & B_{22} & B_{26} \\ A_{16} & A_{26} & A_{66} & B_{16} & B_{26} & B_{66} \\ B_{11} & B_{12} & B_{16} & D_{11} & D_{12} & D_{16} \\ B_{12} & B_{22} & B_{26} & D_{12} & D_{22} & D_{26} \\ B_{16} & B_{26} & B_{66} & D_{16} & D_{26} & D_{66} \end{bmatrix} \begin{bmatrix} \varepsilon_x^0 \\ \varepsilon_y^0 \\ \varepsilon_{xy}^0 \\ \kappa_x \\ \kappa_y \\ \kappa_{xy} \end{bmatrix} \quad (3.1)$$

The load for the tests, N_x , has already been determined. The N_x in-plane load is connected to the deformations through elements of the A and B (sub-) matrices. The previous connects the in-plane loads and responses, while the latter matrix connects in-plane and out-of-plane parameters. Out-of-plane deformations are of no use for the characterizations, even contributing to uneven loading of the specimen. Symmetric laminates have all zero B matrices, therefore this kind of stack-up is desired. Furthermore, A_{16} (and A_{26}) term connects the axial loading to an in-plane shear response. This is also a coupling to be avoided, as it takes another step away from a homogeneous state. This is achievable with balanced laminates, meaning for every (θ) orientation angle, there is a ($-\theta$) ply in the laminate. Altogether, ideally, the specimen therefore should feature a symmetric and balanced laminate.

3.3.1. Failure mode hypothesis of variable stiffness laminates containing gaps

Here the main hypothesis of the present thesis is formulated, regarding the failure process of variable stiffness laminates containing gaps. The failure process of a QI laminate is used as a reference case, as it features several distinctly different orientations. The known damage onset and gradual failure of such laminates provide an insightful thought between orientations and failure events for any arbitrary laminate. The work of Sánchez-Heres provides a nice insight into the problem [88], and Figure 3.6 aids the understanding. A QI specimen's fracture surface might lead some to think that the damage is due to initial fiber breakages, followed by matrix failure. This faulty idea could come from the fact that matrix materials could take up significant strains through deformations, and global strains are uniform in the laminate. In reality, the poor matrix strength is the weaker chain, even though it is not the main load-bearing component of the system.

Upon a tensile loading, the 90° plies develop transverse cracks, which process gets initiated at higher loads for the 45° layers. The density of transverse failures increases and saturates during the damage process. The mentioned fractures propagate and start to form delaminations between adjacent layers. The final failure is fiber fracture but without the admirable support of other plies. Therefore, the last ply failure is at the 0° plies. The main load-bearing plies' failure is enhanced by the other off-axis ply failures.

Following this concept, the failure progress of variable stiffness laminates is speculated to be initiated by the off-axis plies, with respect to principal load direction. This follows the previously stated matrix-dominant nature of the gap strength knockdowns. The number of the off-axis plies in VSL is assumed to be less than in a QI case; however, it is thought to initiate analogous events - transverse cracks, saturation, coalescing of fractures into delamination, and then fiber failure. Merging this idea with the question of the effect of gaps yields the hypothesis that gaps negatively affect the off-axis tows, thus introducing a strength knockdown. Hence, the axial fiber dominant specimen should feature some off-axis tows with gaps, where failure is expected from the effects of the defects.

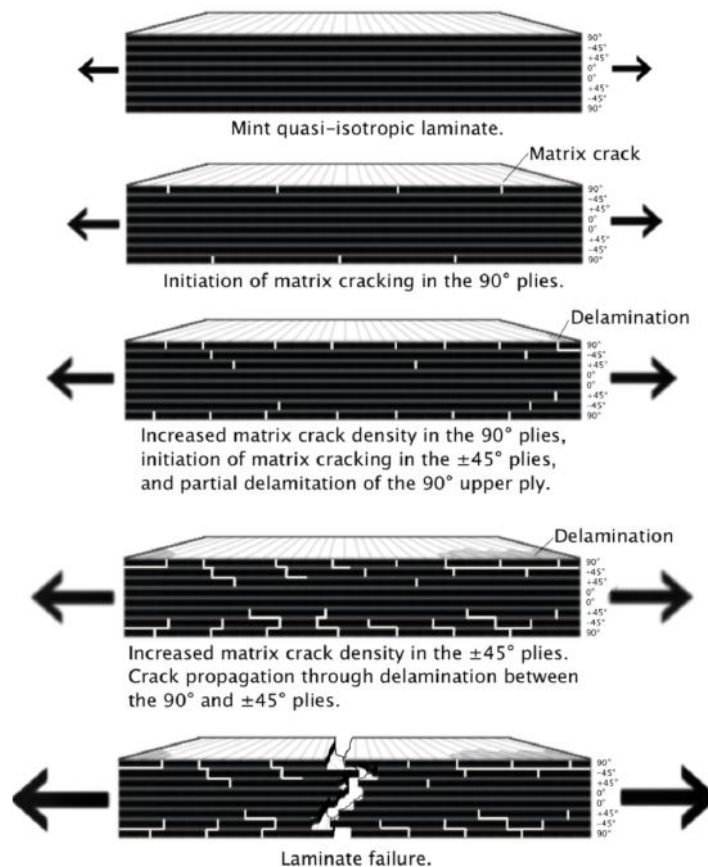


Figure 3.6: Progressive failure process of QI layup [88]

3.4. Manufacturing

Some of the state-of-the-art research featured specimens with a hand-lay-up method like the one of Suemasu et al. [78]. The solution mitigates the need for a costly AFP machine, however, bears some problems. The major one is the fact that tow positioning, and thus gap sizes and orientations are much more controlled and accurate using a robotic arm than using manual labor.

Between tows, there might be some smaller gaps from the positioning of the robot, in the sub 1 millimeter range. These gaps are resin-filled, matrix-dominated areas, and significantly larger than interfiber distances. These long and narrow slits could serve as a gateway to cracks between plies. This could be investigated for a subsequent research study.

The importance of orientation was already presented. Therefore, it can be concluded that the usage of actual AFP robots is desired for accuracy reasons. Since the matters to be characterized are, in real life, manufactured in the mentioned way, it only makes sense to also use the same exact method, with all of its features.

Exploitation of fiber steering has some limitations from the manufacturing side. The tows during lamination are forced to deform to a given radius. An originally straight tow is essentially bent into a radius. Using engineering sense, we can also feel that the inner side of a tow is under compression, and the outer side is under tension. The problem is visualized on Figure 3.7. An inherited limitation is the minimum feasible radius. Under small radii, tows can either develop wrinkles on the compressed side or can flip off starting from the tensioned side.

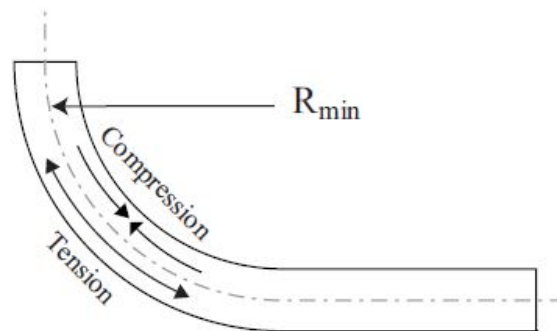


Figure 3.7: Tow placing with forced deformation for steering [81]

Residual stresses are inherent features of composite laminates [89]. During curing, the anisotropy and coefficients of thermal expansions (CTE) cause the phenomena. If not dealt with properly, the final parts can develop warping and other troubling features. In a macro state, the compression and tension of tows might influence performance, probably in the crack propagation direction of the interply media. This could be either compressive or tensile states, as a result, it can both help or mitigate delamination respectively. A specimen with fiber steering could incorporate this phenomenon. This could be an additional variable of influence, but at the same time, could be a pronounced feature in real-life applications. Usually, a minimum radius is the range of 0.4...1 meter for thermoset applications [90], as a consequence, steered fibers will have less deviation in element-level coupons when compared to straight fiber applications. This research will not focus on this macromechanical concept, but the steering of fibers is not excluded if significant advancements are offered by the concept.

3.5. Realistic defects

Strong comments were made on research works [65, 67, 70, 77] conglomerating several defects to have more pronounced effects. In a realistic case, two or more gaps are staggered to alleviate strength knockdowns and large thickness differences. This is especially true for gaps that run parallel. If two gaps are not aligned, a single point will feature a doubled amount of defects. However, with more nonparallel gaps, further agglomeration can be avoided through offsets. Although this being said, applications should vary in all kinds of defect configurations, choosing a representative one is not easy. To counter this, a different approach is used, following a 'best case scenario'. In this research, one, or two layers with gaps will be introduced, with no severe defect agglomeration. The latter is allowed if

needed for the symmetric and balanced layup configuration.

The output results, are considered to be conservative in raising awareness to the minimum amount of knockdowns or magnitude of effects. Conservative, as if even one layer of defects enforce issues, the outcomes strongly and surely emphasize the importance of the studied defects. With agglomerated defects, one cannot accurately judge the severity of problems in more usual cases. Another strong reason for the lower number of defects is to observe the purest nature of gaps and their effects. Multiple defects could lead to interactions, which could mislead the research from capturing fundamental effects.

The gap width is another variable of effect. To quantify gaps irrespective of tow width, gap sizes will be referred to by the percentage of tow width in some cases. For example, for a tow with a width of 10 millimeters, a gap size of 3 millimeters represents 30% relative gap size. At 100% relative gap size, a new tow can be laid between the adjacent ones. Choosing an absolute value for a defect would not be fully helpful, as e.g., a 3-millimeter gap should be a different case for a 6 and a 25 millimeter wide tow. Thus, as a looser requirement, the gap should remain under 100% relative gap size and a minimum of 1-2 millimeter absolute gap size. The latter is stated to have a distinct cross-section, without partial healing through curing or to avoid strong resin pockets. This way, the failure process might be better detected through testing.

3.6. Failure mode

The ASTM standard for "Compressive Properties of Polymer Matrix Composite Materials" [91] discusses failure modes (12.5. paragraph) for the tests carried out according to it. For fiber-reinforced composites, the strength values are admirably high, which carries some difficulties, especially for load introduction. The standard association determined common failure modes and chose acceptable from the list. Figure 3.8 (left) shows visual representations of some failure modes, grouped according to acceptable and non-acceptable ways respectively. The failure modes have common codes to mark failure mode, area, and location (presented on Figure 3.8 right). If the failure mode is unacceptable, the document orders the tester to investigate the force introduction into the specimen. Tab adhesive and inside grip failure locations must be avoided, as these do not exhibit correct data.

This philosophy is required for the tensile tests of the research, meaning failure location is only accepted at the gauge section, where it presents useful information. From another aspect, this means the same as for the mentioned standard - no failure at grips, but taking it further. Acceptable failure locations should be gap or gap-related points. The standard society cares to mention the key factors in undesirable failure, namely:

- Tab alignment
- Tab material
- Tab adhesive
- Grip type
- Grip pressure
- Grip alignment

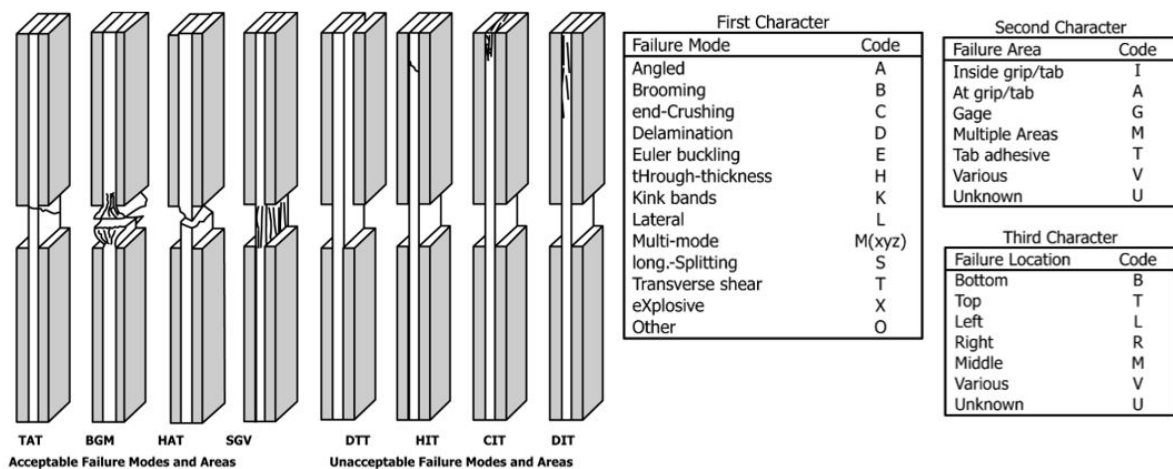


Figure 3.8: ASTM failure mode naming convention for compression tests [91]

3.7. Test output

The testing pyramid has been introduced in section 3.1. It must be noted, that as the test is chosen to be a level higher than before, scientific output and value must also be higher than the simple basic-level coupons. Thus, the greater efforts pay off. Low-level coupons usually output only a single value of interest, like ultimate strength, modulus, or similar. For the element-level specimen, the most desired information are location of failure and failure process. The failure load here is already assumed to be a requirement inherited from lower-class testing.

To be able to extract more data from the specimen, after the onset and potential early damage propagation the specimen itself must remain intact for further testing, otherwise, the research output remains on the coupon level. This opens up a lot of ways to investigate the mentioned desired outcomes, both in- and ex-situ. The various methods which can be implemented shall be discussed here.

The first major desired information, failure location can be detected as Falcó et al. [64] did in their work previously mentioned. Their experimental work featured the digital image correlation (DIC) method on the small coupon tests. The DIC method is a digital tracking method, based on camera images, and a comparison of these images through time [92]. The part under scrutiny must feature a distinct optical pattern on its surface. The unique points of the pattern are tracked by a software algorithm, therefore original and deformed points are known in space. The difference between the two is the displacement, which can be turned into strains using mathematical expressions. One camera is enough to detect such information, although there are difficulties in some cases. If the displacements stay in 2D space, one camera is sufficient. If, however, there are out-of-plane displacements, one camera works with significant error. Such displacements are detected to be strains, when in fact, they can be even only rigid body motions. To counter this, an additional camera is needed at a different spatial point. This way, non-planar specimens can also be tested. Common features of DIC specimens are the black and white speckles. Upon a white base coat, black dots are painted on the checked surface, which results in a very high contrast and accurately distinguishable spatial field. Such a pattern is presented on Figure 3.9 with a post-processed image featuring a strain plot [64].

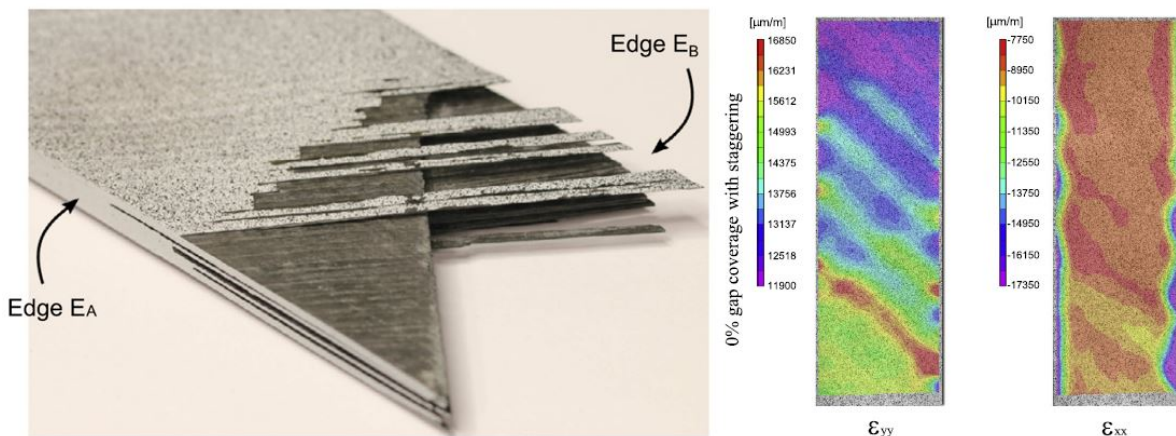


Figure 3.9: DIC specimen (left) and stress plots from the post-processed data, transversal and axial stresses respectively (right) [64]

Heavily loaded points and cracks usually appear as strain-intense areas in DIC tests. These are wished to be captured with the testing to be done. Apart from this, other post-situ tests could help in the full exploitation of testing efforts. Such tests can be simple images using microscopes, similarly to Figure 2.15. In an ideal case, cracks and their paths are recovered. However, even the geometric changes through curing offer valuable insight into the topic. Using these basic inputs, research tools can be refined further. More advanced is the X-ray imaging, already presented on Figure 2.16.

DIC only captures surface events accurately, as naturally, light cannot transfer information from within. However, elastic waves run through the bulk material and, therefore are able to give feedback behind the surface. These waves act as the information carriers in ultrasonic scans, a common NDT testing method in the industry [93]. Ultrasonic waves have high frequency (for composites, usually in the range of 1-10 MHz) and low wavelengths. Any defect, void, or crack serves as a hurdle to such waves, therefore some interaction happens in such areas, which can be even a simple reflection. These

interactions can be detected and processed, therefore damage can be assessed in size, location, and severity.

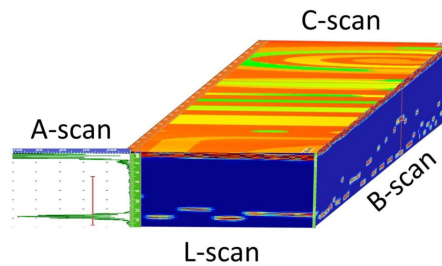


Figure 3.10: A, B, and C scans presented in axonometric view [94]

There are three types of ultrasonic scans in common use, these are:

- A-scan: Waves are sent through a ligament of material at only one spatial point. The output is a function, showing the distribution of detected wave amplitude in time. Two peaks of amplitude across the range usually represent the front and back walls of thin-walled structures. If there is a void between the two, the back wall peak shifts in time, caused by the echo of the damage. As the damage is closer to the instrument, less distance has to be traveled, resulting in shorter flight time of the wave.
- B-scan: Technically an A-scan along a line. A resulting output is a 2D image, showing events through a section.
- C-scan: An A scan over the surface of an object. The output is also a 2D image but projected to the out-of-plane direction.

To help the understanding, Figure 3.10 visualizes the scans in axonometric view [94]. An ideal contender for damage detection would be a B or C scan for the research. To summarize this section, the research methodology needs to offer more than direct values, preferably serving information on failure location and failure process. The process to be used is to be decided according to the available resources.

3.8. Summary of Requirements

This last section summarizes the previous ones from the chapter. This is done in a structured way, by presenting the requirements on Table 3.1.

Table 3.1: Table of requirements

Req. No.	Requirement type	Definition	Value	Unit
1	Testing level	Element level testing	-	-
2	Max load	Load corresponding to desired failure	250	kN
3	Representative structure area	Primary loadpath	-	-
4	Representative structure area	No cutouts at gaps		
5	Stress state	Significant axial, transversal and shear stresses for gaps		
6	Stress state	Homogeneous load state across gauge section		
7	Testing case	Uniaxial tension		
8	Laminate thickness	Minimum thickness	1	mm
9	Specimen layup	Pronounced anisotropy of the layup		
10	Specimen layup	Few off axis plies to inspect hypothesis		
11	Specimen layup	Symmetric and balanced laminate		
12	Manufacturing	Usage of AFP robot		
13	Gap layers	Maximum gap layers, and with no defect agglomeration	2	
14	Gap size	Maximum gap size	<100%	% relative gap size
15	Gap size	Minimum gap size	2	mm
16	Failure mode	Failure at desired location, strictly not at grip locations		
17	Failure mode	No catastrophic failure, intact specimen after testing		

4

Design of specimen

Building upon the foundation of requirements, this chapter serves to introduce the development of the specimen and its final form. Altogether, the chapter forms an answer to the second subquestion of optimal design and partly answers the modeling subquestion. The latter will be completed with a discussion/comparison of the used model and experiences with real-life testing. The mentioned questions in detail are:

- What is an optimal design for an AFP specimen, based on the requirements discussed?
- How can a specimen like this be modeled?

4.1. Used failure criteria

Before discussing modeling, the used failure criteria must be presented. In the research, the state-of-the-art LaRC05 failure criteria [95] are used, which is already implemented in the Abaqus FEM software. This criterion performed outstanding in the Second World-Wide Failure Exercise (WWFE-II), which was an international activity in which several criteria were compared to a wide range of testing data [96]. Some may say it is state-of-the-art as of now. The criteria distinguish four types of failure modes, namely:

- Matrix cracking
- Fiber kinking
- Fiber splitting
- Fiber tension

4.1.1. Matrix cracking

The main governing equation of the matrix cracking criteria is:

$$F_m^{crack} = \left(\frac{\tau_T}{S_T - \eta_T \sigma_N} \right)^2 + \left(\frac{\tau_L}{S_L - \eta_L \sigma_N} \right)^2 + \left(\frac{\langle \sigma_N \rangle_+}{Y_T} \right)^2 \quad (4.1)$$

The equation indicates failure if the index is larger or equal to 1. τ_T , τ_L and σ_N are the transversal shear, longitudinal shear, and normal tractions respectively. These are the traction (stress) components in the potential (or possible) fracture plane. The potential fracture plane is a plane where the highest possibility of fracture is indicated in 3D space. The McCauley brackets for the normal traction component denote the positive mode choice. If the normal mode is tensile (positive), the value is used, if compressive (negative), zero is used instead. The traction values are inherited from both the in-plane and out-of-plane stresses, with a maximization problem with respect to the variable α . This term α is a fracture angle that maximizes the failure criteria function. Therefore, the maximizing value of the α variable presents the orientation of the potential fracture plane. The traction components are as follows:

$$\sigma_N = \frac{\sigma_{22} + \sigma_{33}}{2} + \frac{\sigma_{22} - \sigma_{33}}{2} \cos(2\alpha) + \tau_{23} \sin(2\alpha) \quad (4.2)$$

$$\tau_T = \frac{\sigma_{33} - \sigma_{22}}{2} \sin(2\alpha) + \tau_{23} \cos(2\alpha) \quad (4.3)$$

$$\tau_L = \tau_{12} \cos \alpha + \tau_{31} \sin \alpha \quad (4.4)$$

Figure 4.1 from the works of Pinho et al. [95] tries to help the understanding of the meaning of the idea of the 'possible fracture plane'. For pure compression, the value can be obtained through experimental work, which is denoted as α_0 . This is a common constant in equations, see Puck criteria [56]. For the rest of the research, $\alpha_0 = 53^\circ$ will be used, as it is a well-representative value for carbon composites, and it is also the default value in the software. Apart from these variables, the equation features S_T, S_L transversal (out-of-plane) and longitudinal (in-plane) shear strengths, and η_L, η_T friction coefficients. The friction coefficients are:

$$\eta_L = \frac{S_L \cos(2\alpha_0)}{Y_C \cos^2 \alpha_0} \quad (4.5)$$

$$\eta_T = -\frac{1}{\tan(2\alpha_0)} \quad (4.6)$$

Note, Y_c denotes the transverse (90°) compression strength. Furthermore, the transverse shear strength can be calculated using the following formula [97]:

$$S_T = Y_c \cos(\alpha_0) \frac{\sin(\alpha_0) + \cos(\alpha_0)}{\tan(2\alpha_0)} \quad (4.7)$$

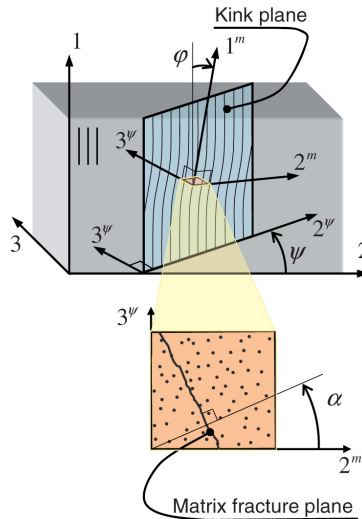


Figure 4.1: Possible fracture plane visualised by Pinho et al. [95]

4.1.2. Fiber kinking and fiber splitting

Both fiber kinking and fiber splitting are compressive failure modes, therefore less of interest in this research. Hence, only the main equation is presented, which both share. Fiber kinking is the micro-buckling (and fracture) of fibers, while fiber splitting is 'only' the interfiber matrix failure under shear-compression state. This being said, fiber kinking is usually preceded by fiber splitting, therefore the justification of a common equation can be easily seen. The failure mode depends on the axial stress - in larger compression values than $X_c/2$ (half of the axial compression strength) fiber kinking takes place. In lower magnitudes, a matrix failure is indicated as fiber splitting. To put it differently, the distinction lies in the relative dominance of axial compression. This comes from experimental observations, as the fiber buckling is only observed at significant compression levels. The distinction is important for crack propagation modeling only, for first-ply failure (FPF), no major difference can be found. The governing equation is as follows:

$$F_f^{kink} = F_f^{split} = \left(\frac{\tau_{23}^m}{S_T - \eta_T \sigma_2^m} \right)^2 + \left(\frac{\tau_{12}^m}{S_L - \eta_L \sigma_2^m} \right)^2 + \left(\frac{\langle \sigma_2^m \rangle_+}{Y_T} \right)^2 \quad (4.8)$$

The m exponent notation refers to the 'misalignment frame' stresses, obtained by tensor transformations. The misalignment frame stresses are further built up by the 'kink-band frame' stresses, which are the stresses rotated in the fiber-kinking plane. This shall not be discussed further.

4.1.3. Fiber tension

Fiber tension is the most straightforward one out of all is governed by the equation:

$$F_f^{\text{tens}} = \frac{\sigma_{11}}{X_T} \quad (4.9)$$

Which is a simple comparison of applied axial stress and axial (tensile) strength.

4.2. Material input

Next to the used failure criteria, the material input will also be presented here. For the material data properties of initial simulations the industry leader, Toray Advanced Composites' TC250 matrix system is used in combination with high-strength fibers [98].

Table 4.1: Material stiffness inputs for the simulations [98] [99]

	Unit	TC250-HTS-40 12K	MTC510-UD150-HS-37%RW
E_1	MPa	140000	110000
E_2	MPa	9800	8200
E_3	MPa	9800	8200
ν_{12}	-	0.3	0.34
ν_{13}	-	0.3	0.34
ν_{23}	-	0.4	0.4
G_{12}	MPa	4500	3600
G_{13}	MPa	3000	3000
G_{23}	MPa	3000	3000
t	mm	0.15	0.15

Due to the high costs of the tow materials, later this is changed to the available material of SHD composites. The exact definition of the material is MTC510-UD150-HS-37%RW, meaning 150 gsm material with an MTC510 epoxy matrix system and high-strength fibers. The cured resin content of the material is 37% weight percentage. This exact material was used in the research of Ramji et al. [99]. The data input is collected from the cited publication. The thicknesses for the Toray product are given to be 0.15 mm, which value is also kept for the other counterpart, based on the same areal weights. For both materials, the stiffness and strength inputs are presented on Table 4.1 and Table 4.2 respectively.

Table 4.2: Strength values and additional inputs for the LaRC05 failure criteria [98] [99]

	Unit	TC250-HTS-40 12K	MTC510-UD150-HS-37%RW
X_t	MPa	2100	2100
X_c	MPa	1730	988
Y_t	MPa	56.5	54
Y_c	MPa	200	200
S_T	MPa	92.5	99
α_0	°	53	53
ϕ_0	°	2.5	2.5
S_L	MPa	92.5	75.35
η_L	-	0.082	0.376
η_T	-	0.287	0.287

For both cases, the ϕ_0 input, which represents a local misalignment angle of fibers (manufacturing deviation, connected to fiber waviness in plane), is kept at 2.5 °, using the same value as Gouskos and Iannucci [97].

4.3. Applied simulation model

To give a clearer understanding of the modeling aspects, the general thought for the specimen shape is briefly introduced. Observation of processes is very hard if it is deeply hidden within the specimen. Thus, the general thought is to put the gaps (therefore some tows which mark the gap) onto the surface of the specimen, allowing better insight. The deeper plies are decided to be gap-free, and designed to give a shape to the testing panels. Gaps are created between tow strips, therefore the front and back side are basically decided to feature an advantageous pattern of tows, which is the main feature to develop with the tool. It must be mentioned again that the tow drops, and consequently the gaps therein produced, had to be at the central region of the specimen to minimize or completely reduce edge effects at the gaps' location. The gap-free inner plies are referred to as 'supporting' or 'backing' plies from now on, and the surface tows are also named 'surface' or 'additional' tows, as these are the major targets of the observation. A sketch of the concept is presented on Figure 4.2.

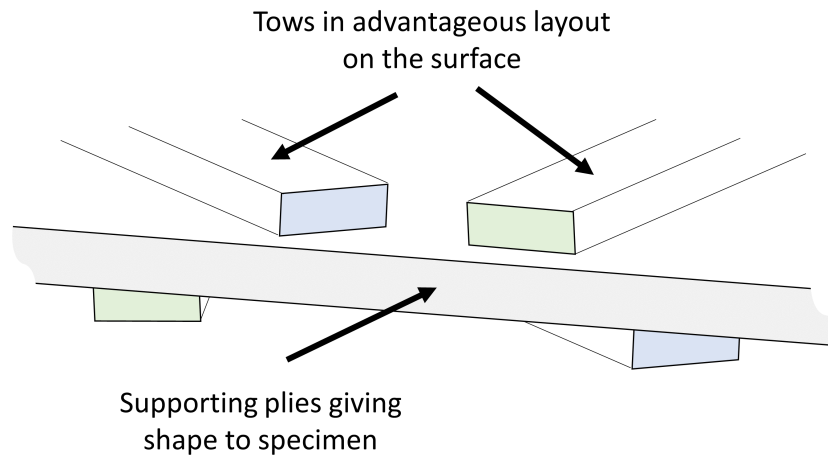


Figure 4.2: Initial thought for the specimen layout.

The simulation work is founded on the 'supporting' plies, which give the specimen a form and allow gaps to be loaded up. 'Founded', as in these layers were not or barely changed through iterations, thus being a reference to any additional detail. To the base supporting plies, 'surface' tows, and similar layers are contacted using a rigid, perfectly strong tie constraint. The design aspects of such parts will be discussed in detail in the subsequent work. From the simulation side, this approach allowed trying many tow patterns and geometries, since the majority of the model, the supporting plies and the load introduction could remain the same as the design evolved to a final one. One design iteration required only the new tow shape generation, which is substituted into the place of the old concept with the mentioned tie constraint. This being said, the tows and the supporting plies could feature different element types. For the tows, the usage of solid elements to capture out-of-plane effects, spatial distributions and other aspects were thought to be priority, the choice was obvious. For the supporting plies, shell elements should have been somewhat faster than solid counterparts, but the additional information was thought to outweigh the computational time increase. The supporting plies and 'surface' tows are modeled as flat, rectangular cross-section items, not accounting for post-curing deformed ply geometries. For this thesis research, solid 'brick' elements (C3D8R) are used for both additional tows and supporting plies. This type of elements are capable of indicating edge effects at tow edges and at specimen edges, moreover, at clamping regions, the stress concentration effect can also be investigated.

The mesh size is determined after a convergence study, which is presented in Appendix A. The mesh size in the tows have a size of 0.25 mm, while the supporting plies have 1 mm of size. The initial setup is visualized on Figure 4.3. The loading onto the specimen is through reference points. The top and bottom reference points are rigidly coupled to the top and bottom specimen edges respectively. The bottom point then is constrained in all degrees of freedom ('encastre' boundary condition), simulating a clamped case. The top point is constrained in all directions except the vertical displacement, which is controlled during the loading. For final checks and for the grip zone inspections, a more detailed model was created, as will be discussed in the corresponding section (4.6).

In the creation of the model, research time was a major influencing factor. Since every design process is an iterative process, the design tools have to give results in a rapid but effective manner. The greatness of FEM lies in the capability of dealing with every concept, by solving smaller, simpler parts (elements) of it. The usage of FEM as a tool was never a question, but the details of the modeling were. The element choice for the supporting plies increased computational time for increased value, however, some other simplifications had to be made elsewhere.

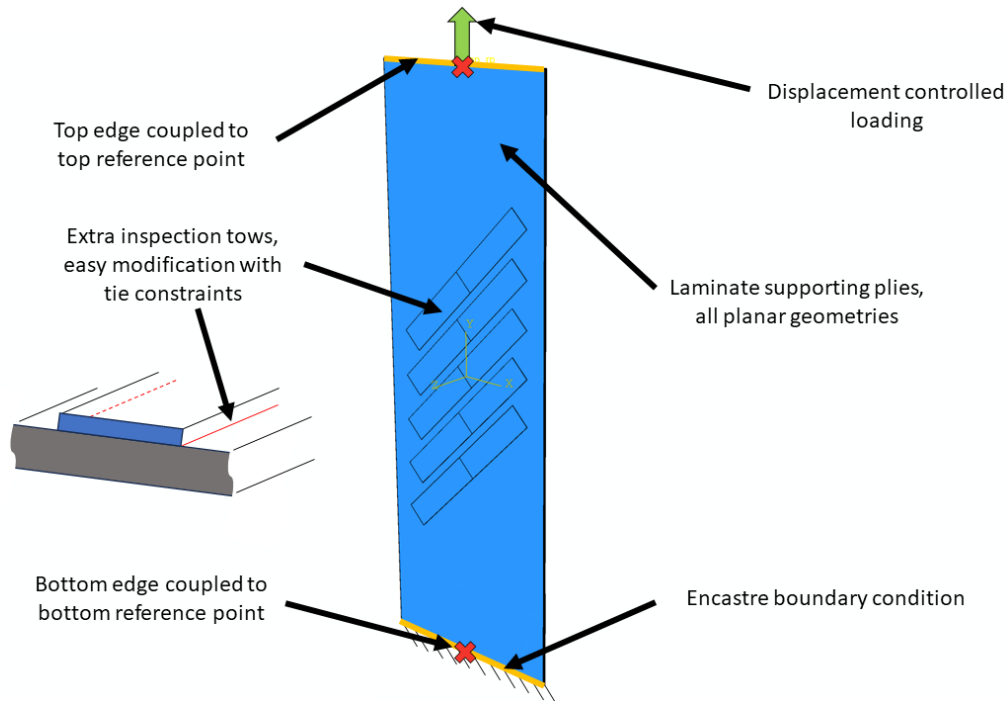


Figure 4.3: Initial simulation approach used for the thesis work.

First, delamination was ignored as a failure mechanism. One reason for this has been conveyed in the literature study chapter (chapter 2), the variation of strength against this failure mode is not entirely known in multidirectional laminates. This being said, using some averaged or estimated SERR values could still convey an educated guess if one will, with a price of computational resources and time. This aspect was rejected already in the early stages of the research because such a model would only output a questionable result, or might even mislead the design process.

Next to this, geometrically the post-curing cross-sectional features are also drastically simplified. In the literature study phase, a cross-section of a cured laminate with gaps or overlaps has been presented on Figure 2.15. Another cross-section, focusing on the ply deformations is shown on Figure 4.4 (from the works of Guin et al. [71]). As can be seen, a gap enforces deformation onto the adjacent plies in the laminate during curing, simply because the neighboring plies do not have support in a local zone; thus, the layers have room to move under the curing pressure. In the applied model, ply waviness (and therein resin pockets also) is neglected, also for two reasons. On one hand, the lack of information on the final, realistic cross-section after curing. Many parameters influence this waviness, including gap size, ply parameters, layup, and also others next to some stochastic processes. To put the problem into a different perspective, with only transversal gaps in a specimen, the layer waviness can be simply described by the side view/section. If however, the gaps are in multiple directions, the adjacent layers are deformed into complex 3D shapes. Moreover, the thickness variation and fiber volume fraction change significantly. A model featuring accurate ply waviness thus should be based on extensive numerical data. On the other hand, complex 3D modeling of realistic laminates would also require a significant amount of dedicated time, and for the worse, require individual remodeling of every single concept. Retrieving representative geometry with corresponding parameters is a challenge in itself for one instance, let alone iterating designs with it. Hence, the waviness has not been modelled to save time also.

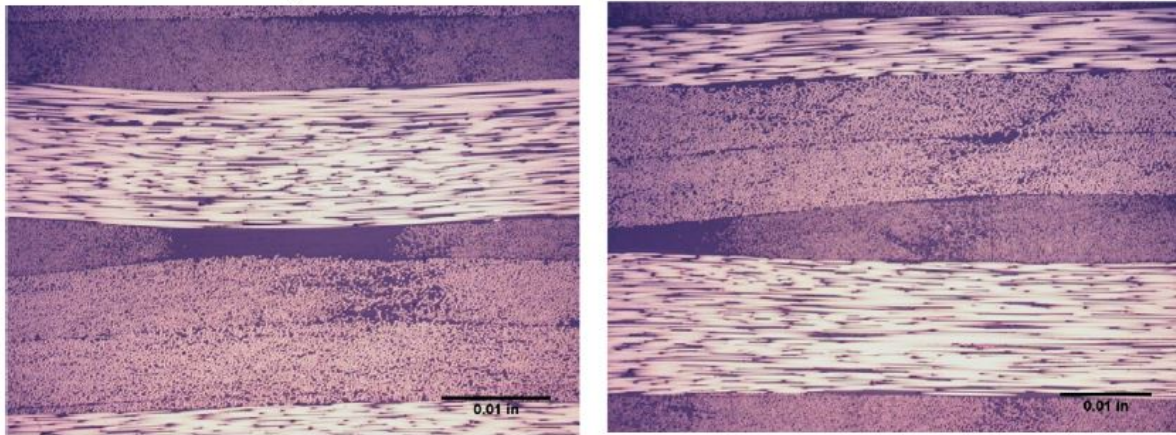


Figure 4.4: Ply deformations around embedded manufacturing defects [71]

The simplification is similar to the works of Falcó et al. [68], already introduced as probably the most prominent work in the research topic, together with their related experimental work [64]. Their FEM modeling also neglected out-of-plane waviness and used resin-rich pockets in the mentioned zones. To aid understanding, Figure 4.5 presents the whole approach. The plies and resin-rich zones are modeled using solid elements (C3D8R), but in total, their model was detailed in damage progression. This aspect was covered with cohesive contacts (delamination) and User Material Definition (UMAT) subroutine for damage evolution in solid media (ply or resin pocket crack propagation). The simulations showed a good correlation with experimental data, even in the progressive damage phase. This fact also further pointed to the modeling approach choice.

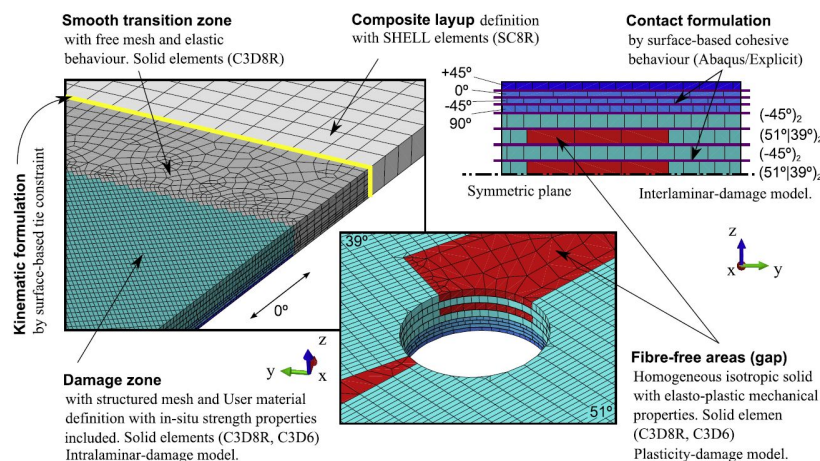


Figure 4.5: Simulation approach of Falcó et al. [68]

The thesis simulation model calculates with local cross-sectional data but neglects out-of-plane ply waviness and also resin-rich pockets amongst others. Therefore, drawing any numerical strength knockdowns with respect to variables like gap size and tow geometry is unjustified. Especially the mentioned gap size sensitivity curve would be hard to trace, as a small gap size, the gap goes from a pristine layer to a pronounced resin-rich zone really quickly. This demands a model which could be generated with all geometrical features included.

Out of research outcomes, strength allowables are sought the most. Understandably, it is a direct and very strong tool in pushing structural efficiency. However, for the given limited time, this research will only focus on the testing method, the observations, and failure processes. An accurate strength knockdown characterization with parameter sensitivity is reasoned to be enough challenge for complete PhD cycles, rather than limited time Master's theses. For that, higher-level numerical tools, including automated/scripted parameter sweeping are envisioned. This being said, the process still needs a founding work, which align with this thesis' focus. Hence, the pursued outcomes currently are the areas of highest importance, from which steps forward are possible.

4.4. Initial concept

After stating the inputs, modeling approach, and the main outputs sampled, the initial design and its shortcomings are discussed. The initial concept was based on fiber steering, and trying to have significant orientation differences over a smaller panel size.

The first panel features five curved tows on each side of the specimen, similar to an 'S' shape. This is achieved by tows switching turning direction (at the center of the panel). The curve consists of constant radius circular arcs, with a radius of 400 millimeters. This is usually the absolute lowest value for a steering radius for the smallest width prepregs - like 1/4 or 1/8 inch. The widths of 'surface' tows are set to be 1/2 inch, which would have been built up by several passes of the AFP machine. A tow, at specimen grips has an orientation angle of 0° , while in the middle of the panel, it has an angle of 45° . With stacking tows adjacent to each other at the upper and lower edges, gap closeout is achieved. It is achieved in such a way, that by vertically translating one tow, the gap size could be adjusted to a desired value. The gap size is set to be a vertical and horizontal translation of one tow width, meaning roughly 2.75 millimeters of gap size. The panel is represented on Figure 4.6.

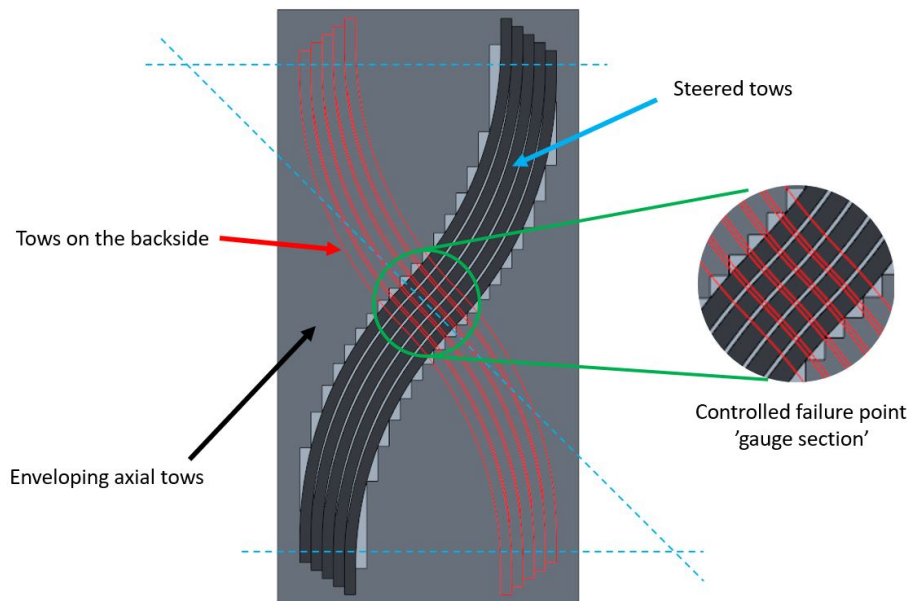


Figure 4.6: Initial panel concept

The same 'S' shaped tows are placed onto the other side of the specimen, however, in a (vertically) mirrored orientation. This way, the laminate balancing is achieved on a larger scale, though not in some local points. Between the two curved/external layers, the backbone of the specimen is about 0.3 millimeters of gap-less, monolithic, straight fiber laminate. These are referred to as 'supporting' or 'backing' plies (as they back up the tows under investigation). With this, the total thickness is only 0.6 millimeters, which is not sufficient to fulfill the thickness criteria. Nevertheless, for the first few initial concepts, it was used to have more pronounced effects. Later on, the thickness was adjusted, as will be discussed in the subsequent parts. These supporting layers give the specimen its shape and also create a laminate field around the gaps. This laminate field essentially conveys loads to the gaps. The panel width is 340 millimeters, while the height is 675 millimeters, not including the load introduction area.

Additionally, the initial and novel idea was to envelop the 'S' tows with axial fibers, creating triangular gaps with all kinds of aspect ratios. This way, both translational and triangular gaps can be investigated within one specimen. On top of this, the tows are closed out from external edges, and thus from edge effects. Upon simulating the panel, the result represented on Figure 4.7 was obtained.

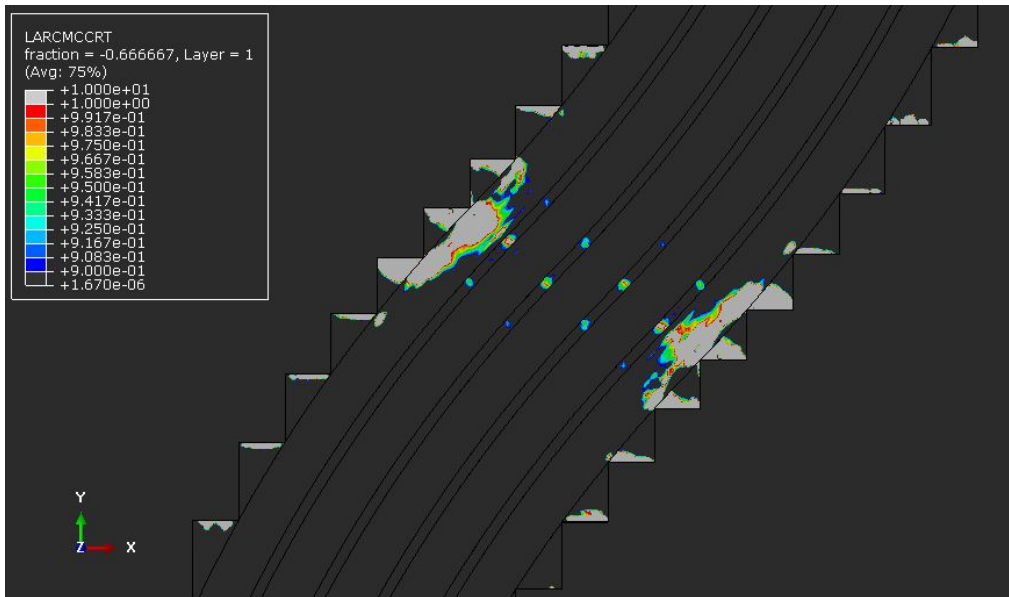


Figure 4.7: Matrix failure plot for the initial panel concept

The plot scale is set between 0.9 and 1, meaning that all material with a lower failure index than 0.9 appear as black, whereas all failed media appear as light grey. The enveloping axial tow terminations cause an abrupt stiffness change, which could lead to numerical singularities. Hence, the material failure at the triangular gaps further away from the gauge sections is thought to be the result of the FEM method. However, failure at the gauge sections for the triangular gaps is pronounced, therefore onset of matrix cracks is thought to happen. The outermost tows show a strong zone with higher indices than 1. As one can see, the tows are not loaded homogeneously, since inner tows are further away from damage onset (below 0.9). This is thought to be a causation of the triangular tows, which drop the load onto the outer tows directly. Thus, the main conclusion from the first iteration is not to attempt the characterization of both types of fiber-steering gaps. Other than that, the failure peaks in the gaps promise some validity to the research, as local failure peaks can be detected there.



Figure 4.8: Second iteration of the initial concept without enveloping tows and extra clamping reinforcement.

In the subsequent development process, the supporting plies are thickened and the concept of enveloping tows is discarded. The backing plies in the subsequent simulations are kept at 1.2 millimeters, equivalent to 8 plies of the tow material. The laminate was 'virtually tested' for several orientations

and found that above 15° with respect to load direction, the supporting plies prematurely fail (before the inspecting tows). Thus a major consequence is to not have orientations larger than $\pm 15^\circ$. This happens to align with the requirement of pronounced anisotropy over the specimen (coming from representing a primary load path and VS method exploitation). The final orientations are $[0/15/-15/0]_s$. The $\pm 15^\circ$ plies reduce the testing force within the limits, while 0° layers reinforce in a 3rd direction. Having a laminate reinforced in a minimum of 3 directions is a common rule of thumb for laminates (see [2] for similar). The supporting laminate stack-up ensures a mostly symmetric and balanced laminate over the specimen, even though the extra tows disturb this feature. Additionally, axial tows are kept at the clamping area to give some aid against grip zone failure. The design is presented on Figure 4.8, and its simulation output is displayed on Figure 4.9 with dashed lines to mark the contours for easier understanding.

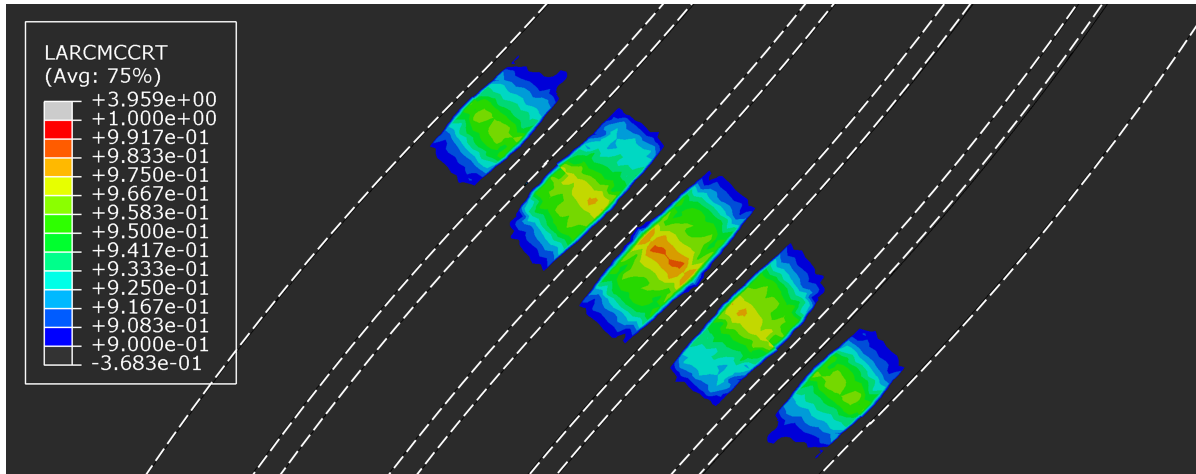


Figure 4.9: Matrix failure for panel with increased thickness and no enveloping plies

As one can see, the tows fail in the middle of the panel as before. However, the load state tendency switched, and now the innermost tows are loaded up slightly more. Moreover, failure is connected to the exact center of the tows, only in one line. This means, that over the (almost) rectangular gauge section, the load state is not homogeneous. This statement is supported by the σ_2 plot of the same simulation on Figure 4.10. The plot scale is set between 10 and 35 MPa values, and the colouring method is the same.

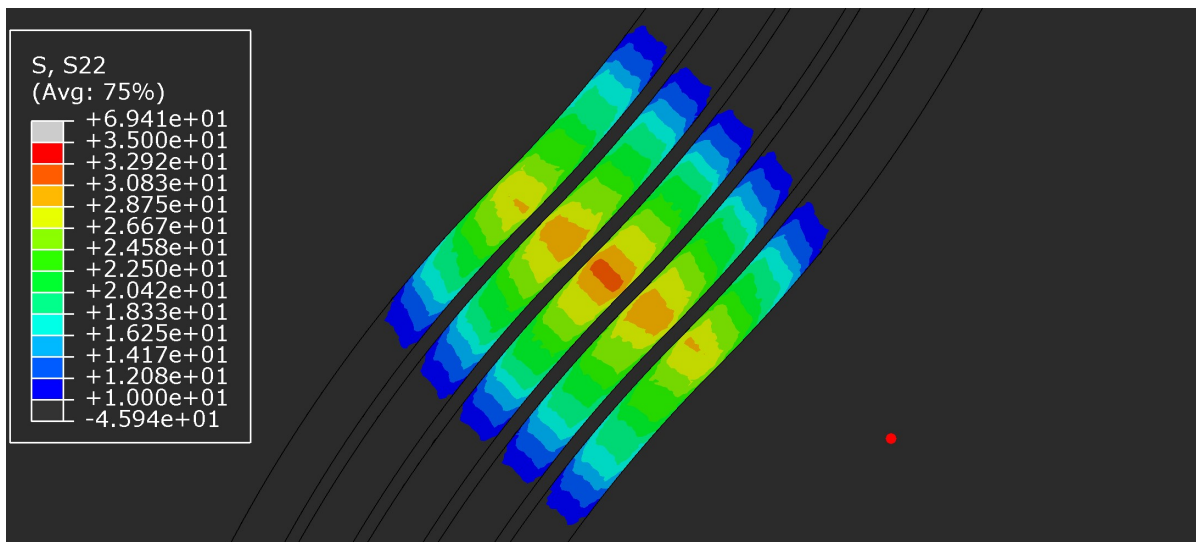


Figure 4.10: Transversal stress plot of the initial concept without envelopes and with larger thickness

The non-homogeneous damage nature is inherited from the undesirable distribution of transversal stress. This distribution is argued to be a causation of the out-of-plane displacements. The gauge section, having both + and - 'S' tows becomes balanced, while in other areas, a significant out-of-plane deformation is detected. This results in an accumulation of loads in the central area. To aid the understanding, the out-of-plane displacements are plotted on Figure 4.11.

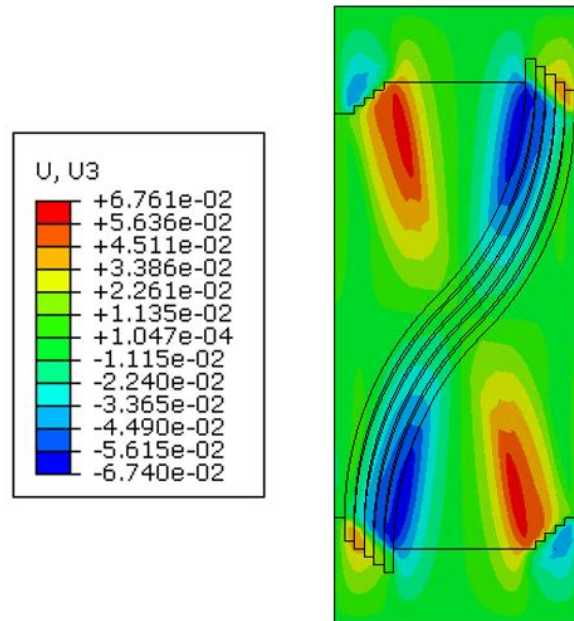


Figure 4.11: Out-of-plane displacements of the initial panel concept

Apart from this, the in-plane shear stress plot (shown on Figure 4.12) gives a great indication of processes for gaps. The shear stresses jump in the tows, right at the area where there are gaps on the other side. The jump is in the 3-5 MPa range, although not much in itself, however, when compared to the shear strengths of 90-100 MPa, an indication for some percentages of knockdown can be anticipated in some cases. This number correlates with the smaller knockdowns observed in the literature. Outside the rectangular gauge section, there are strong triangular zones with increased loading. These are zones to avoid, which will reappear in subsequent designs. Altogether, the shear stress plot gives a slight reinforcing feedback on the hypothesis of gaps affecting off-axis tows.

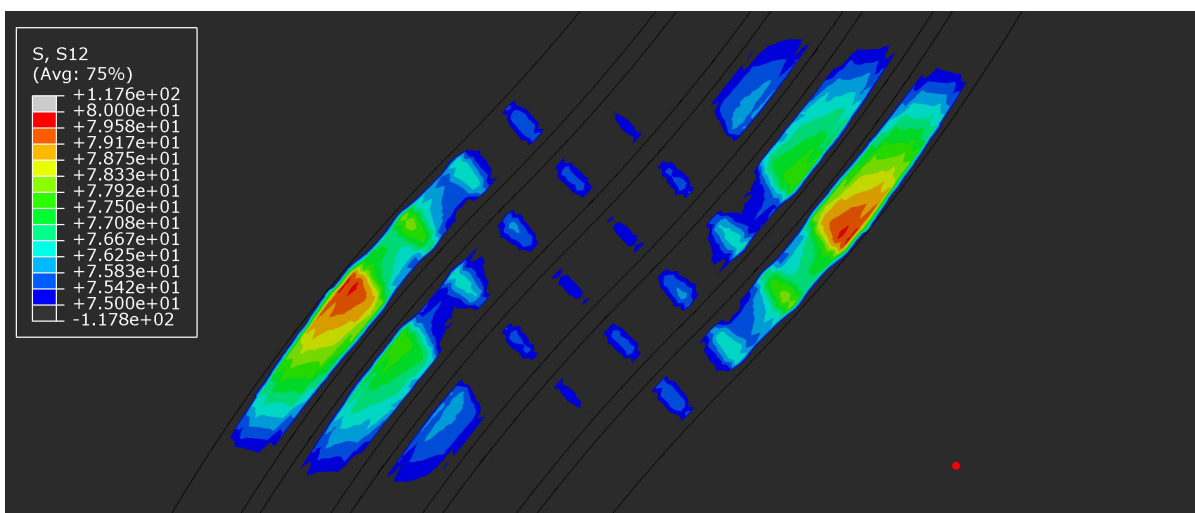


Figure 4.12: Shear stress plot for the original curved fiber concept

The initial concept provided good information on the process, even though it has some fundamental problems with it. The first is the failure location without a connection to gap effects, and the second is the failure point force, which is 540 kN, exceeding the testing machine limits. Not only this but the fiber steering of narrowest tows to the bare minimum radius limits the manufacturability of the presented design. Noteworthy mention, the globally unbalanced nature of the panel also causes some trouble, which needs to be resolved. Thus a new concept is designed, detailed in the next section.

4.5. Final concept

The final concept (Figure 4.13) is based on the previous specimens' gauge section. The five full tows are kept, as with fewer tows/repeating units, the homogenization of the state is believed to worsen. The front still has $(+\theta)$, while the back has $(-\theta)$ tow angles. The paths are completely straight, because the length of the laid tows is set to be 100 millimeters. In this small length, steering can hardly be implemented. Moreover, feasible radii do not yield significant orientation differences. The minimum feasible length of one tow placement is 65 millimeters. This limitation comes from the AFP machine to be used. The corners of the gauge sections have tows with shorter lengths. These are designed to be manually placed at the desired locations, and the function of these is purely to homogenize the stress state. Essential, as will be presented in further discussion, for the aspects of homogeneous stiffness distribution and improving the balanced nature of laminates. No failure data result will be drawn from these 'sacrificial' tows. Appendix E contains a more detailed drawing of the specimen.

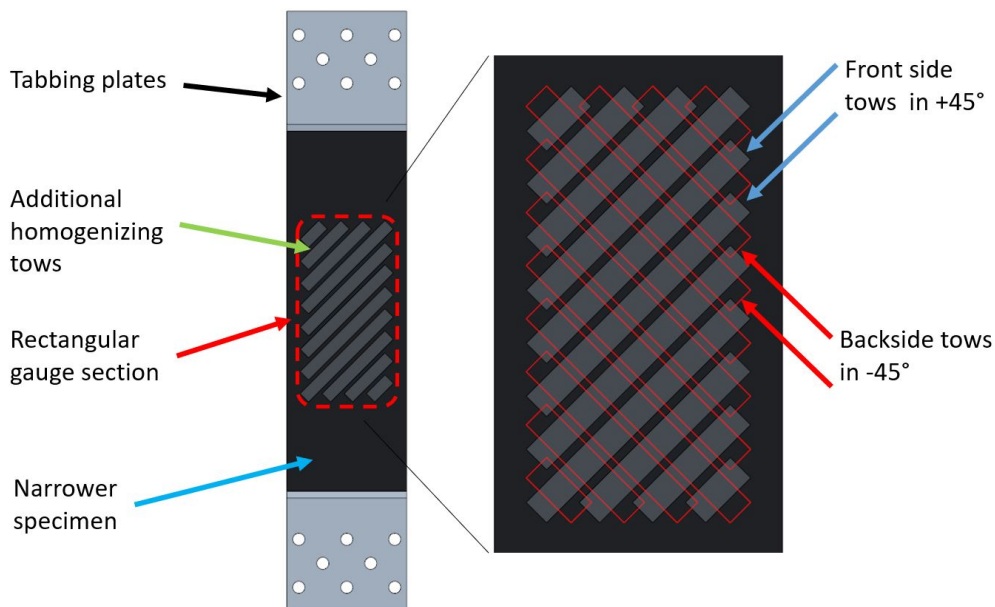


Figure 4.13: Final specimen concept

A fundamental difference lies in the specimen width, as it is reduced to 100 millimeters. The supporting layup is kept the same, hence the inspecting load is reduced significantly, to below the upper limits of the testing machine. The tows do not reach the edges of the specimen. All gap sizes are set to be 3 millimeters. The tow widths are 10 millimeters wide, thus, the configuration results in a 30% relative gap size. For the final panel, the utilized material is MTC510-UD150-HS-37%RW.

The simulation's matrix failure output is presented on Figure 4.14. The outcomes are very promising. The tows under inspection exhibit repetitively pronounced peaks of matrix failure index at gap locations of the opposite side, similar to a grid. This reinforces the hypothesis that gaps affect surrounding matrix or other layers negatively. The first point of failure is indicated at the top and bottom of the gauge section, though these areas are not to be evaluated. The failure pattern stabilizes after the first 1-2 centimeters, into a quite homogeneous zone. Additionally, a tendency can be observed in the horizontal/width direction. Going from the edge inwards the tows are loaded a bit more (plot 'going from green to yellow'). To conclude, failure in the front side is anticipated to start at backside gap locations, and inside the tows. For the back side, vice-versa, failure is indicated at front side gap locations, but also within the tows. The FPF force of the tows is 162 kN, well below the 250 kN limit, allowing potential gradual failure process experiments above damage onset.

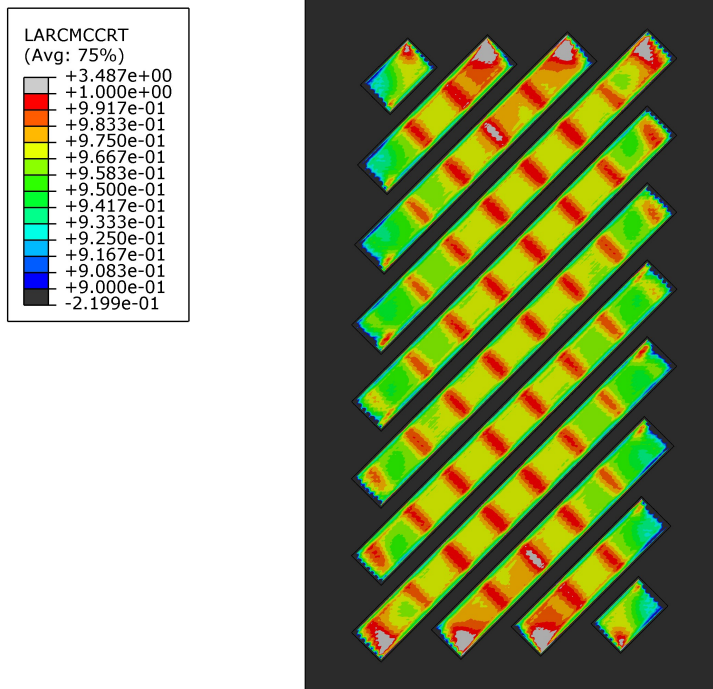


Figure 4.14: Matrix failure plot of the final specimen design showing failure in front tows at backside gap locations

The importance of sacrificial tows was mentioned earlier. Figure 4.15 shows the specimen without the extra truncated tows. As can be seen on the left side, the load state of the tows is far from homogeneous, and the outermost tows have pronounced failure areas (the plot shows a load state below damage onset, but the distribution tendency stays constant during the loading). The reason might not be obvious, however, it is simple. Visualizing the front and back tows together (right side, red dashed), it is clear that a triangular zone (marked grey on the diagram) does not feature extra reinforcing tows. This weakness causes extensive deformation mostly in-plane but also out-of-plane, forcing extra loading on the surroundings of the triangle. Therefore, the sacrificial tows make a more homogeneous stiffness distribution in-plane and also balance the laminate better.

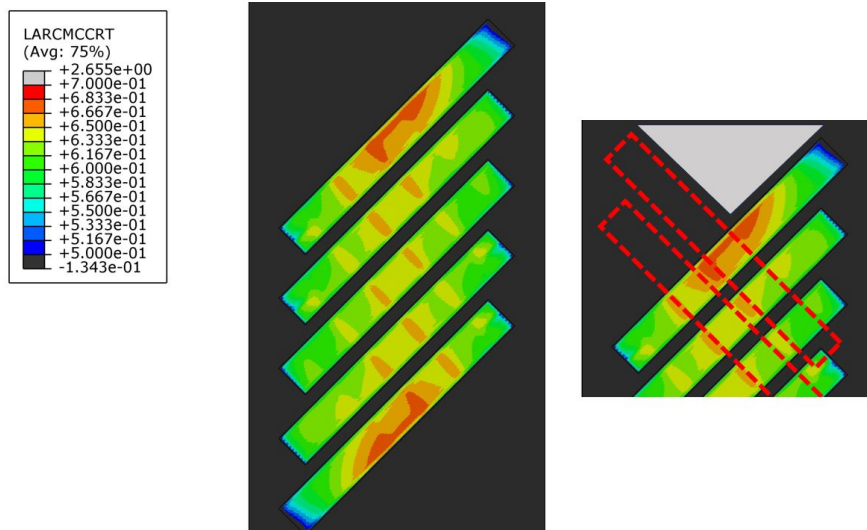


Figure 4.15: Specimen simulation without extra sacrificial tow. Inhomogeneous laminate zones at the top and bottom caused a crooked load state

Apart from the sacrificial tows, longer specimens also help the homogenization. The ASTM D 3039 [100] standard discusses specimen geometry requirements, which are presented in the original form on Figure 4.16. The minimum length requirement specifically says "gripping + 2 times width + gage length".

This is also an important rule to obey for homogeneous loading. With sufficient distance between the gauge section and the gripping area, the stress concentration does not influence the gauge section. Easy to see the validity through the poisson ratio effect - in the center of the specimen, there is a large contraction, while at the grips, transversal displacements are constrained. Eventually, these differences mean internal stresses. On another note, the well-known St Venant's principle implies that over sufficiently large distances, the effects of load introduction become very small. For the final design, the simple ASTM guideline ("gripping + 2 times width + gage length") for length is also kept in mind.

TABLE 1 Tensile Specimen Geometry Requirements

Parameter	Requirement
Coupon Requirements:	
shape	constant rectangular cross-section
minimum length	gripping + 2 times width + gage length
specimen width	as needed ⁴
specimen width tolerance	±1 % of width
specimen thickness	as needed
specimen thickness tolerance	±4 % of thickness
specimen flatness	flat with light finger pressure
Tab Requirements (if used):	
tab material	as needed
fiber orientation (composite tabs)	as needed
tab thickness	as needed
tab thickness variation between tabs	±1 % tab thickness
tab bevel angle	5 to 90°, inclusive
tab step at bevel to specimen	feathered without damaging specimen

Figure 4.16: Tensile specimen geometry requirements according to ASTM D3039

The previously mentioned MTC510-UD150-HS-37%RW material has a tow width of 20 millimeters. However, the specimen from Figure 4.13 and Figure 4.14 featured a tow width of 10 millimeters. Upon trying the concept for the available tow width, the result presented on Figure 4.17 is obtained through the same simulation process (the image represents a one-millimeter gap size in this case). At this specimen size, a larger tow width becomes a hurdle in making a homogeneously loaded, uniform zone. One clear indication of this is the failure zone at the edges of the last full-length tows. Moreover, because of the larger tow width, the same gauge section could only facilitate 3 full-length tows, instead of the previous 5. The lower number of these repeating units also means a lower number of gaps, reducing the data sampling points amongst other problems. The failure zones are non-negligible at the top and the bottom, and sacrificial tow usage in the corners can hardly be implemented. After all these issues mentioned, it must be also pointed out, that the peaks are not so strong as in the narrower tow case. Therefore, wider tows are thought to be less sensitive to gaps, according to the used low-fidelity model.

As a last attempt to make use of the wider tows and to be able to place the gauge tows by the AFP machine, a hybrid tow width specimen is also simulated (Figure 4.18). Sacrificial tows in this case are planned to be hand laminated, as these parts are not to be evaluated. The fine mesh in use caused some high-frequency numerical oscillations, which could also be somewhat detectable on Figure 4.17. Nevertheless, the output is considered realistic apart from this noise. The sacrificial tows became thinner and thus helped the design to create a more uniform gauge section. It is clear to see the effects, which resemble the final concept shown on Figure 4.14. The tendency of larger tows to be less vulnerable to gaps is still holding up since the failure peaks are again not as strong as before (for the 10-millimeter case). The fully 20-millimeter tow concept has shortcomings next to the hybrid width case and has a less promising gap effect. These contributed to the choice of using 10-millimeter tows, for the sake of more pronounced results. More pronounced, as in featuring stronger failure index peaks and more homogeneous loading. The material is decided to be the same, only split into two halves and to be placed by hand. This choice violates a requirement, namely the usage of AFP for the whole specimen (coming from representative placement accuracy, etc...). Here, a compromise is made in order to have better and more prominent testing outcomes, nonetheless, the manufacturing quality must be as close

to the AFP as possible, mostly in terms of accuracy. As a reason, the specimen will still remain a valid and founded way of characterization. The process to counter the problem features a precision template and laser positioning, and will be further discussed in the corresponding manufacturing and testing chapter.

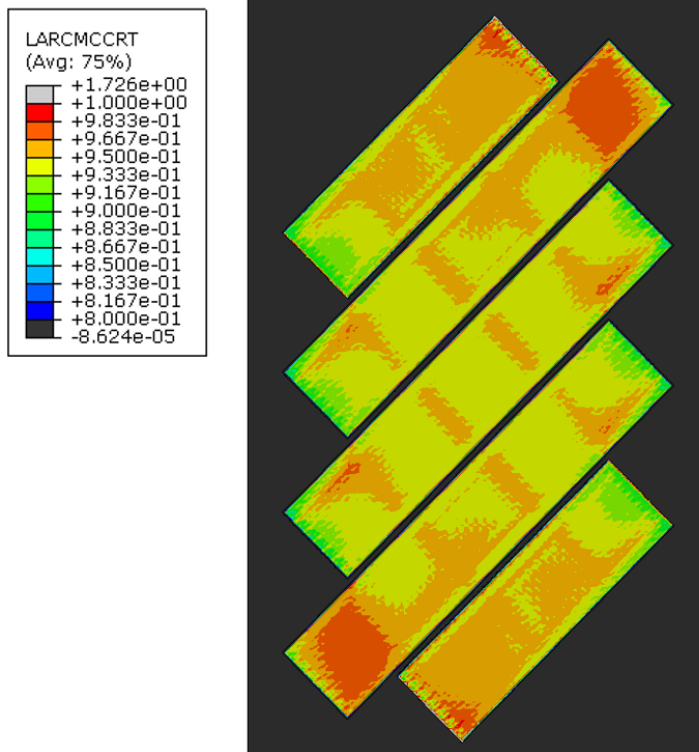


Figure 4.17: 20 millimeters version of the final panel design

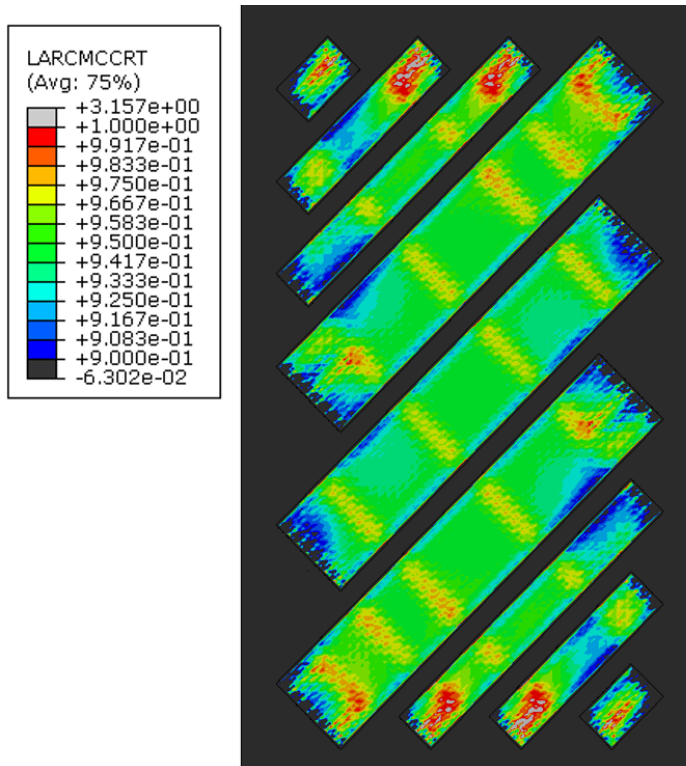


Figure 4.18: Hybrid tow width specimen simulation output

4.5.1. Load introduction and tabbing

One of the important requirements for the specimen is that no failure is accepted at the load introduction area. The work of Adams and Adams [101] presents a great overview of general rules for tabbing composite specimens. Tabbing is essential in controlling the stress ratio between the specimen gauge section and gripping sections. In an ideal case, gauge stresses should be larger than gripping area counterparts, eventually leading to gauge section failures. The first problem with load introduction comes from the nature of friction. The well-known formula for frictional force, $F_s = \mu F_c$, describes the two major parts of such forces - friction coefficient and clamping force. The multiplication of these two values gives the frictional force, which for load introduction, must meet a given value. Smooth surfaces need large clamping force to meet the requirement, which could crush the specimens, leading to undesired failure mode. If, however, surfaces are rough, less clamping force is needed, avoiding the problem. Avoiding one problem makes another, namely the grips could bite into the specimen, again leading to unsuccessful testing. Applying tabs to grip sections protects the specimens from these damages by suffering the bites themselves. Next to this, the net section of the zone increases, moreover, it is damping grip edge stress concentrations. As one might see, the tabbing for composite specimens is equivalent to 'dog-boning' isotropic specimens, only in a different spatial plane. The mentioned width tapering in the case of composite specimens is less effective since fiber splitting and other matrix failures usually develop in the tapering area.

Sudden material discontinuities impose a stress concentration, which is also a problem with simple tabs. To counter this, tabs are usually tapered towards the gauge section, gradually guiding the load into the net section. The following graph (Figure 4.19) from Adams and Adams [101] creates a nice representation of the stress concentration with respect to the tab tapering angle. Note, that the vertical axis represents normalized far-field stresses, also called gauge section stresses.

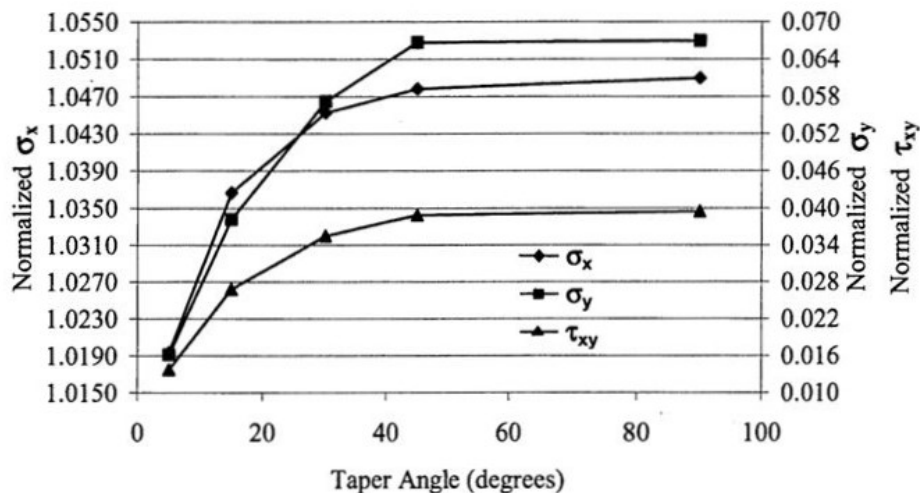


Figure 4.19: Stress concentration dependence with respect to tab tapering angle

The tapering angle shows a significant effect on the stress component. Generally, the smaller the taper angle is, the better. Ideally, a tapering angle should be between 5...15 degrees to alleviate the unwanted effects as much as possible. Next to tapering, the stress concentration effects can be lowered with optimal material choices too. The parameter sensitivity is visualized on Figure 4.20.

Tab material choice has even stronger effects than tapering angle. Again, as a general tendency, the softer the material, the better. Following the curve, ideally, the sub-50 GPa materials are the way to go to alleviate material effects. Amongst the mentioned parameters, tab thickness and tab length also have an effect on the tab termination stress concentrations. These have much less of an effect and will not be discussed further here.

For tabbing, infrastructural limitations are also considered. The ideal case would have been a 5° tapered and quite soft material, like a GFRP mat plate. Such materials are generally used for tabbing and for electric purposes (because of the electric insulation properties), as they are mass-produced in plate form. These are less available than conventional metallic sheets, being also harder to manufacture. Aluminium tabs are also known in the industry and have an advantageous feature,

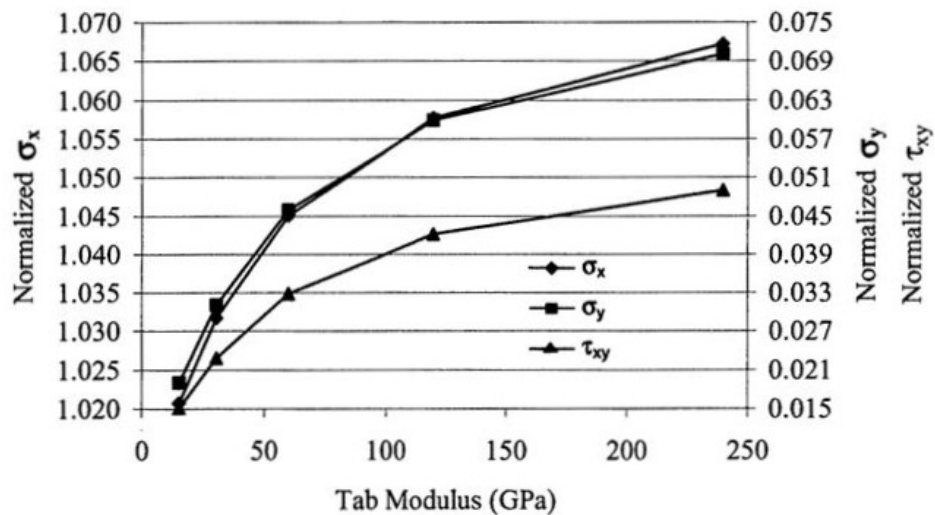


Figure 4.20: Stress concentration dependence with respect to tab material

namely plasticity, helping against fracture at the gripping region. Besides, it is easy to manufacture, allowing it to have useful tapering.

The final tabbing is chosen to be a 1-millimeter thick aluminium plate with 10 ° of tapering, presented on Figure 4.21 (left). The material - AL6082 - specifically is chosen to have 'mid-range' properties, namely around 250-300 MPa of yield strength, while keeping sufficient plasticity. The adhesive is chosen to be the 'Scotch-Weld EC-9323 B/A' product, with outstanding shear strength value for both metallic and composite applications. The adhesive's shear strength is checked for the testing machine's ultimate 250 kN load, with a simple calculation, namely the ultimate force divided by the total sheared area. The safety factor is 2.096 on adhesive failure, for the calculations, see Appendix B.

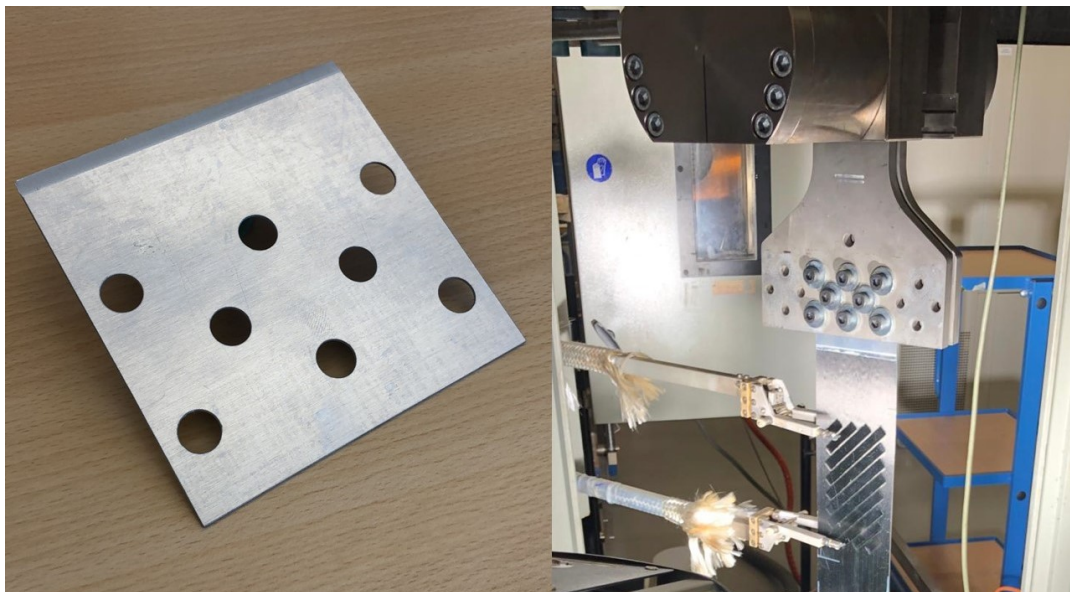


Figure 4.21: Final specimen tab (left) and specimen in the upper hydraulic grips with clamping plates (right)

With the tabbing itself, the load introduction has not been resolved completely. The machine to be used needs to transfer these loads onto the tab surface and in a desired uniform fashion. The universal tensile testing machine has hydraulic grips, which could crush the specimen if it is pressed directly. The hydraulic grips have circular pistons, which impose another threat to the homogeneous loading. Not only these but purely frictional loading up to 20 tonnes of force yields a serious hazard in case of any explosive failure for the testing environment.

To counter this, an intermediate step is implemented at the load introduction, by means of a clamping element featuring bolts on the specimen side. This is a commonly used method (see the works of Ravi et al. [102] for a subcomponent level clamping), as distributed bolts also distribute the load quite homogeneously. Not only this, but the bolts with the bearing load impose a secondary load path in case of a slip or other frictional problems. The bolts' pretension can be tuned by a torque wrench, protecting the specimen from over-stressing the clamping area. The other end of the clamping elements is connected to the hydraulic grips. Thus, the pistons can apply stronger force for the strong monolithic steel, giving a larger safety factor against slipping at the clamps. The original clamp facilitates specimens up to 300 mm wide, though the final design is only 100 mm wide. The eight central M10 bolts should have sufficient pretension to load up the specimen more than the testing machine's 250 kN limit (by a safety factor of 1.7). For this calculation, see Appendix C.

4.6. Simulation of grip zones

To have a check on the load introduction, a final simulation is carried out including the previously discussed tabbing plates. In the new simulation, instead of connecting the top and bottom edges of the specimen to the reference points, now the grip zone surfaces are tied to the respective points. All degrees of freedom are tied except the gripping directional translations. This DoF instead is used to simulate the clamping force of the load introduction. Apart from this, other aspects of the simulation are analogous to the original one. The understanding is aided by Figure 4.22. The fact that the grip surfaces are kinematically coupled to the loading meant that the approach should be conservative with respect to load transfer since the load is introduced purely on the surface of the model. In reality, bearing loading is thought to make the state more favorable.

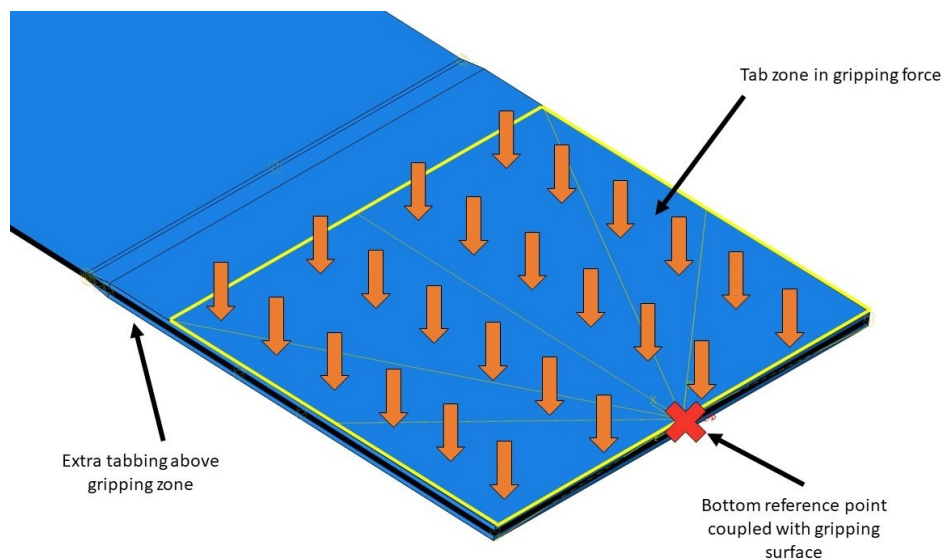


Figure 4.22: Final specimen simulation including tabbing area and clamping force.

Upon running the simulation, the results show a sudden matrix failure at the element borders along the tab termination and a smaller one along the gripping force introduction. About the first one, it is common to have a peak in stresses/failure indexes in FEM where there is a sudden stiffness change. This peak, upon mesh refinement, goes to larger values, but the scope of the failure rather shrinks with element size. This is an indicator of numerical singularity, therefore it is thought to be only an inherent phenomenon of the method used. The same evaluation is used for the gripping/free tabbing zone switch, which is less pronounced and only affected the specimen edges. The decision is easier due to the fact that fiber failure is not indicated, so in the event of matrix cracks, the residual strength of the laminate is assumed sufficient. Inside the grips, the equivalent stresses for both the tabbing plates and laminates are under the magnitude of 25 MPa and, therefore deemed safe for testing. Outside the clamped surface, the tabbing plates are anticipated to go into the plastic region of the material.

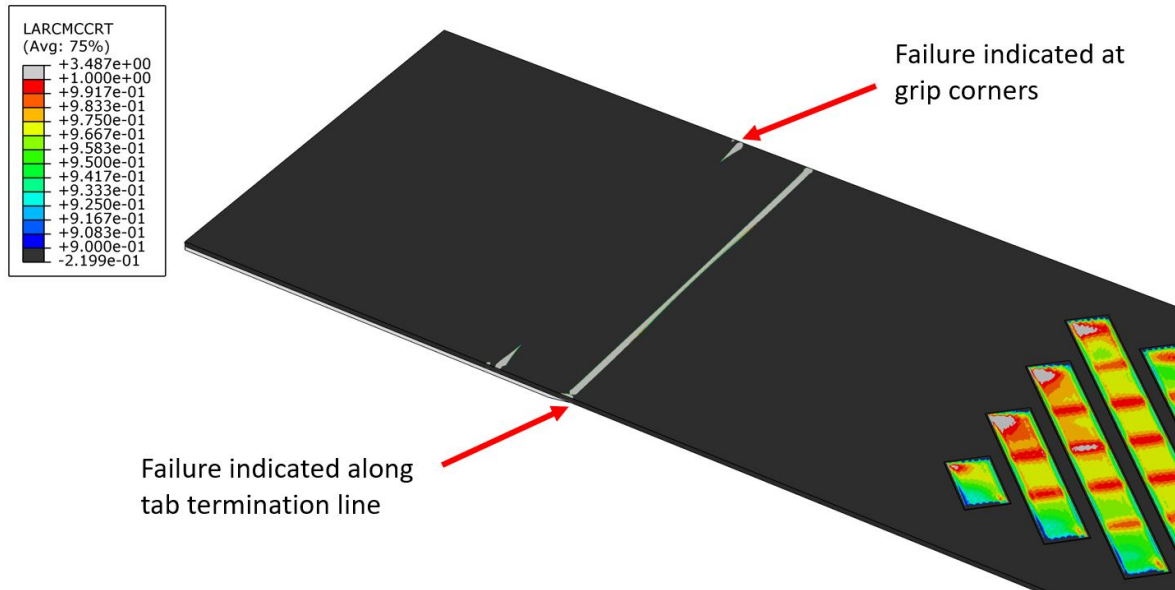


Figure 4.23: Stress singularity at tab termination and clamping force introduction.

4.7. Testing methods

The information output from the samples is wished to be maximized, therefore advancing further from the more basic coupon test outcomes. For this, DIC measurements are available at hand for in-situ strain detection, which is chosen for the research. Above the mentioned, (ex-situ) microscopical cross-sections are sought for subsequent research, as this way there is geometrical and material information to develop from. This process is also chosen for the thesis project. Ultrasonic scans are readily available at the university laboratory, however, the usage is thought to be only justified for cracks that propagate into the laminate and need tracing.

4.8. Design summary

The chapter starts with the simulation aspects (research tool). The design, being an iterative process, required a tool with rapid run times, therefore some neglects/simplifications were implemented. One major decision is the simplification of ply waviness to simple, straight, rectangular cross-sections. Delamination, as a failure mode is neglected, and not only for speeding up the simulation process, but also the literature study chapter proved to have question marks in the knowledge of materials' resistance against this failure mode. Moreover, the lack of data finalized this decision. The tool is not able to accurately predict strength processes over small gap sizes, where the geometries go through a large change over a small variation of defect sizes. Thus, drawing numerical knockdown values over proper scales is not feasible to carry out with respect to the main variables (gap size, tow width).

The next section of the chapter is the introduction of initial concepts and the pathfinder process to a promising specimen. The first thoughts revolved around steering tows in a way to control the failure zone across a specimen. Enveloping the tows, which are the focus of research, proved to be a wrong path, as simulations show an interaction between triangular and translational gaps. As a consequence, neither of the defect types have the potential to be correctly characterized. After removing the mentioned enveloping tows, the anti-symmetric strips on each side of the specimen foreshadowed the importance of the balanced and symmetric layup requirement against the global specimen layup. Even though the failure plot distribution is undesirable, the shear stress distribution envisions the problem with gaps - the absence of reinforcement tows imposes a greater load onto the surroundings, eventually 'overstressing' them. Nevertheless, the initial designed panels have major problems with both the magnitude of failure load and the manufacturability of tow steering.

The final concept started with the reduction of specimen size to be feasible for the testing equipment available at the laboratory. The concept features a symmetric and balanced base/supporting layup, upon which a few surface tows are placed at $+45^\circ$ and -45° angles for the respective sides. The resultant failure index distribution give a periodic, grid-like pattern in the extra tows, supporting the hypothesis of gap locations affecting off-axis tows. The load state of the tows under scrutiny proved to be homogeneous, thanks to so-called sacrificial tows. These tows help the load distribution, and even though they are anticipated to fail first in matrix failure, the axial residual strength is expected to help until the important surface tows exhibit the desired failure process. Specimen length gives additional help in the homogenization process, by damping the effect of grip zone constraints.

Despite the really promising simulation results, manufacturing and resource concerns conflict with the final design. The available tow material is 20-millimeters wide, while the favourable concept has tows that are 10-millimeter wide. The usage of wider tows exhibited inherent problems in creating uniform gauge section zones. Additionally, the larger tows are observed to be less vulnerable to gaps, reducing the chance to capture the main research problem. Attempts featuring narrower sacrificial tows next to wider, AFP-laid tows show some improvement. This being said, the reduced gap sensitivity of wider tows still raise some concerns. After all considerations, manual lamination is chosen for the extra $\pm 45^\circ$ tows on each side, with manually slit (halved) tows. The rest of the layup is still available for the wider tow AFP process. Despite violating a design requirement, the automated manufacturing one, a lamination process featuring acceptable accuracy is developed. The process will be discussed further in the corresponding chapter 5.

With a hopeful gauge section concept, the specimen design is finalized by elaborating on the details of tabbing and load introduction. With the help of tabbing guidelines, premature grip zone failure is countered, while the introduction of bolted clamping plates help the load introduction in homogenization, specimen protection, and safety. In-situ DIC and ex-situ microscopical cross-section images are chosen as investigation methods of the topic.

5

Manufacturing, experimental work

This chapter serves to introduce the specimen manufacturing and detail the experimental observations. The chapter starts with the manufacturing aspect, introducing the methods carried out until the finished panels (a total of six specimens were created). Then the testing procedure is documented (section 5.2), with the details of the testing outcomes. The AFP manufacturing process was done at the Smart Advanced Manufacturing XL (SamXL) centre, while the testing was carried out at the Delft Aerospace Structures and Materials Laboratory (DASML).

5.1. Specimen manufacturing

The material used is a toughened epoxy resin combined with high-strength carbon fiber, namely the 'MTC510-UD150-HS-37%RW' product from SHD Composites. This is a toughened epoxy resin system combined with high-strength carbon fiber. Typical applications are 'general purpose' and 'visual' components [103].

The available tow have a width of 20 millimeters, but in the surface tows, a 10-millimeter wide tow was found to be more desirable, as per the design outcome presented. For the support plies, the wider tow is advantageous, as fewer passes are needed to lay down the layers, therefore speeding up the process. Thus, for the tows under scrutiny, the original 20 millimeter width was halved manually, by the use of long metallic rulers and handheld cutting blades. The final tow widths were measured to be 10 ± 0.2 millimeters, which is in relative terms a larger deviation compared to the original 20 ± 0.25 millimeter, but in absolute terms they are comparable.

Moreover, tow ends in AFP systems are not under tension during lamination, which causes laid tow width change. This is an inherent problem of the manufacturing method because the tow termination (cutting) happens before the compaction rollers, therefore the rollers only run over loose material. This no-tension case causes a width change in the magnitude of 1-2 millimeters, depending on tow widths. Considering this, the deviation could be less important. Ultimately, in the context of anticipated fiber flow during curing, the tow-splitting accuracy is deemed acceptable. The length of the tows have the same order of magnitude of accuracy, which in relative terms (compared to the range of 100 millimeters of strip lengths), are also considered acceptable.

At this point, the tow shapes are manufactured up to normal standards, but positioning, especially with respect to gap sizes are of much importance. Hand layout of thinner tows could violate the requirements against a representative specimen if tow placement cannot be up to AFP quality. To counter this, an intricate placement method is used, assisted by a master template (see Appendix F). The template has the outer dimensions of the final panel, while also featuring grooves at the surface tow locations. It has a manufacturing tolerance of ± 0.05 millimeters from the water jet cutting machine. Thus, only the positioning of the template is needed, the tows with respect to each other are controlled by this simple device. The positioning is done by featuring two self-leveling laser lines. The process goes as follows, with illustrations on Figure 5.1 until Figure 5.4:

1. The robotic arm places tows onto the curing plate at the corners of the future specimens, marking out the machine coordinate system on the plate. These tows serve as references only.
2. The self-leveling laser lines are then positioned to the reference tows. These laser lines project the machine coordinate systems onto the whole plate.

3. The mentioned laser lines are transferred at the edges of the plate onto PTFE films. These films stay on the plate until the end of curing and are assumed not to move during manufacturing or curing.
4. At this point, the machine reference system is transferred to the curing plate. The laser lines can be re-positioned at any time to any marking, thus providing sharp and accurate reference lines. Two intersecting, perpendicular lines are sufficient to position anything over the 2D domain. The crossing point marks the desired spatial point, while either lines also mark the orientation. The use of laser lines is essential since these also project onto already laid plies, which would cover other types of markings - making it an "un-coverable" and "un-erasable" line.
5. The initial reference tows can be removed, leaving a clear area for the lamination process.
6. With the help of the water jet cut master template, the hand-laid tows can be laminated. The master template is positioned by the laser lines. The individual, prepared tows are placed inside the dedicated grooves.
7. The AFP lamination can take place after removing the template. After the automated placement, the laser positioning of the master plate can take place for the second batch of tows for the backside. This process is completely identical to the first case.
8. The laminate is fully placed, and ready for the vacuum bagging process.

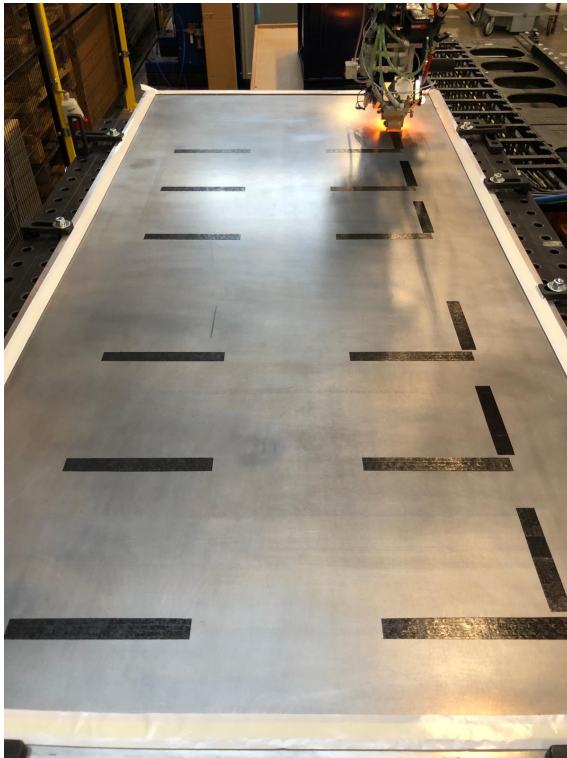


Figure 5.1: Reference tows laid by the robotic arm.

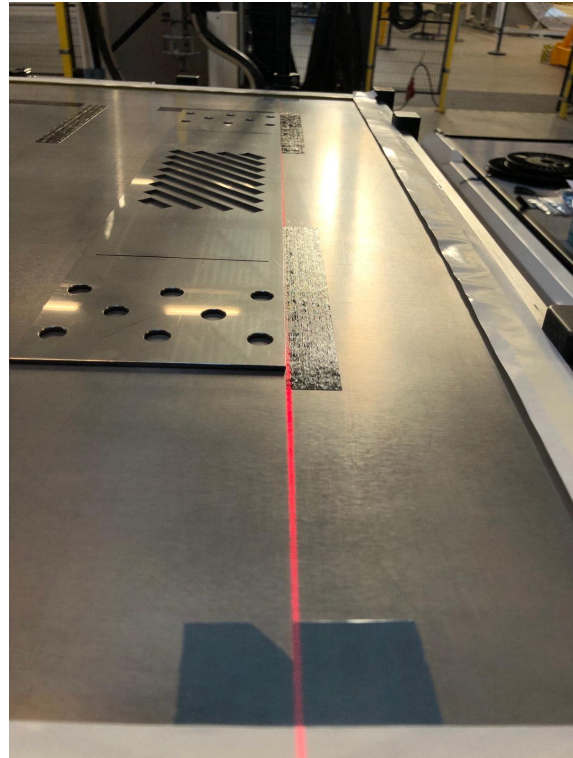


Figure 5.2: Reference coordinate system projected onto PTFE films. Master template positioned in the system.

The used robotic arm is a KUKA KR210 R2700 Extra product with 8 degrees of freedom (see Figure 5.7). The AFP head is an ADDcomposites AFP-XS product. Because of non-uniform tow widths and the previously introduced width deviation with tension, an offset (gap if you will) of 0.4 mm was set for the machine above the 20 mm tow width. This value was set after testing which offset came closest to a no-overlap no-gap state based on visual checks. The tows had a staggering of 50% or in absolute terms, 10 mm. The importance of this method has already been pointed out in literature ([63] [64] [76]).

At the first 10 mm tow length, the 'runway' speed was reduced to 5 mm/s. This slower speed is generally enforced to help the adhesion of the tow at laydown starts. This value is then increased to the 'laydown speed', which was set to 200 mm/s. The total time of AFP placement (so not including the manual tows) was 9 minutes per specimen. The compaction piston pressure was set to 3 bars. The

350 watt heating lamp was set to be 25% of the maximum power output. This low heating was enough for the laydown because the used prepreg material has high stickiness.

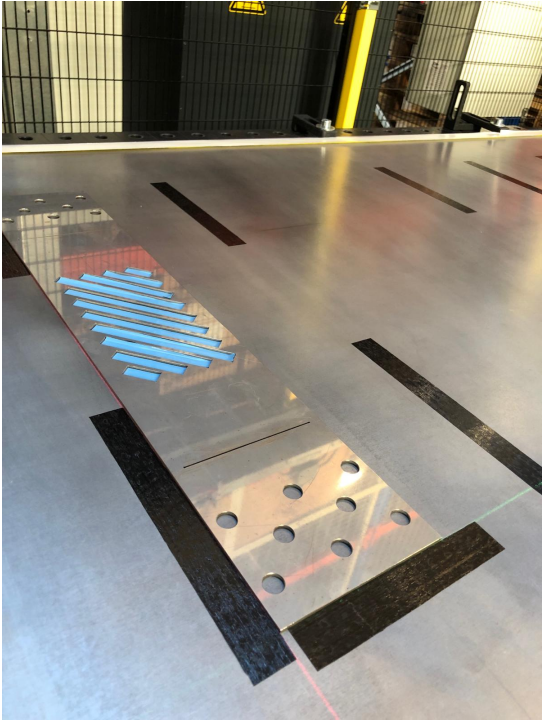


Figure 5.3: Jig plate positioned to laser lines. The template already used for lamination of the first layer with gaps



Figure 5.4: In-situ gap size measurement after lamination.

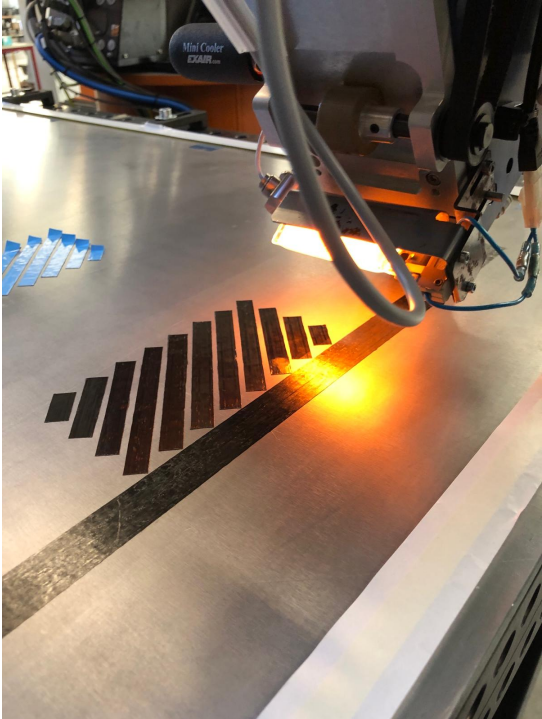


Figure 5.5: Automated laydown of material onto the hand-placed surface tows. The first axial AFP tows prove an accurate manual work.

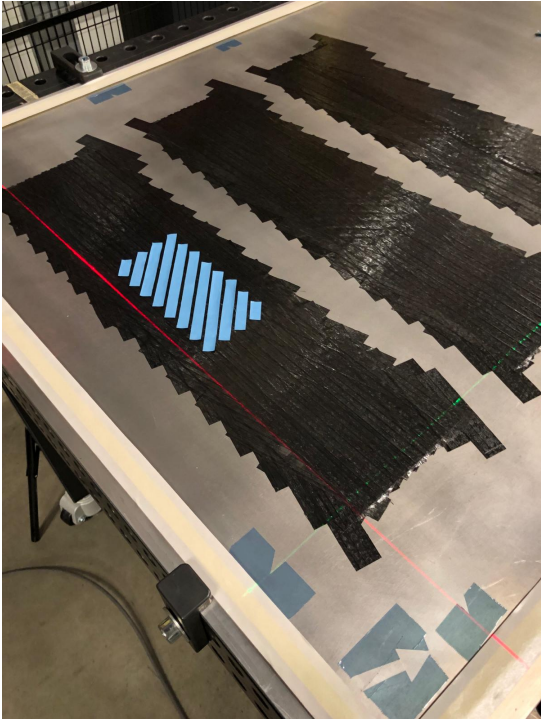


Figure 5.6: Laser lines on AFP laminate. The master template had already been removed after the final layer of surface tows.

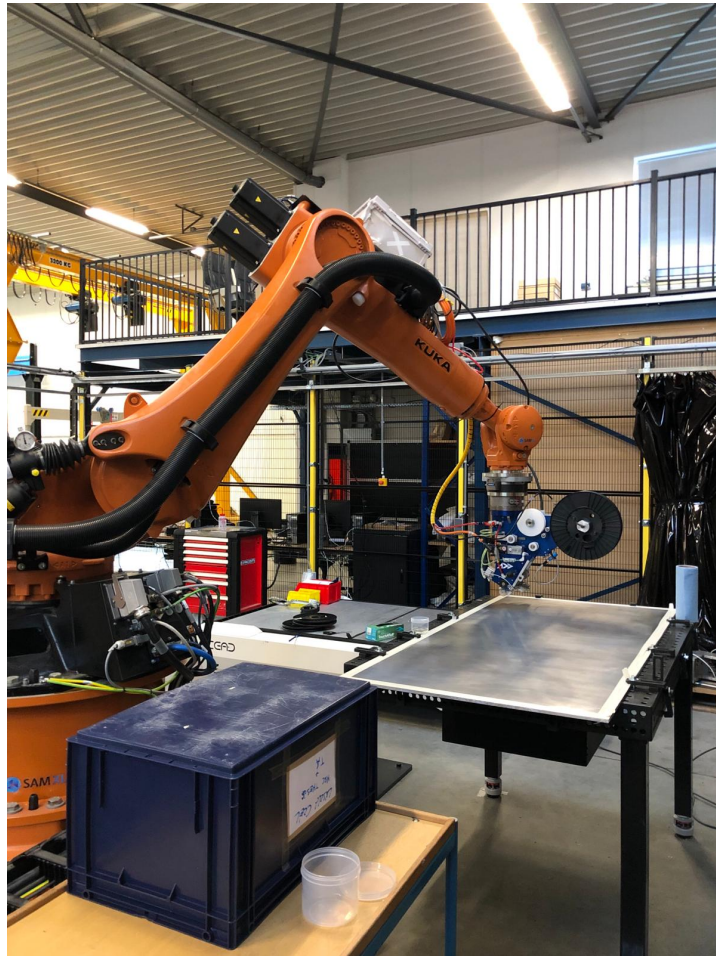


Figure 5.7: Used KUKA robotic arm with AFP head.

There were however some minor problems along the way with the automated process. The six specimens were processed as:

- Specimen 1: Tow developed folds on the first and sixth layers. During the spooling of the prepreg, a misalignment might have happened which forced a fold onto the tow in the AFP head. The folds were less than 1 millimeter in total width.
- Specimen 2: Went as planned, with no troubles.
- Specimen 3: At the last (eighth) layer, the tow got stuck at the so-called pinch roller, which applies tension onto the material. This then damaged the tow, which rapidly got laid down. Complete removal of this tow was not possible due to sticking down to the laminate, therefore it was patched by hand with some extra material where needed.
- Specimen 4: Tow starts were at incorrect positions in layers six, seven, and eight, meaning the tows started deeper inside the specimen. Since there was an extra offset to all directions for accurate trimming reasons, the problem did not affect anything in the final configuration. The reasoning for the problem is based on the braking of the AFP spools. During the process, the backing foil of the prepreg is spooled onto a shaft, which is also controlled by a magnetic brake. The braking pressure was eased after the previous problem, which made the foil loose. This loose foil caused inconsistent tow feed, resulting in insufficient material at laydown starts.
- Specimen 5: Went as planned, with no troubles.
- Specimen 6: Went as planned, with no troubles.

Apart from these issues, several others did not get to the final laminates, because with visual process monitoring, these were stopped in time. The majority of the problems are inherited from the sticky nature

of the prepreg tows. The tows must be aligned in a coordinated manner before the compaction rollers, which on the used head is solved by a so-called 'chute'. The chute is a longer, milled groove with about the same width as one chosen tow. In this about 10 centimeters of groove, the material gets aligned, however, at this stage, already without any backing foils. Any roller misalignment before the chute section could force the strip of material to develop folds or to develop wrinkles. A significant portion of the manufacturing time is taken with troubleshooting these problems, therefore advancing research on process improvement should be a rewarding endeavor.

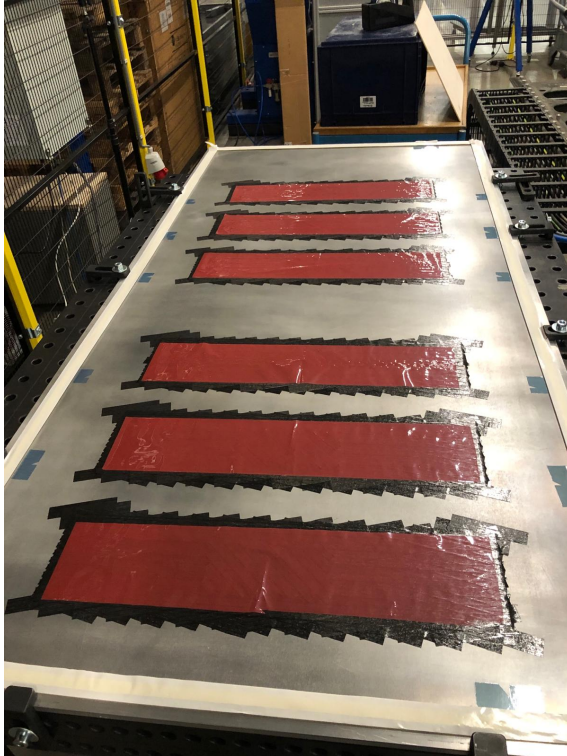


Figure 5.8: Release film on the complete laminates

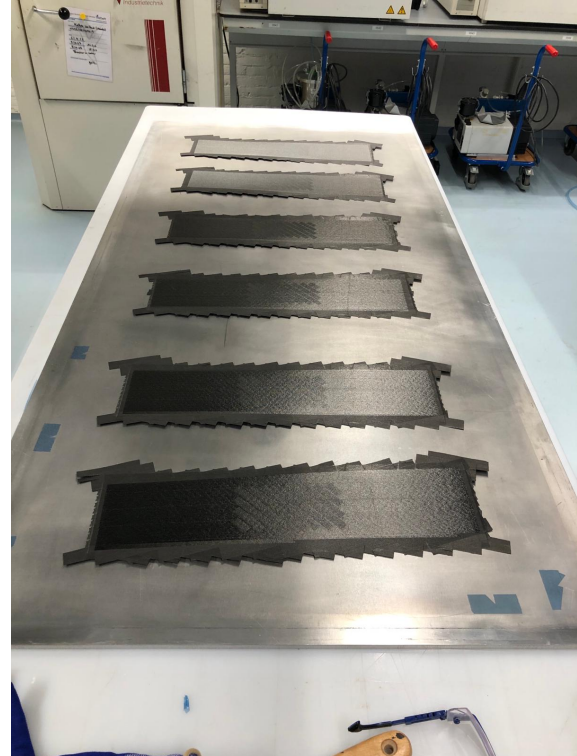


Figure 5.9: Cured specimens on the manufacturing plate.

Apart from the combination of hand layup and AFP, the other steps of the manufacturing process was according to industrial standards and practices. The plate, prior to the described lamination process, was thoroughly cleaned and treated with Marbocote 227 release agent. The placed layers received an AeroVac A4000 FEP unperforated release film on the top to control the resin content of the laminate in the middle with some free laminates all around (Figure 5.8). Above this, there was a 'Stitch Ply A' peel ply product, as a release layer. This step is implemented to ensure uniform vacuum on the important central parts of the laminate. The window-like zone of prepreg which did not feature any release film allowed vacuum to surround the stack up, and these zones were eventually discarded during the trimming process. Above the peel ply, Air weave N10 breather blankets were stacked on top of each other, in total 2 layers. This insulated the non-tooling side, eventually contributing to less temperature gradients between the plate and non-tooling sides. 'Wrightlon WL 7400' vacuum bag was used with 'AT 200Y' sealant tape to compact the laminate.

The curing cycle was chosen to be 1 hour at 120 C°, with 5 bars of pressure, as per the material data sheet. The autoclave software already had this material cycle implemented and saved, therefore it was used. Prior to the mentioned 1 hour at 120 C°, a dwell of half an hour was set at 90 C° (with 3 bars of pressure). This being said, the monitored curing cycle is presented on Figure 5.10.

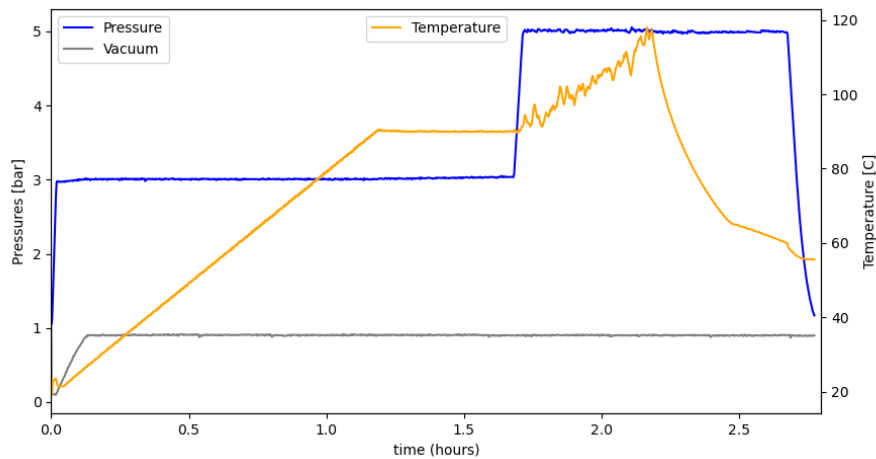


Figure 5.10: Logged curing process parameters.

As can be seen, the temperature ramp-up and the dwell went as planned, but the final ramp-up encountered some serious issues. The instability of the step is significant and even worse, the whole next plateau at this temperature is skipped. The origin of the issue is unknown. Although the curing cycle was strongly cut short, the final specimens were still judged as fully cured upon visual and physical investigation, and also based on microscopical images (which will be shown in section 5.2).

The cured laminates had a small warp, which was anticipated from the anti-symmetric layup. The laminates could be flattened by one gentle finger push, which means the specimens are also compliant with the ASTM specimen guidelines (Figure 4.16). The laminates upon both visual inspection and physical touch were found to be smooth, with no significant out-of-plane texture from the additional tows. An important observation, however, is the cured gap size. As Figure 5.11 shows, the gap size was reduced from 3 millimeters to about 2. Some tows were observed to be 'floated' away due to pressure during the liquid flow state of curing. This inhibited drawing any specific conclusions with direct respect to an exact gap width, nonetheless, the influence of the manufacturing defects could still be inspected in a general manner.



Figure 5.11: Cured gap size width of around 2 mm instead of the 3 mm set during lamination

The master template was also used for the drilling of the holes, as it had cutouts for this manufacturing step as well. For the drilling of 10 millimeter holes, 'brad point' drill bits were used, which differs from the usual drill bits in cutting geometry. These types of drills cut at the circumference of the hole, instead of the whole circular section, leaving a cleaner cut for composite laminates, without excessive delaminations. The exact drill bit is presented on Figure 5.12.



Figure 5.12: 'Brad point' drill bit used for the drilling of bolt holes.



Figure 5.13: Cutting machine with a diamond blade used for the fine trimming of the specimen.

As a next step, the laminate was trimmed to final dimensions. It must be noted, that a positive offset of 0.5 millimeters was applied per side. This was for the tabbing plates, so in case of any slight misalignment, the tabbing plate is still bonded on the whole surface, and no plate is overhanging. The trimming was done on a dedicated machine with a diamond-coated cutting disc developed for fiber-reinforced composites. This machine ensured parallel cuts for the longer sides while leaving an almost polished level surface finish. The cutting feed was 0.1 millimeters per passing, thus, the total specimen was cut in 13 passes, all with coolant water. The specimen inside the cutting machine is presented on Figure 5.13.

For the tabbing of the specimens, Scotch-Weld EC-9323 B/A high-strength adhesive was used. The laminates were surface-treated with 120-grit sandpaper, while the tabbing plates were sandblasted. After masking the untabbed surfaces, the adhesive compound was applied to the surfaces with some 100-micrometer glass beads, which control the bonding thickness over the tabs. The curing adhesive assembly was put into a vacuum bag with lower vacuum values (0.7 bar absolute pressure). The vacuum bagging ensured a homogeneous pressure over the entirety of the bonded area. Above the bagging, some extra weights were used to counter any remaining inhomogeneity from the warping of the laminates. The process is presented on Figure 5.14.

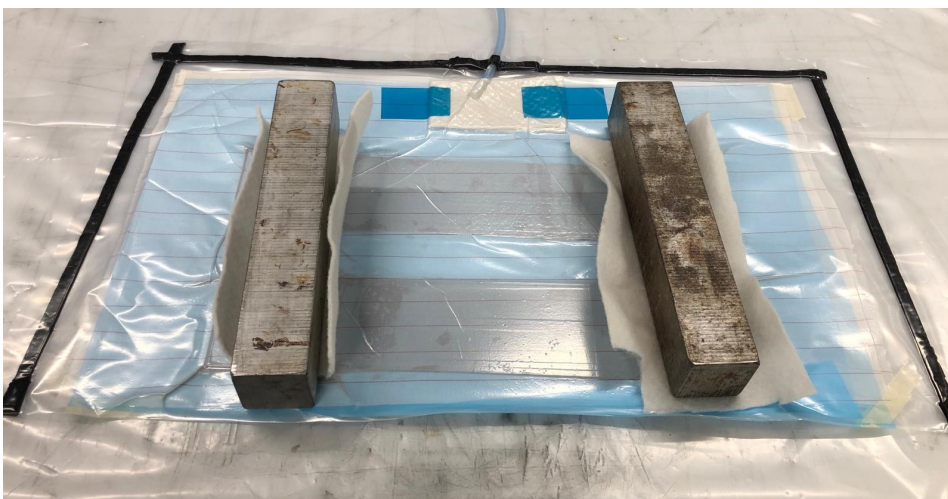


Figure 5.14: Tabbing process during the curing of the adhesive.

The Digital Image Correlation (DIC) method was chosen as an in-situ measurement of the tensile tests. Out of the six produced samples, four were chosen to feature DIC, while the remaining two would stay clean. By doing so, the location of micro-cracks would be evident in those specimens, because the DIC process requires a high contrast, random speckle pattern over the investigated field. Since one clear specimen could just happen to be an outlier in tendencies, two were chosen for the sake of higher confidence in capturing visual tendencies and events.

The available 3D camera setup had a resolution of 2448x2048 pixels ('vertical' x 'horizontal'). As a rule of thumb, one speckle should be at least 4-5 pixels large, this way, the output will have less scatter and noise. Since the specimen width is 100 millimeters wide and 2048 pixels should cover this dimension at best, the speckle size becomes:

$$\text{Speckle size} = 4..5 \frac{\text{specimen width}}{\text{resolution}} = 4..5 \frac{100}{2048} = 0.195..0.244 \text{ mm} \quad (5.1)$$

The field of view of the camera was anticipated to be almost filled out with a specimen, however, with also having some background at the edges. In other words, a complete fit is impossible to achieve, so as a conservative approach, some visible background was expected next to the specimen. In practice, this means the real speckle pattern should be somewhat larger than the calculated size (0.25 mm and larger). The DIC kit contained stamp rollers, which have speckles with precisely defined sizes. As a reference, the 0.013 inch (0.33 mm) roller was used for reference on blank paper. After painting the samples with a bright, clean white base, the black speckle patterns were carefully painted over it. The final specimens are displayed on Figure 5.16.

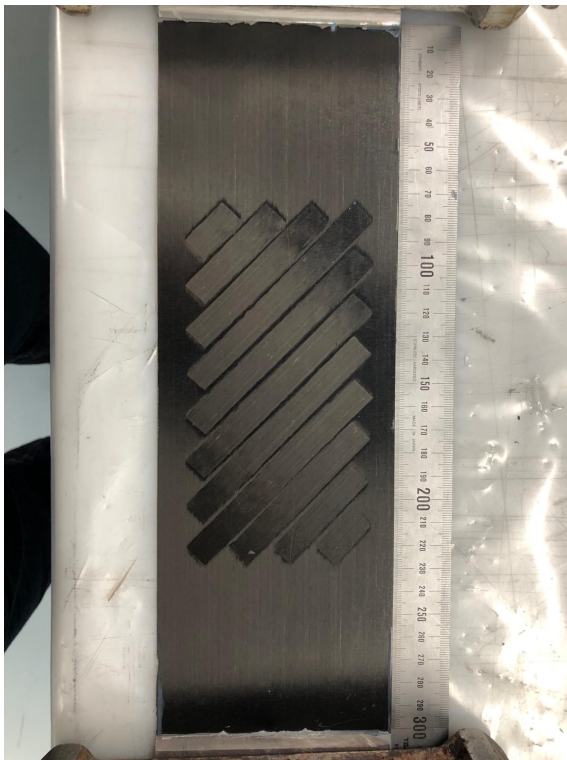


Figure 5.15: Finished specimen's gauge section.

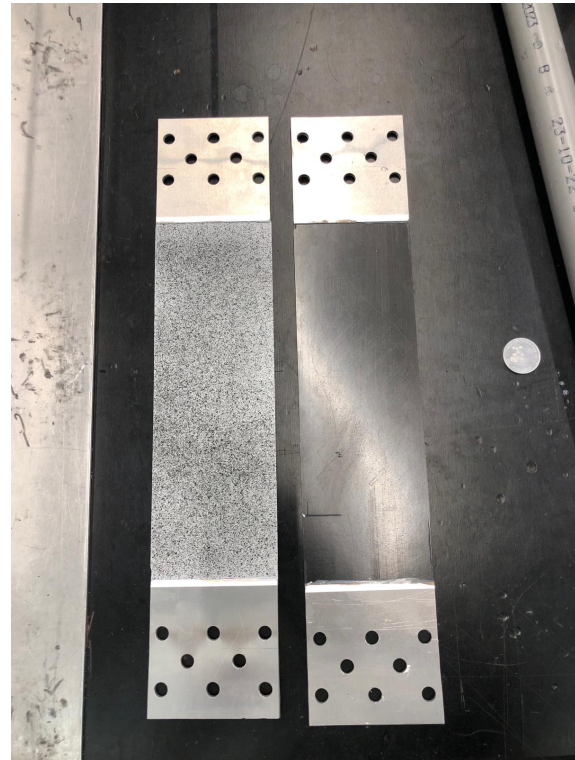


Figure 5.16: Final specimens with and without DIC patterns, all tabbed up.

5.2. Testing

5.2.1. General testing outcomes

The tensile tests were carried out on a Zwick Z250 universal tensile tester machine. The testing setup is presented on Figure 5.17 and Figure 5.18. The first two samples were the ones without speckle patterns, and the last four had DIC recordings.



Figure 5.17: Clean specimen with clamping plates.

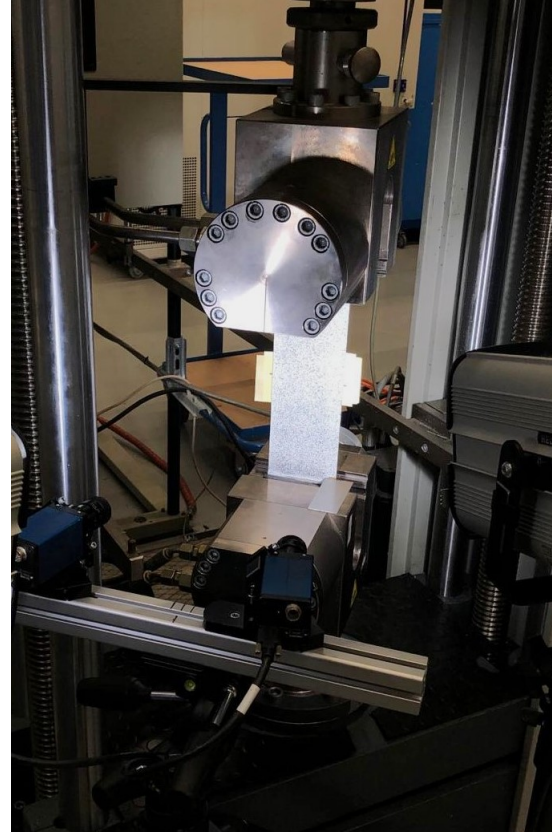


Figure 5.18: Specimen with DIC speckle pattern.

It must be noted, that the specimens were not tested in the order they were manufactured. After torquing down the bolts of the clamping plates, the first specimen was inserted into the machine. Upon loading, clamping problems occurred between the hydraulic grips and the clamping plates, perceived as slips at 70-90 kN loads. It was assumed to be originating from the frictional coefficients being lower than expected, which eventually was proven. Cleaning of the grips from hydraulic oil and grease helped to achieve higher loads (110 kN) but still wasn't enough compared to the 160 kN range. Increasing the hydraulic pressure from 250 bars to 350, and applying 'drywall sanding screen' proved to be enough eventually to reach forces in the desired range. The latter is, as the name suggests, used in drywall applications, and is essentially a mesh with sandpaper-like surface on both sides. In practice, it raises the coefficient of friction between the adjacent surface pairs.

The first specimen (after three runs with frictional problems) was tested until 140 kN and already showed some microcracks. The cracks were visualized by some white paint dissolved into it, similar to dye penetrant testing. The outcome is presented on Figure 5.19. All other specimens had similar microcracks and distributions. Some major cracks are located at backside gap locations - take the top right corner of the displayed gauge section, where significant cracks are aligned in a straight line perpendicular to the tows. To repeat once more, the main hypothesis was that gaps cause a local matrix-governed failure. However, the testing outcome falls short of reinforcing this hypothesis. Plainly, not enough major cracks appear and/or align with the desired (gap) locations, burdened by the homogeneous distribution of really fine cracks.

Above the disproved hypothesis, there are several other outcomes and observations, which might bear even higher (scientific) value. One of these is that none of the specimens exhibited cracks along

the gap interfaces, at the resin-rich regions. The other outcomes are connected to the DIC results and microscopical images, introduced in the further text.

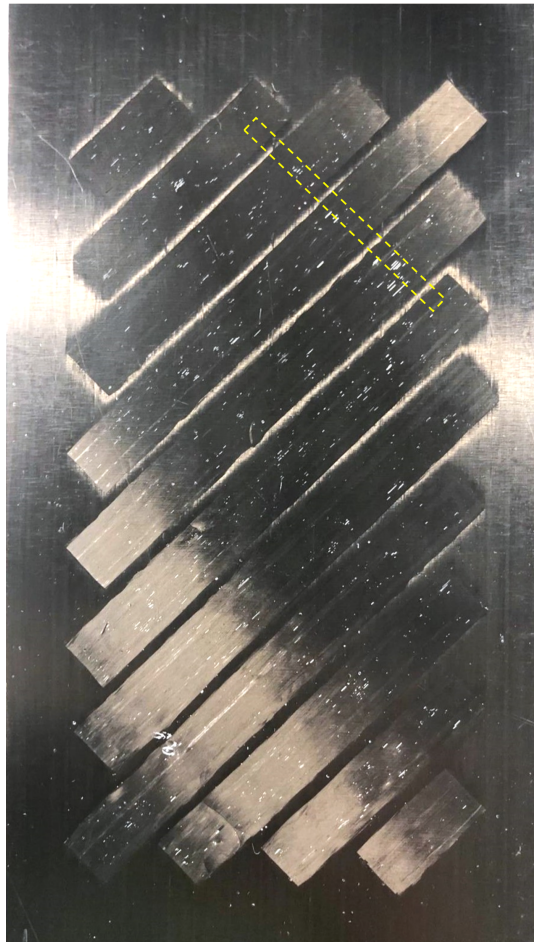


Figure 5.19: Microcracks on the flat side of the first tested specimen.

The next specimen, unfortunately, had a failure inside the clamping zone at 143 kN. At this point, excessive bearing stresses were reasoned for the fracture, since the bolts were almost a press fit during installation. As a solution, the next specimen's holes were re-drilled to be 0.1 mm larger in diameter. This resulted in a looser fit of the bolts. However, the same happened to the third test, with the same fracture surface at 150 kN. This characteristic fracture surface is displayed on Figure 5.20.

While making the holes a looser fit didn't help much, the clamping plates were discarded, and the specimens were directly placed between the grips. A help in this matter came from the geometry of the tab. As Figure 4.21 (left) shows, the tab had a full cross-section towards the tapering for a significant length, as opposed to the bolted area having -20% or -30% locally. Thus, the grips were clamped directly at the start of tapering. This way, the next specimen reached an admirable load of 189.5 kN (almost 1900 MPa of applied stress), and the test was interrupted before an explosive failure. It was mentioned by articles [64, 72, 78] and the author of the thesis, that having gaps at free edges could lead to incorrect characterization, as weak points in such locations should show different behavior. Thus, the edges were closed out from the sample's boundaries. Great feedback for the choice is the mentioned fourth specimen, which developed a thin strand from delaminating the top layers on each side, about 3-4 millimeters wide. This strand is thought to be a result of edge effects at work (and has nothing to do with gaps). If this specimen had gaps at the edges, it would have failed with misleading consequences in the author's opinion. The strand is presented on Figure 5.21.

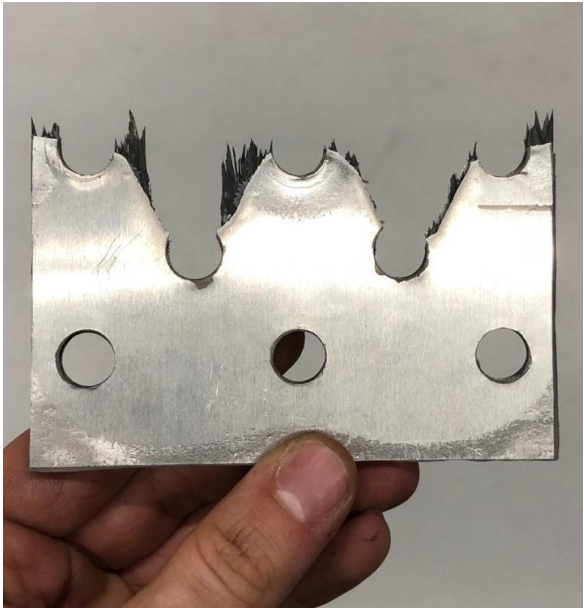


Figure 5.20: Typical fracture surface for the inside.



Figure 5.21: Delaminated strand at the edges of the specimen.

The fifth specimen suffered a net section failure at 167 kN. The crack started from the edge of the specimen and propagated into it while going around the gauge section. This makes sense considering the gauge section has extra layers (tows), meaning that it should be stronger. Simultaneously, a failure within the grips happened once more. Grip failure is speculated to initiate the gauge section, as during failure, stored elastic energy was suddenly released, in a snapping mode. Even if this is true or not, the crack propagation path provided a useful hint about the specimen nature.

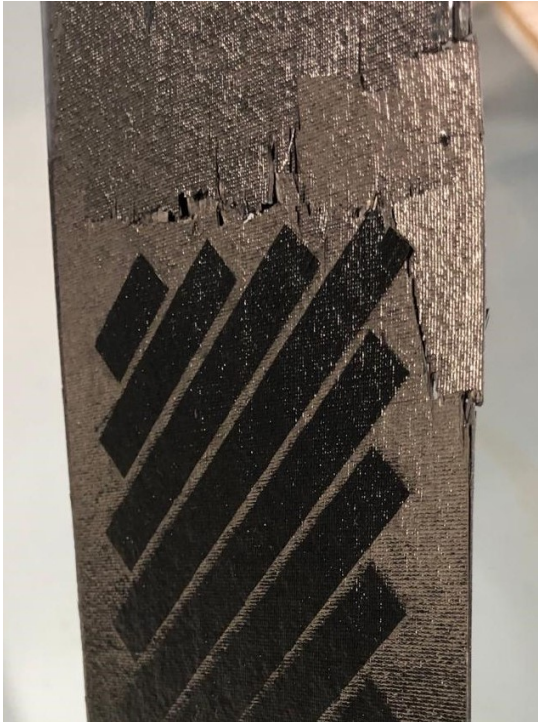


Figure 5.22: Net section crack going around the gauge section.

The last specimen also had a grip section failure at 146 kN, making it four out of six specimens affected by this unwanted failure mode. Although this being said, the failure load was enough to load

up the surface tows enough to facilitate microcracks in all of the mentioned specimens. The cracks, interestingly, were only found on the flat side of the specimen, while the rough side showed no sign of cracks. This is thought to be from the thick resin layer, which had enough deforming capabilities, and not from secondary bending or similar events. The visual observation is reinforced by dye-penetrant testing, which is displayed on Figure 5.23 and Figure 5.24.



Figure 5.23: Flat side dye penetrant testing.



Figure 5.24: Rough side dye penetrant testing.

5.2.2. DIC measurements and results

The DIC process is a non-destructive testing method based on optical principles. The investigated specimen must have a characteristic pattern over its surface, which pattern could be tracked over the measurement process. Differences in tracked images result in deformation (and rigid body motions). By knowing the deformations (and rigid body motions), the strains and curvatures can be calculated for each spatial point, amongst other interesting outputs. The used DIC system was a 3D/stereo unit, meaning that it could capture deformations and strains not only in a planar case but also in 3D space. This was needed because of the initial warping of the specimens, and besides it is always a 'safer' choice, as any small out-of-plane deformations appear as measurement errors in a 2D/mono system. The cameras had a resolution of 4 megapixels (2048x2048 pixels) each and were oriented with about an angular difference of 25 degrees relative to each other. The focal length of the used lenses was 35 millimeters, and the devices were placed about 600-650 millimeters from the samples. The cameras (sensors) had a pixel size of $3.45 \mu\text{m}$. The setup is visible on the already presented Figure 5.18 (the specimens had strong lighting conditions, therefore the equipment is a bit underexposed to show the testing environment). The cameras had some excess field of view, as discussed earlier, and were calibrated using 'calibration targets'. A calibration image is presented on Figure 5.25.

Apart from the calibration, the subset size must be set as well. As mentioned previously, this subset defines the size of the characteristic areas to track. Generally, a larger subset results in lower resolution but also low random noise, whereas a small subset results in higher resolution but also higher random noise. The measurement software (Vic-3D) has a built-in function to suggest an optimal subset size, which yields the smallest measurement error. This value was usually fine-tuned for every specimen, in order to also obtain good spatial distribution of low errors. This process is shown on Figure 5.26. After calibration and subset setup, the average measurement error (therefore the accuracy) was 0.023 pixels. It might sound counter-intuitive to have sub-pixel accuracy, but current software can go into

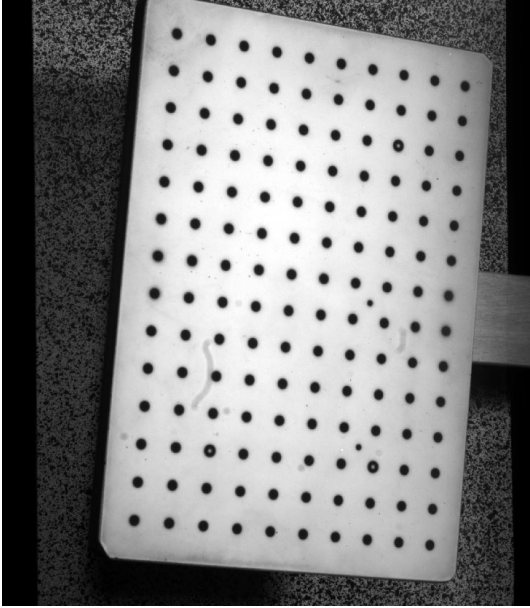


Figure 5.25: A calibration image for the stereo DIC system.

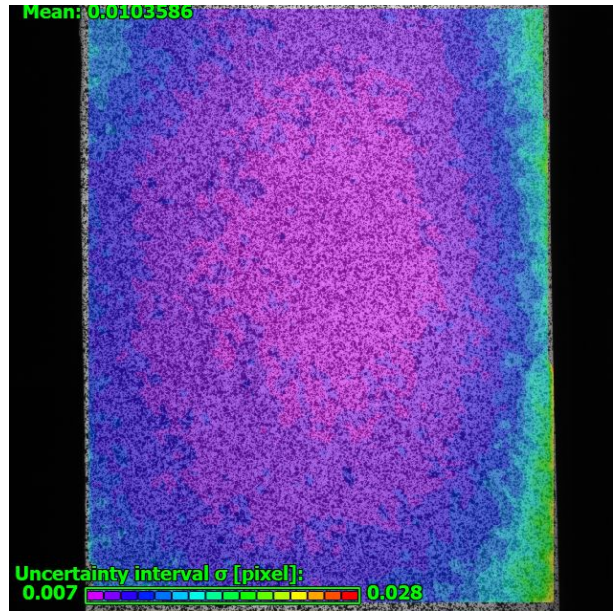


Figure 5.26: Subset optimization algorithm, with accuracy distributions over the specimen.

sub-pixel levels. The mentioned accuracy can be converted into deformations in the specimen plane if one knows the pixel size in the camera, the focal length in use, and the distance of the object from the setup. The latter two give the 'scaling ratio', thus, the value is estimated in the midplane of the specimen to be 0.00149 millimeters:

$$\sigma_{displacement} = d_{pixel} \frac{z}{f} \sigma_{pixel} = 3.45 \cdot 10^{-3} \cdot \frac{65}{35} \cdot 0.023 = 0,00149 [mm] \quad (5.2)$$

In the equation, d_{pixel} is the pixel size, f is the focal length, z is the object distance, σ_{pixel} is the standard deviation in pixels, while $\sigma_{displacement}$ is the same in millimeters. The results of the DIC sampling resulted in the same tendencies and distributions for the important outputs, though the magnitudes have some deviations. This being said, the final failure loads also differ, therefore only one specimen's (Specimen no. 4) results will be discussed here. Except for the initial warping plot, all other values were calculated for the maximum force point (last moment before failure). At this point, the spatial differences are most pronounced for all variables. The rigid body motion is deducted from the data, and all are plotted on a best-fit plane. The mentioned warping plot will not be discussed in detail in the main text, it can be found in Appendix D.

It must be emphasized, that the calculated strain and curvature values are calculated in two coordinate systems. For the longitudinal and transversal strains, the plots are in the loading coordinate system. These are the first two plots. The last plots are aligned with the 45° direction, parallel to the front side tows. Using Figure 4.14, in the last plots the reference X axis is parallel to the blue arrows (though pointing in opposite direction), while the Y axis is exactly as the red arrows are (same direction too). For all diagrams, the reference system is displayed, with red colors marking the plotted direction (if applicable).

The first plot (Figure 5.27) is the vertical engineering strain ϵ_x . This is the engineering strain aligned with the loading. The scale end is 0.012 micro-strain, meaning 1.2% strain. Note, that the lower end (0.9%) is set to articulate the differences best, therefore the total scale represents a 25% absolute difference. Globally we can see a larger strain on the left side of the image, this is thought to be the result of some misalignment in the testing machine (10% between sides). The strains at the edges are at about 1..1.2% strains. This magnitude of deformation is quite plausible at these loads, which can be verified by some simple considerations. The E_1 modulus of the original material was 110 GPa based on Ranji et al. [99], which is significantly lower than the usual high-strength fiber epoxy laminates, which feature 135-140 GPa of axial modulus [104]. Using CLT, the supporting plies should have an equivalent longitudinal modulus of 100 GPa using the material inputs (Table 4.1), and 122.5 GPa using a more common E_1 value. The load corresponding to the plot is 150 kN, and the cross-section was 101 mm², giving an applied stress of 1485 MPa. This with the mentioned modulus values gives 1.485% and 1.2% strains. Therefore, the magnitudes of the output are verified as a first estimate, and rather, the validity of used data input is strongly questioned.

The contour of the front and also the back tows is quite articulated, which appears in a periodic plateau of higher strains and small peaks of low strains. The low strain peaks come from the fact that the additional tows are surrounded by axial plies (at gaps, these plies are visible), which are much stiffer in the loading direction. The strain peaks are in the front tows, as visible, but with respect to the backside tows, it is harder to see. Interestingly, the peaks are at backside gap locations, which gives positive feedback to the research hypothesis that gaps negatively influence the surroundings' matrix phase (the plotted strain is not parallel with fibers, hence matrix distortion is included). The magnitude of peaks is about 4-5%.

Apart from these, the highest and lowest peak areas at the edges of tows could be inherited from the fact that at the termination of tows, the stiffness could drop due to the fiber ends being looser than in a constrained ply. Some singularities are found in the dataset, which are thought to come from speckle pattern problems and/or reflections during testing.

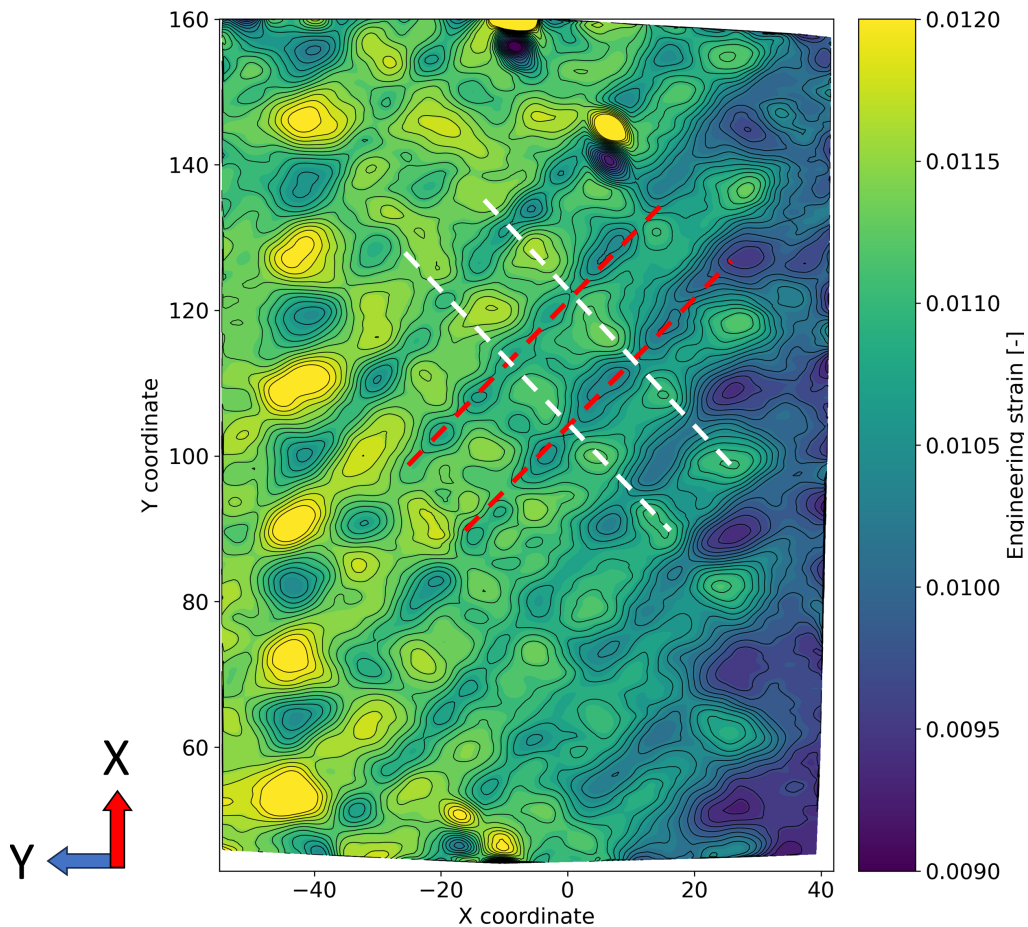


Figure 5.27: ϵ_x strain component distribution. Red dashed lines show frontal gap lines, white present backside gap locations.

The second plot (Figure 5.28) is the transversal engineering strain (or horizontal engineering strain) ϵ_y . This strain component is perpendicular to the loading direction, therefore the poisson ratio give negative strain values (contraction) - note the coloring direction with respect to the scale. The largest contractions are also on the left side of the specimen, which could be anticipated by the previous plot. The tows are less articulated than in the prior case. The tows have smaller contractions than gaps (UD), which is from the fact that tows are more aligned with the 90° direction. The distribution shows some peaks inside the additional strips. The coloring might mislead some, but these peaks are in absolute terms, meaning less contraction can be observed in those areas. Overall, the backside has less effect on this variable, but some peaks still align with the backside gaps, just somewhat less pronounced. This alignment is somewhat contradictory with the previous case, as more tensile strains should mean more contraction too.

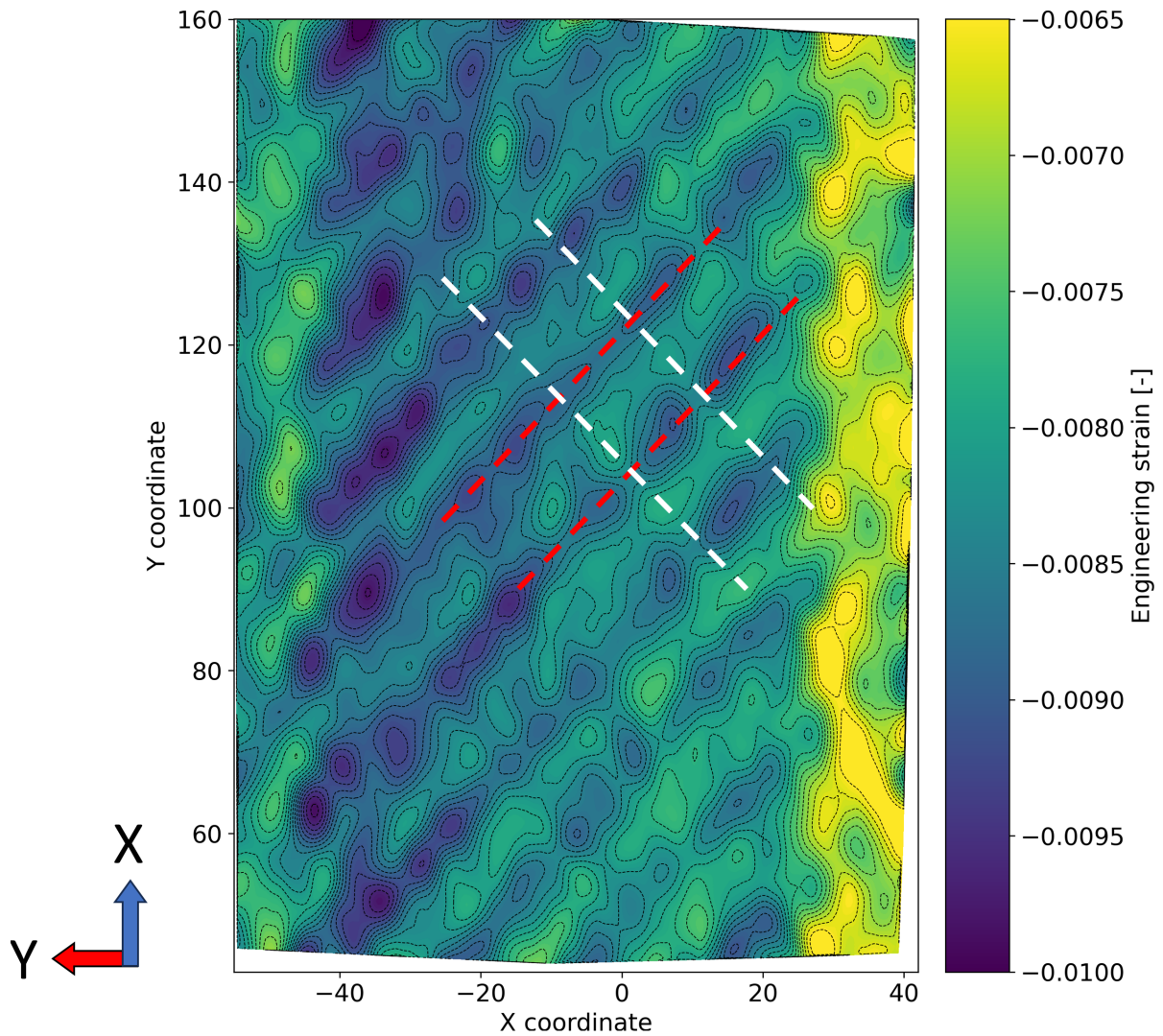


Figure 5.28: ϵ_y strain component distribution. Red dashed lines show frontal gap lines, white present backside gap locations.

The third plot (Figure 5.29) is the first in the rotated coordinate system. The diagram shows the principal strain distribution of the sample. This should be the most important DIC result, as the anticipated failure pattern is mainly governed by shear stresses. The principal shear represents the maximum shear deformation in-plane, similar to the principal strains representing the maximum values of a strain tensor. The coloring scale represents a 17% absolute difference. The absolute values of shear strains change with respect to coordinate systems, even though the distribution is the same in all orientations. The reason for quite high magnitude of values in the presented case is unknown.

The tows are very articulated once again, and the backside gaps also affect the strain distribution. However, the opposite way to the FEM prediction - the backside gaps did not impose extra deformation (thus extra load), but rather less than other areas in the surface tows. The peak shear values are in the additional tows, however, in between the repetitive backside locations, or in other words where the local layup featured 45° tows on both sides. Thus, it is observed that the tows couldn't get loaded up more at the backside gap location for some reason, which was originally anticipated based on FEM results (deeper discussion and comparison between the two in chapter 6).

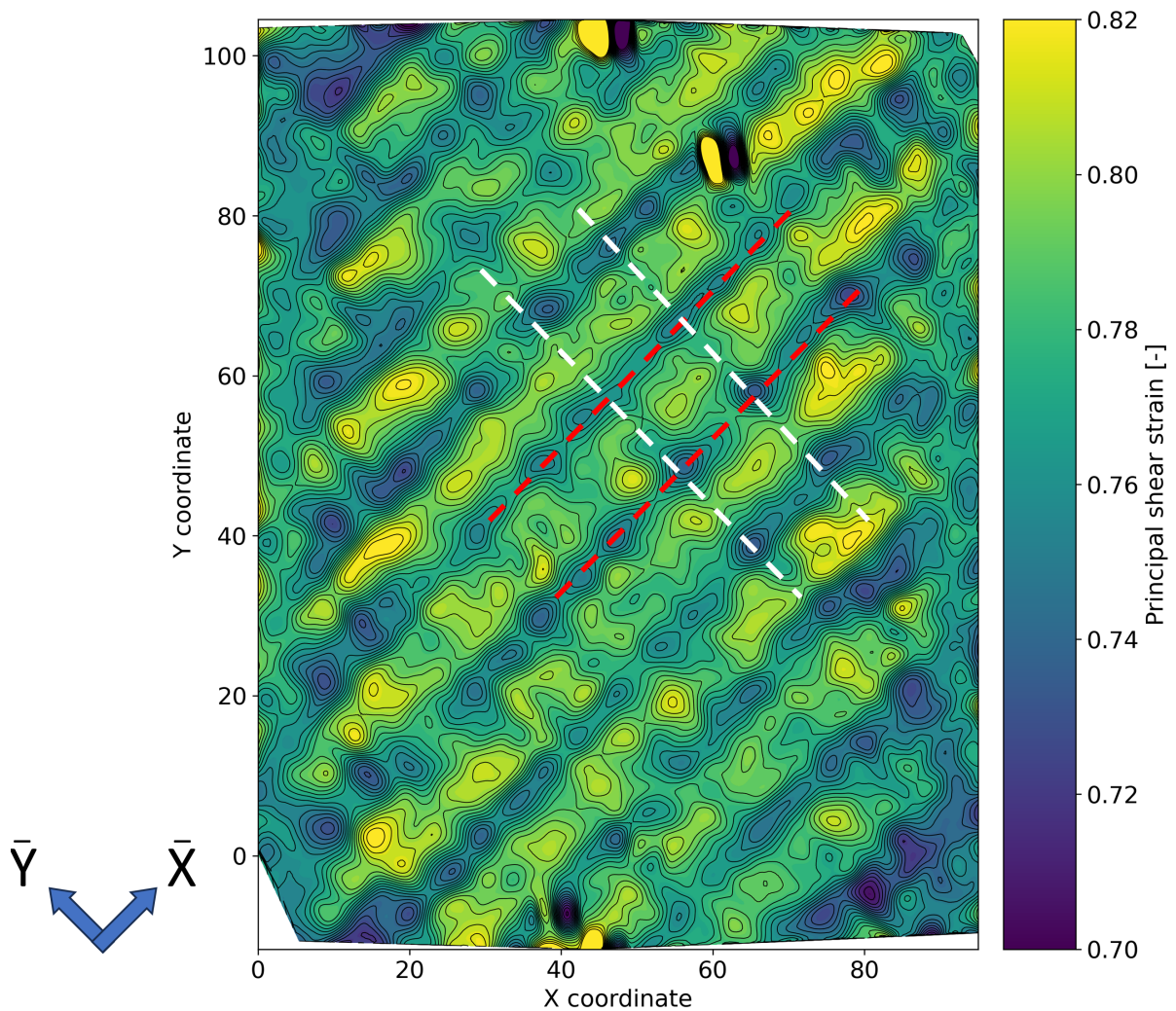


Figure 5.29: $\gamma_{principal}$ strain component distribution. Red dashed lines show frontal gap lines, white present backside gap locations.

The next plot (Figure 5.30) is the curvature along the \bar{X} axis. It might be easier to perceive it as the curvatures in the \bar{X} normal plane. The DIC software calculates the results for diameters, therefore the 2x multiplication must be kept in mind for a full understanding of the absolute value output. This being said the distribution over the field matters more than the values.

The frontal tows are outstandingly pronounced, leaving a positive ('upwards') curve at frontal gaps (bright yellow lines). This, in basic terms, means that upon loading the gaps are revealed, essentially leaving a 'ditch' between the additional strips of materials. Within the tows, the curvatures don't have exact tendencies, rather just leaving one arch or saddle shape between ditches. Therefore the main outcome here is the through-the-thickness motion of the plies, which are thought to be the axial layers flattening out during loading. The out-of-plane difference between a ditch and a local highest point is about 0.02 millimeters, equaling 10-15% of one-ply thicknesses. Therefore, the observation must be dealt with in consideration of its magnitude. The understanding is aided by Figure 5.31 obtained directly from the DIC post-processor software.

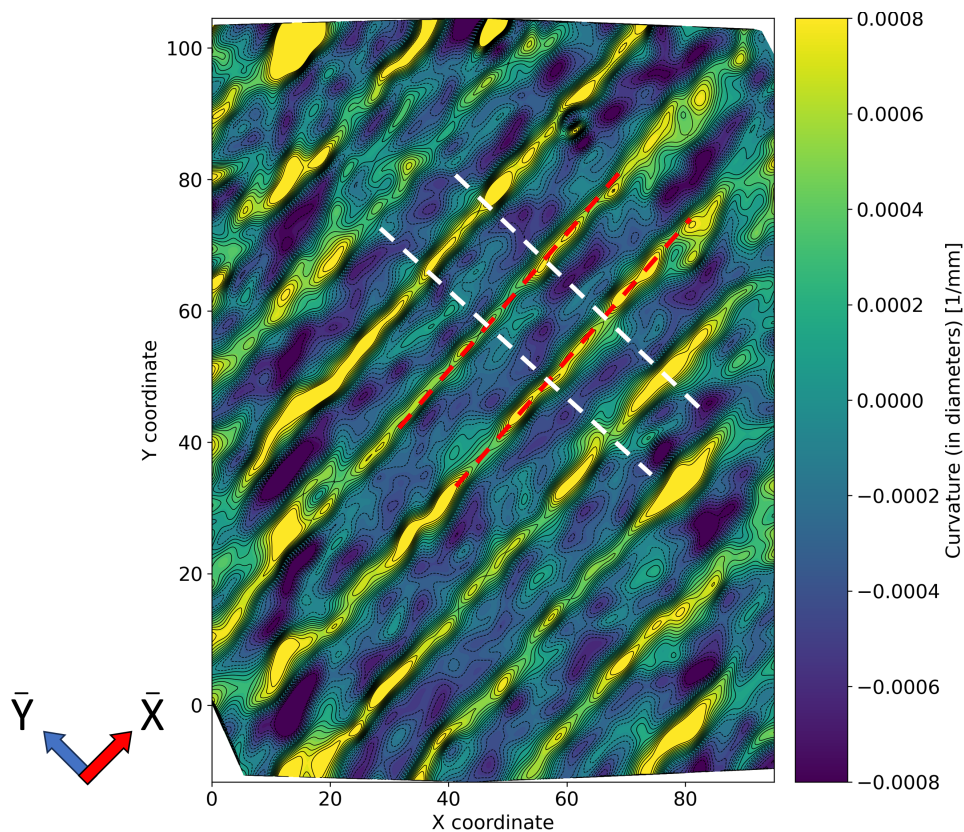


Figure 5.30: Reference directional curvatures in the rotated system. Red dashed lines show frontal gap lines, white present backside gap locations.

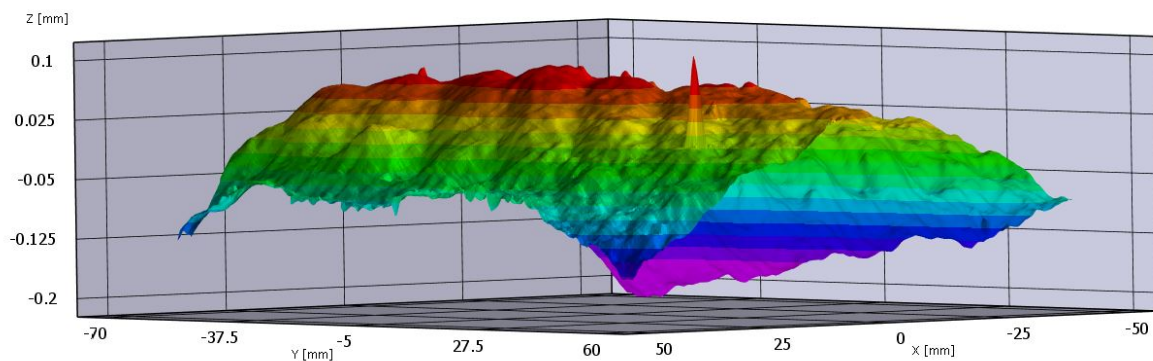


Figure 5.31: Surface topology of the specimen before failure. The gap locations were revealed in the form of pronounced ditches. The Z direction is not to scale.

The last major plot (Figure 5.32) is the curvature along the \bar{Y} axis. Following the previous explanation, these are the curvatures in the \bar{Y} normal plane. This plane is normal for the backside tows, therefore the results are expected to be connected to these additional strips.

The curvatures reinforce these visions, as there is a repetitive pattern along the mentioned layout. Opposite to the ditches in the previous plot, there are dark blue lines with negative curvatures, meaning these are small 'ridges'. These exactly align with the backside gaps, although in magnitude, smaller than the previous diagram's phenomenon. This is thought to be from the same origin, namely the rear side axial plies flattening out upon loading, which eventually push outwards in the front. The repetitive saddle shapes therefore exist in both directions, but the difference lies with the peak/ditch location - from front perspective: frontal gaps become ditches, and backside gaps become peaks. This being said the difference between peaks and local lows is 0.005 millimeters, or 3-4% of a ply thickness, which is also not quite substantial. Figure 5.33 helps understanding of the tendencies on the 3D surface topology. The blue lines of both plots mean the same, though the latter diagram features a rainbow coloring scheme. The Z directional topology is not to scale.

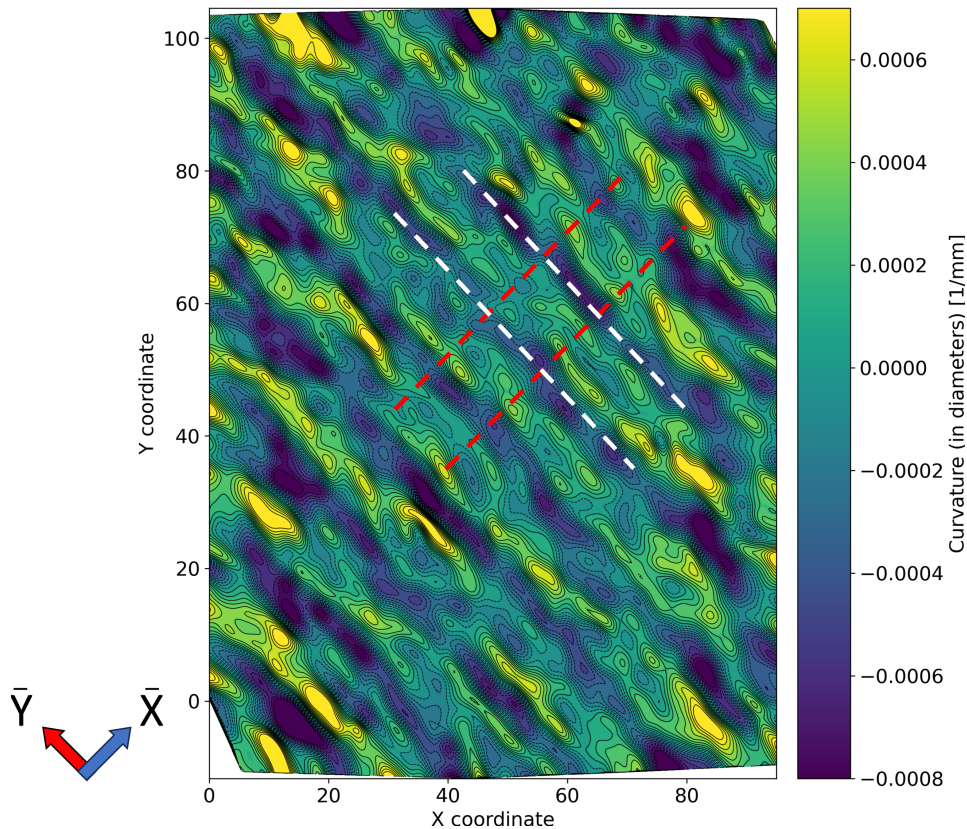


Figure 5.32: Transversal directional curvatures in the rotated system. Red dashed lines show frontal gap lines, white present backside gap locations.

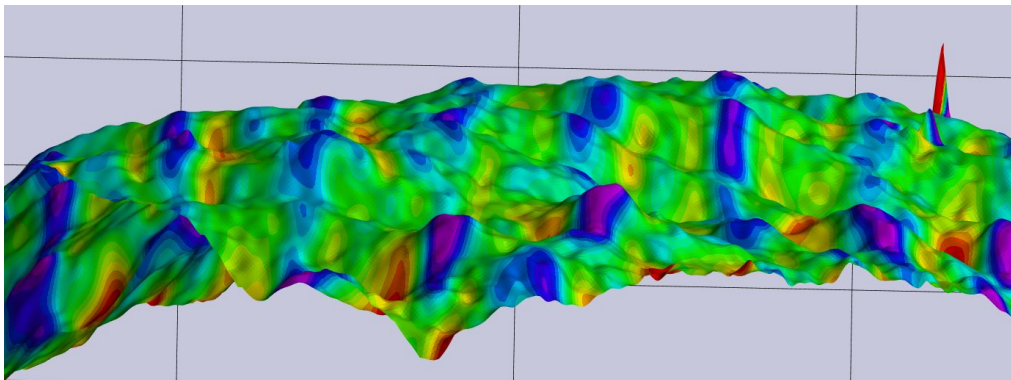


Figure 5.33: Transversal directional curvatures on the 3D surface. The backside gaps built subtle saddle shapes. The Z direction is not to scale.

5.3. Microscopical observations

Several polished cross-sections were prepared for (optical) microscopical observations. All cross-sections were cut perpendicular to the line of gaps, leaving the sections normal to tows as well. First, for the actual gap sizes, Figure 5.34 presents an accurate measurement of a gap post-curing. The original 3-millimeter gap size was actually reduced to about 2.5 ± 0.3 millimeters (from 10 cross-sections). This was thought to be a result of resin getting into a liquid phase and flowing during curing with fibers, as discussed earlier. There is also a variation between the values, as it could be from hand lamination and also from unequal tow widths besides the mentioned aspect.

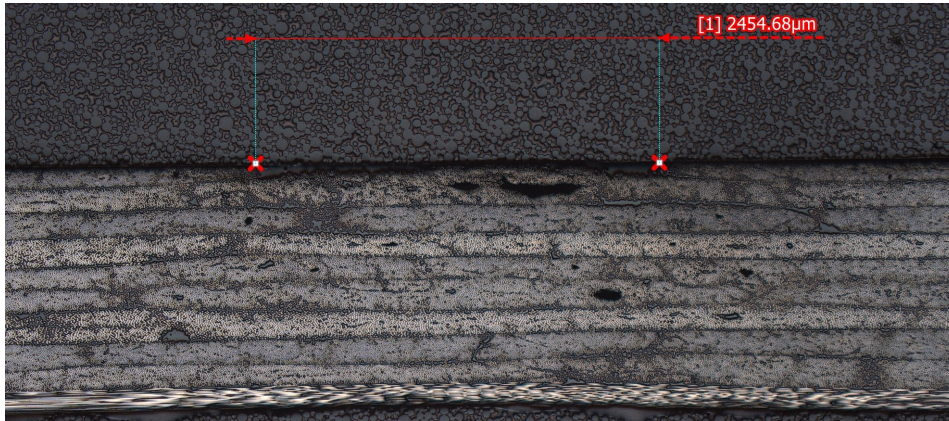


Figure 5.34: Microscopical measurement of gap size.

Figure 5.35 presents some of the other obtained images, including a 0.5-millimeter scale for reference. Gap edges are marked with yellow dashed lines, and the flat side is the bottom side in all cases. All represent a very strong tendency, namely there are a significant amount of voids in the laminate, but strongly concentrated in the gap region. The total thickness of the laminate is quite uniform, thus, at gap locations, the local stack up with one less ply fills up the same thickness. This results in 'ply swelling' of the local layers. The tow edges are exhibiting a 'ramp', with a resin pocket or 'wedge' starting from the last fibers inwards. The extra resin-rich areas are thought to draw matrix away from plies, which facilitates the formation of voids. As visual inspection also tells, the axial UD plies are pushed to the flat side of the sample. In some samples, overlaps can also be detected, which is reasoned to be from the AFP lamination.

5.4. Chapter summary

In this chapter, the specimen manufacturing, testing setup, and experiment outcomes were discussed. Starting with the manufacturing topic, the hand lamination process of tows was introduced with the self-developed method to pursue AFP-level accuracy. Some issues with the AFP process (also in general) were listed. The autoclave curing cycle had some controlling errors, but fortunately the specimens were observed to be fully cured. The manufacturing ended with trimming, tabbing, and DIC pattern painting.

The tensile testing had some considerable problems, all tracing back to friction that was smaller than the assumed value, used to design the specimen in Chapter 4. The friction in the clamping area built up quite 'fast', meaning even the areas closer to top/bottom edges, inside the grips, were fully loaded to the maximum forces. Since the tabbing area had holes for the bolts, the reduced net section triggered net-section fracture in numerous samples. Nevertheless, the load introduced in each specimen was sufficient to lead to microcracks.

Some larger cracks were aligned with the simulation-predicted locations, though the outcome falls short of satisfactory proof of the main research hypothesis - gaps impose failure on neighboring matrix materials of plies. The cracks were only observed on the flat side, even dye penetrant tests couldn't indicate microcracks on the rough side. Edge delamination on one specimen, however, proved the importance of non-free edge gap characterization.

The DIC measurements exhibited a clear indication of the repetitive tow-gap nature of the samples. Interaction between gaps and strains was observed in both normal and shear strains. The more important plots conveyed the feedback on the undesired distribution of microcracks- the major strain peaks were shifted from the predicted gap locations. Thus, it was found that the gaps reduce stiffnesses,

which was discussed in the context of principal shear plot. Maybe bearing even more scientific value, the ply-flattening nature was discovered in the specimens, appearing as subtle ditches and ridges in the out-of-plane topology and curvature plots.

The microscopic cross-sections presented a flow of fibers (gap size reduction), apart from other ply deformations. A great number of voids were observed at the gap locations in an otherwise well-consolidated laminate. Uniform laminate thickness meant an imposed swelling for the layers, essentially meaning the surrounding material flowed to the empty spaces of gaps.

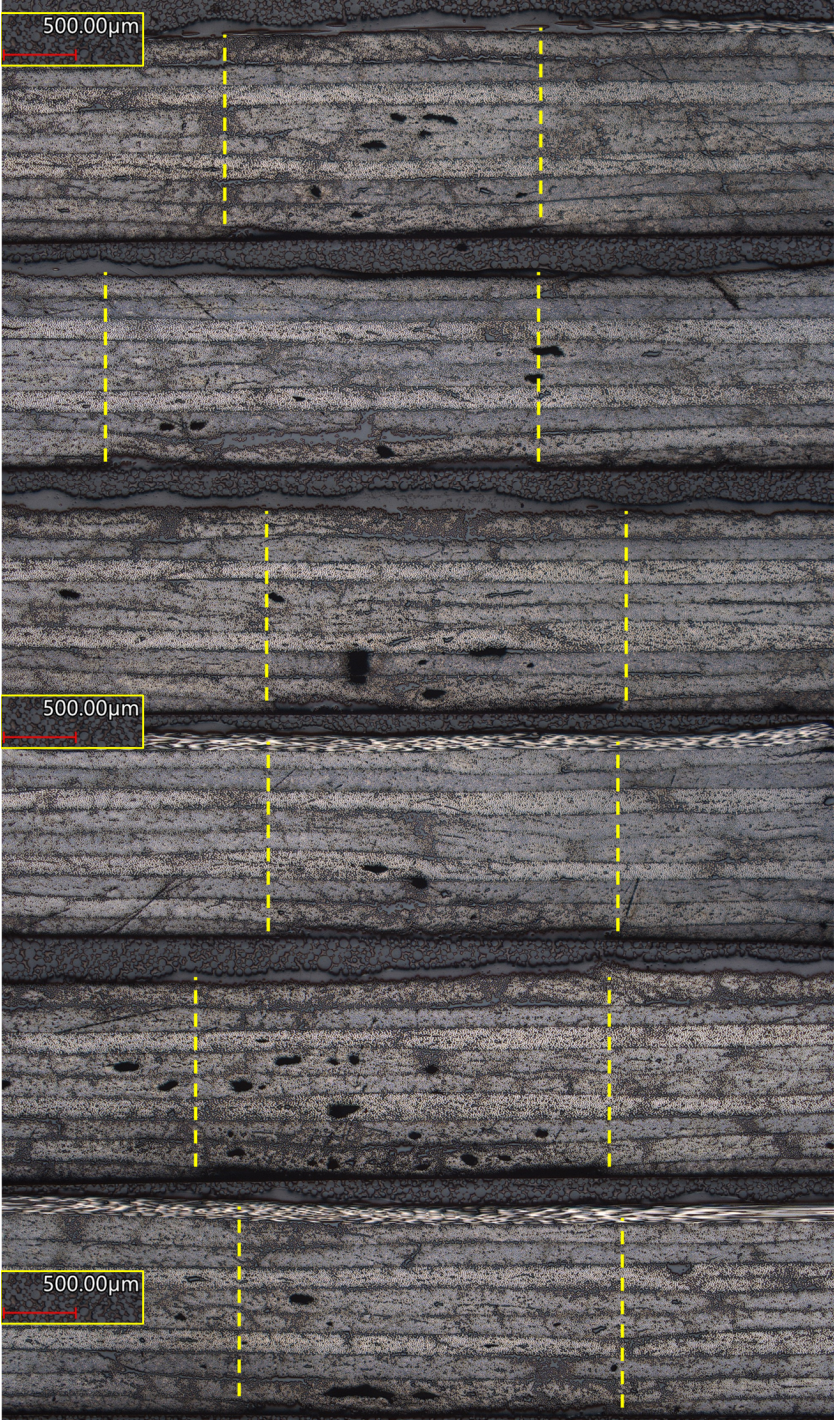


Figure 5.35: Microscopical images of gap locations.

6

Discussion

This chapter summarizes all that has been done and puts it into perspective, answering the research questions, and then finishing with future recommendations.

6.1. Answering the research questions

The section will discuss the main topics of the research parallel to the research subquestions and eventually with the main research question. The research questions are listed here once again:

Main question: **Assuming that gaps are manufacturing features that drive the properties being characterized, how can the effects of gaps be generally characterized?**

Subquestions:

1. What are the requirements for a specimen to realistically represent fiber-steered structures?
2. What is an optimal design for an AFP specimen, based on the requirements discussed?
3. How can a specimen like this be modeled?
4. What are the observations in real-life tests? How does the model correlate with test data?

6.1.1. Specimen requirements

In chapter 3, 17 requirements were set for a desired characterization specimen, based on a wide range of aspects. The main requirement and concept was the choice of element-level testing. The Literature Study chapter (chapter 2) already cited major research articles that pointed out the need for higher-level testing designs. The lowest level of testing, the coupon tests were and are predominantly used in material characterization (hence, only these experiments could be found in the research area). The material word shall be emphasized, it is the basic knowledge for structural design, however, it cannot capture structural aspects. In this research, the defects from the variable stiffness process are reasoned to be structural features. Thus, the need for a step towards larger panel-like specimens was justified.

This proved to be the right choice on several levels. The gaps were closed out from free edges, therefore the edge effects were mitigated. Seeing one of the samples with edge delamination (Figure 5.21), but without any larger damage to gaps inside the panel, the importance was proven on a basic level. Moreover, the variability in strains was observed by the DIC systems, which couldn't have been detected in smaller coupons. The latter wished to be underlined - the load found its way across the zone, as stiffnesses vary between gap and non-gap locations. This allowed loads to 'go around' the defects, therefore not overloading them locally (e.g. shear strain peaks not at gap locations). The literature presented coupons with defects across the full cross sections. In these cases, loads can't find a better way, therefore obviously imposing failure with considerable knockdown. While, in reality, the gaps might not get loaded up to failure, thus the coupon results could present an enlarged problem of the defects compared to what it is in reality.

A primary load path zone was chosen as a representative structure point for characterization. This meant pronounced anisotropy, no cutouts, given thickness, and a complex stress state (with respect to gaps). This was reasoned to be of more importance than, for example, window cutout areas or other

discontinuities. Therefore, for further studies, the choice of other representative areas is encouraged, but with a consideration of taking everything gradually. The full focus on the mentioned areas could lead to a deeper understanding with time, compared to ending up with a wider but shallower knowledge with the future recommendation. The balanced and symmetric laminate aspect eventually caused some problems in the homogenization of the stress state, justifying the requirement.

Some requirements were inherited from the available laboratory equipment. Multiaxial loading of laminates with any tool could help the deeper understanding of defect characterization. Even though there were (smaller) equipment limitations, the research provided a great amount of valuable results.

The gap size requirements were found satisfactory for a first sampling. Eventually, the broad sweep of different gap sizes and different tow sizes is envisioned for a full solution of gap characterization. The research test samples featured two layers with gaps, which provide a best-case scenario, and exhibit the problem in its purest form. The number of layers with defects is recommended to be increased for further studies, above any other requirements. This way, some stronger defect affection could be captured, with respect to strength and stiffness, further indicating the importance of the problem. This being said the serious agglomeration of defects (also found in literature) is still not encouraged, as they are not representative and picture the problem worse than it is. A hurdle to maximization of structural efficiency, if you will.

The desired failure location criteria were proven to be essential. The testing still pointed out an increased demand for design focus. Even though the samples were loaded up to microcracks and in one case, up to net section failure, the four grip section failures were nevertheless barriers to a possible informative event. It must be pointed out, the 'desired failure and intact specimen' requirement has a second aspect, the post-testing intact specimen. Without intact specimens, the microscopical images couldn't have been obtained. To conclude, the 'failure' requirements are eventually highlighted and thought to be essential in further research.

The 'AFP robot usage for manufacturing' point was partially violated with the work carried out. This did not have strong consequences, only because the used process had sufficient quality. Therefore, for researchers with worse infrastructure, the possibility shall be opened using hand lamination, only if the used process delivers representative test specimen up to standards. The standards, however, are somewhat subjective and up to the person.

No additional requirements were found during the latter stage of research, only changes to the existing ones, as discussed.

6.1.2. Optimal design

This subsection only focuses on the design aspect of the project, discussed in chapter 4 (Design chapter). The other topic, the used simulation tool will be discussed in the subsequent section.

The initial ideas for an ideal specimen revolved around utilizing fiber steering, and thus controlling the failure points of specimens to a well-defined gauge section. The first steps and simulation outcomes conveyed the wrong direction for characterization. Eventually, it turned out, that the correct method requires a well-defined homogeneous area, in which only one problem is wished to be solved and in a pure form. Breaking down this statement, first, the well-defined area is realized in a quasi-homogeneous, rectangular gauge section in the final specimen. As could have been seen, the initial curved trajectories resulted in large out-of-plane displacement and stress inhomogeneity over the whole panels. The indicated failure was concentrated over one line, rather than a homogeneous distribution (of peaks), which would grant equal opportunities for all materials. If the gauge section was incomplete, failure points were at undesired edges, therefore the sacrificial tow usage was needed. The concept was proven with DIC measurements, as globally, no significant distortion was experienced on the laminate surfaces.

The second part of the statement, 'one problem in the pure form' appeared in two points. On one hand, the concept which made an attempt to characterize both triangular and translational gaps failed to effectively do so. The two defects had a mutual affection, excluding both from accurately capturing the phenomena in their nature. This concept of focusing on one process was eventually found to be working and thus recommended for future research. Here it is noted, that the research into triangular gaps is encouraged, for which a basic concept sample is visualized on Figure 6.1. Here, one or two strips of UD material are laid in an inclined angle on the surface, and surrounded with enveloping axial tows, thus creating triangular gaps. With the inclination angle, the triangular shape can be controlled to any arbitrary aspect ratio. On the other hand the statement 'pure form', the fact that the research

used only two layers of defects, the problem was captured without any significant noise or affection. It was helpful for this work, as it was a pathfinder research, rather than an advanced study. To conclude, for the first steps, this approach is encouraged, however, on a direct buildup of translational gaps and increasing the defects could show more insight.

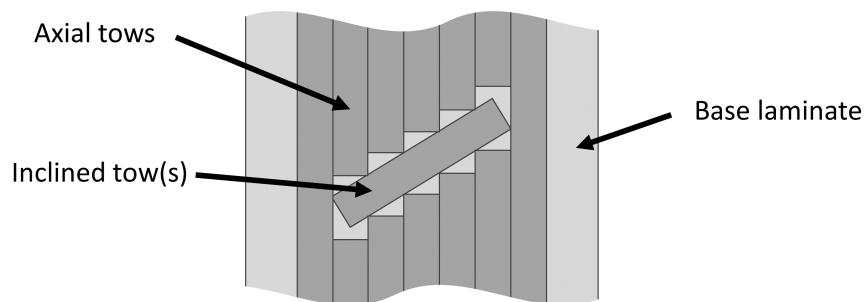


Figure 6.1: Proposed concept for characterizing triangular gaps.

There were increased efforts in the grip zone design of the specimen, however, it was not enough as the tests proved it. The tab termination point proved to be stable, which is the usual critical point. This was helped by the fact that common tabbing guidelines were followed. Nonetheless, some specimens failed inside the grip sections. Overseeing the problem was inherited from the simulation method. Even without the bolted connection, premature failure occurred with the sole use of hydraulic grips. This means the failure was not coming from bearing loads but from insufficient net sections in general. Within the grips, the net sections were already loaded up to a nominal level, even at close locations to the top/bottom edges. With the bolt holes serving as net section reductions, failure was deemed to happen. The understanding of the problem is aided by Figure 6.2. Note, that the stress distribution doesn't account for singularities for easier understanding, and the tendencies are not up to scale neither.

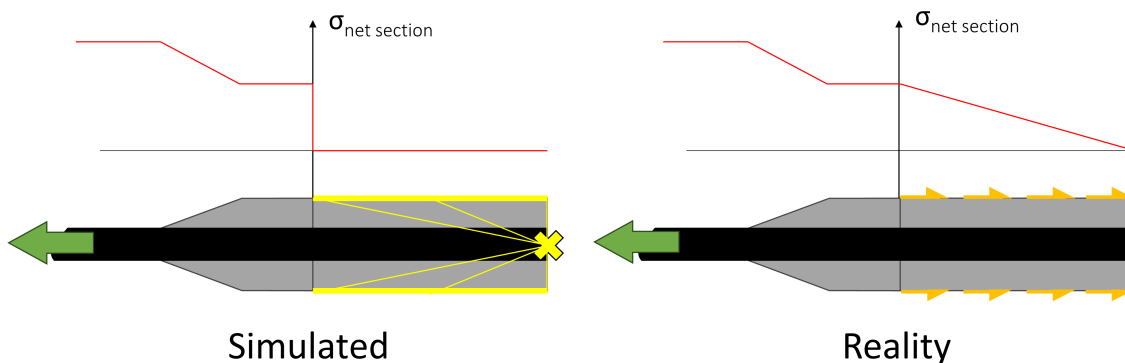


Figure 6.2: Net section stress build-up: simulated vs. real life observation.

To counter this problem in future tests, the usage of pure hydraulic grip mode could work if there are no holes in the region. This would mean some safety hazards but might lead to the prevention of small slips, which would eventually outweigh the concern. Improving the roughness of clamping surfaces could reduce the micro-slipping problem even further. Using the initial bolted connection method, it would work if the width of such a region is wider, thus lowering the net section stresses. This, however, would only work if the width of the gauge section of the specimen remained the same, leading to a 'dogbone' specimen. The usage of such geometry could be realized with water-jet cutting. While this method usually leaves some delamination at the edges, the damaged zones could be sanded away by manual processes. Such a concept is visualized on Figure 6.3.



Figure 6.3: Proposed improved concept with dog-bone shape.

The envisioned concept has one more advantage. Note the sketch features the 'hourglass'-like transition 'inside' the gauge section. Inside, as further from the top or bottom borders, closer to the horizontal midplane. Since the extra tows reinforced the central area, failure could take an easier way around the zone, as it happened with one specimen (Figure 5.22). If the smallest width is further away from gauge section boundaries, the failure should be guided through the gauge section rather than around. This being said, the dogbone specimen is not in use for composite specimens, for some reasons. Above manufacturing concerns, the main one is the common failure at the dogbone transition zone, which cannot serve any useful data.

The DIC and optical microscopy measurements delivered the expected results. In case of gaps deeper inside the laminates, the usage of ultrasonic testing is strongly advised, as for example, DIC could only capture surface trends. Otherwise, the design of the measurement setup is judged as satisfactory.

6.1.3. Modeling of VS laminates

The issue with the simulation regarding the grip section failures has been discussed already, which is somewhat connected to this question too. Following that discussion, the rest of the modeling question could be answered through the used tool and its comparison with real-life observations. The FEM model predicted a repetitive failure pattern over the gauge section of the specimen. Tested samples, however, did not indicate such processes. It has been mentioned that, based on simulation outcomes, the process should be based on the shear stresses of the laminate. Comparison of the principal shear strains of the FEM prediction and the measured DIC plot yields the diagram presented on Figure 6.4.

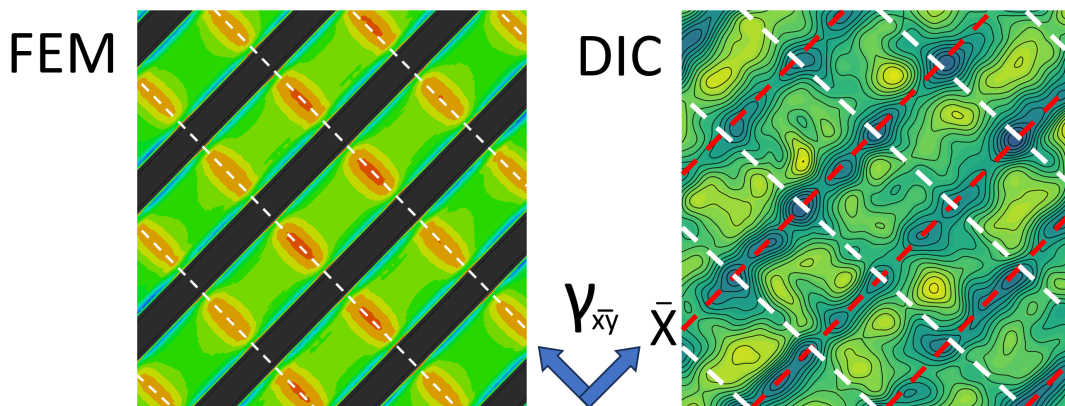


Figure 6.4: Comparison between strains of FEM model and DIC testing.

As one can see, even without comparing the values, it can be seen that there are serious differences even between tendencies (therefore magnitudes are not detailed further). Of course, the DIC

result presents inconsistencies (some data scatter), which could be a product of microcracks or general imperfections. The FEM model indicated strain peaks at backside gap locations (anticipated failure points), while DIC proved principal shear strain peaks within a zone bordered by front and backside gaps. While similar tendencies with differences in magnitude could point to incorrect material data properties, the strain trends definitely indicate fundamental modeling problems. The inputs mentioned in chapter 5 were suspected to be inaccurate, but not off by magnitudes, thus the difference should lie between the major modeling simplification - geometry. The significantly deformed, post-curing plies, burdened further with voids, were presented on Figure 5.35. The plies have a pronounced 'ply waviness' on the images. The used FEM model, at the gauge section, featured straight plies, with the surface tows also being rectangular in cross-sections. Therefore, it can be stated, that the original model accounted for the local layups (number of plies and orientations), but not for the post-curing ply deformations. This ply waviness deviation is judged as the major reason for the deviation between the prediction and test results.

In literature, the 'fiber waviness' phenomenon is known and actively researched. This being said, the topic is not only connected to AFP/VS gaps, for example, it also covers the problem when the hole laminate as one integral part has a waviness too. The work of Alves et al. [105] reviews the state-of-the-art, and states that the waviness has a drastic effect on mechanical performance. Moreover, the need for higher-fidelity models was emphasized by the author, in order to accurately predict laminate behavior. The thesis research agrees with and emphasises the two conveyed points of Alves et al. First, the thesis research emphasizes the demand for connecting the research of laminate gaps with the fiber waviness phenomenon. Since the latter also has major effects and is an inheritance of the former, the two together cover the "effects of gaps in variable stiffness laminates". Second, the correct modeling of VS gaps for characterization purposes must feature the post-cured ply deformations, in a higher fidelity model than used in this research.

As another aspect, the used input data could also deviate to a certain extent. This was supported in the DIC results' basic validation. However, the impact of this deviation is thought to be an order of magnitude smaller than the cross-sectional simplifications. Not accounting for delaminations between layers proved to be acceptable neglect, since the interfaces along surface tows or inside layers did not exhibit this kind of failure. The neglects of resin-rich pockets at this gap size is also deemed to be acceptable, as the large stiffness change between a composite layer and resin diminishes any effects imposed.

An additional thought, the change 'rate' of impact on mechanical performance is thought to be more significant at small gap sizes, where the defect is forming from a no-gap to a fully pronounced gap (or 'full-wave' waviness of plies). At very low gap sizes, the defect is just a sudden discontinuity, while at the pronounced magnitude, the plies are already deformed to a 'full wave'. Above the 'fully formed' gap size, no major difference is anticipated by the author of the thesis - a '10-' and a '20-millimeter' gap yields more or less the same result. Concluding this, the characterizing model must accurately follow the geometrical processes at 'gap forming' defect sizes, thus tracing the whole spectrum with respect to the gap size variable.

Model proposal for future research

Based on the research and discussion, the "how" of modeling is summarized here in a concrete approach. The understanding is aided by Figure 6.5. As mentioned, the numerical tool would start from a high-level numerical tool, an automated FEM simulation. The validity can be easily seen since the number of variables is too much, not to mention the combinations of them. Purely experimental characterization of such a problem is too costly and time-consuming. The FEM model would simulate on a macro-level, therefore not modeling fibers and matrix, nor modeling a whole specimen. This way the model space is comparable to the defect magnitude, allowing sufficient accuracy and satisfactory computational time. The simulation is envisioned to be automated by a script that generates a laminate with defects arranged in it and assesses the severity of the defects based on gap size, location, defect agglomeration, and ply waviness amongst other variables. The assessment values should be stored in a "map" of the laminate, which could be either a 2D or 3D matrix. The loading should happen on the cross-sectional boundaries of the model, by applied stresses or strains. This approach therefore could exploit multi-axial stress states also. After running the calculation, the obtained result should present the failure onset point in 3D space. Feeding back the outcome to the assessment map, the failure can be connected to the stored variables. As with all modeling processes, this method also requires veri-

fication and validation in discrete points. After sampling sufficient simulations, the tendencies for the variables could be visualized fairly easily. The basic scripting approach to automate model generation and tracing tendencies for variables has been mentioned by Alves et al. [105] also, as a promising trend for research.

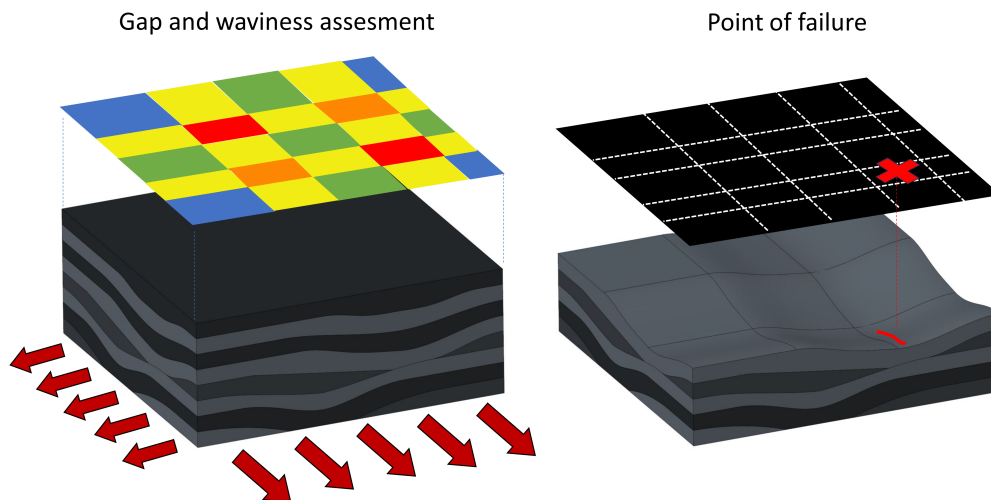


Figure 6.5: Proposed modeling approach for complete characterization of the effect of gaps.

6.1.4. Testing observations

The second half of the subquestion about the correlation between the applied model and the testing results has been answered in the previous section, hence here only testing observations will be considered. As a first step, the cross-sectional observations are discussed (for one larger magnification, see Figure 6.6, otherwise Figure 5.35). The main problem of ply deformations comes from the fact that all areas of the laminate have the same thickness, whether they have additional tows or not. This means, that at gap locations, there are significant deformations in the plies to take up the same thickness. First, the tows adjacent to gaps were deformed to have a ramp, as they gradually thinned towards the gaps. Not only the shape but the initial gap size also changed, as it was reduced by 15-25%. These are thought to be from the same phenomenon, namely the fibers flowing away during the liquid flow state of curing. The flow process is known in the scientific community as "shear flow" [106], in which resin and fiber flow together (otherwise, when only the resin flows between fibers it is "percolation flow"). Second, the ply waviness - the plies above the first layer were pushed into the laminate, thus imposing a non-negligible waviness. This waviness is gradually recovered by the plies, as from bottom to top the layers gradually flatten out.

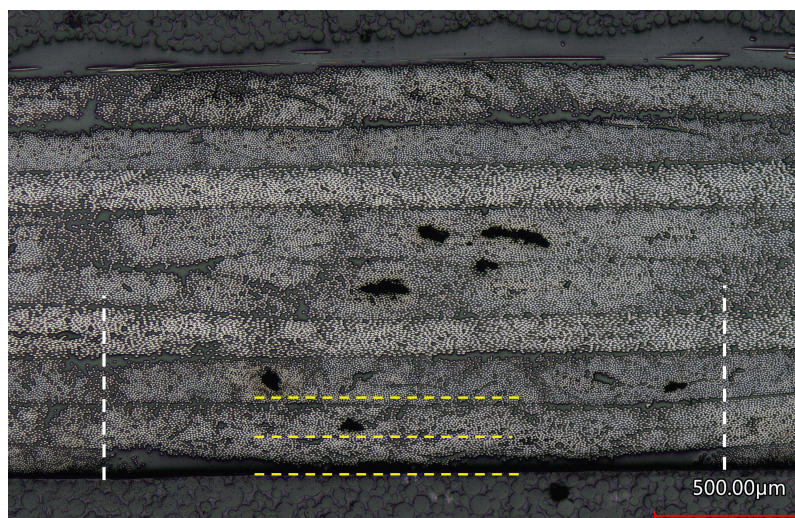


Figure 6.6: Swollen ply at gap location with voids.

The plies also show an interesting nature of 'swelling'. Looking at Figure 6.6, the bottom supporting ply shows a significant thickness increase, through which it can take up basically two-ply thickness in itself (yellow dashed lines showing one ply thickness). However, at the additional tows/gap edges (white dashed lines), the plies are back to nominal thickness. This swelling results in a notable drop in fiber volume content. This, and the fact that the gaps also feature two resin 'wedges' means that locally a large portion of the available matrix is drawn from the laminate, which is thought to be the reason for the voids. For the laminate, a non-perforated release film was used, which should have preserved the originally set fiber-matrix ratio. The fact that the laminate features a thicker line of resin at the top hints the issue of resin being squeezed out. A major outcome of the thesis is these voids were only discovered at gap locations, very distinctly. The incorrect curing cycle could have also contributed to these defects, the exact statement could only be said after further investigations. Research into this direction is highly encouraged. The microscopical observations, apart from the voids align with the outcomes of Guin et al. [71].

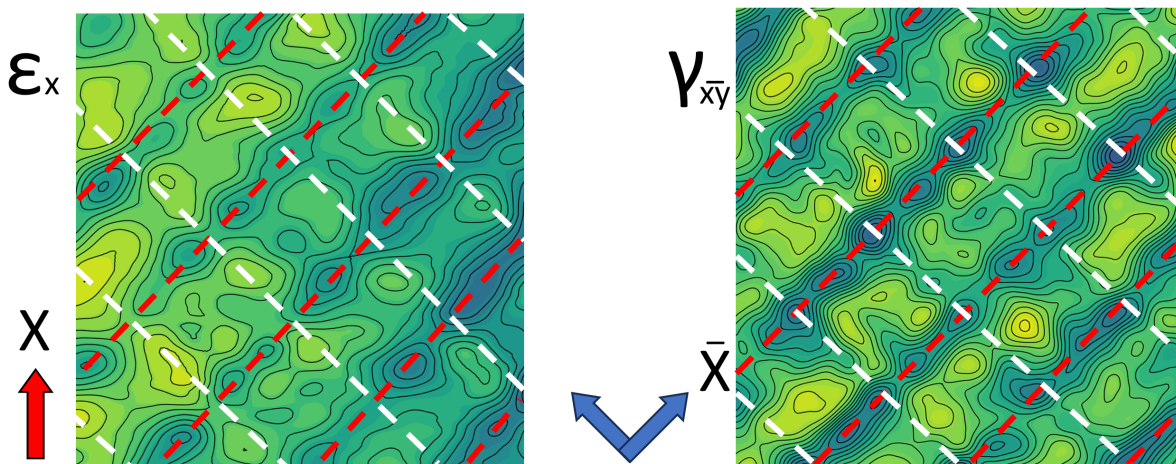


Figure 6.7: Axial and principal shear strain DIC plots.

Figure 6.7 presents the axial strain and the principal shear strain from the previously shown diagrams (in their respective coordinate system, also see arrows). As a brief summary of all plots, gaps were found to affect the strain distribution of the specimen, not only from the front side but also from the back. The affection materialized in repetitive patterns of strain intensities. Note, that the image shows front side gaps with red dashed lines and white for the backside gaps (the gap width is larger than the used lines). On the left side of the image, the axial strain peaks were mostly aligned with the backside gap locations within the surface tows, which proves that in a global response, the phenomenon can be perceived. On the right side, the principal shear distribution also proved an affection, however, in the other direction. The repetitive peaks were inside the rectangular zones bordered with gaps. As a main takeaway, the gaps therefore affected the laminate responses in deformation intensities in any way.

For the author of the thesis, the deformation inhomogeneity is a synonym for material knockdowns. An analogy is wished to be made with the gaps and knockdowns, based on all observations and experiences. In fatigue, open holes are critical features, because of the stress concentration factor they bear. The generally known, factor of 3 exists between the general applied stress and the local stress peak at the hole edge. This stress concentration factor is a materialization of the stresses piling up at the edge, while the material at the hole edge is just like everywhere else. If one just investigates a general test, a premature failure can be observed, with respect to the applied stress, with respect to the system as a whole. A similar nature is envisioned in the laminates with gaps. One-ply can be over-stressed locally, which can be perceived as a knockdown on a large scale. The 'stress concentration' of the imperfect laminates is introduced during the lamination process when gaps become a part of the system. The gaps are the open holes, and the neighboring environment plies are the surroundings of the hole, which eventually become the weakest link in the chain. Therefore, the perceived performance loss is down to a small-scale local problem. Conclusively, it is stated that there is a strength knockdown in the tested laminates, based on the DIC observations.

The reason for the strain inhomogeneity is thought to come from the local layer absences (covered by the FEM tool), and also from the previously considered ply/fiber waviness. The waviness of plies is known to impose a stiffness decrease [105]. The loads are assumed to find the most convenient way, commonly put as "stiffness attracts loads". Using this notion, for the principal shear plot, the gaps from both sides imposed such a local softening, that the additional tows couldn't be loaded up to significant stresses. To conclude, first, the affection for stiffness must be understood, so that the stress states can be known/modelled accurately. The strength-wise characterization could only be a second step, after this founding work.

The DIC also presented an insight into laminate behavior with the curvature plots. As it was seen, front-side gaps got revealed in the form of a 'ditch', while backside gaps formed a smaller 'peak'. The magnitudes of these out-of-plane displacements were very small, nonetheless were distinct. The phenomenon is reasoned to be a result of the ply waviness within the laminates. The explanation is aided by Figure 6.8. As the curing imposed waviness onto the plies, upon loading, the layers are thought to be flattening out. On the gap side, this should result in the observed ditches, while the other side should exhibit peaks, although a smaller magnitude, as the ply waviness is less and less strong in the layers.

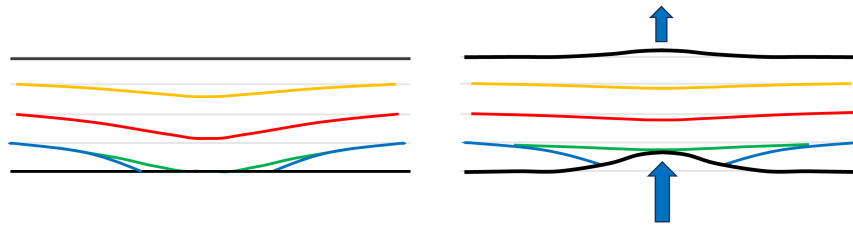


Figure 6.8: Swollen ply at gap location with voids.

Last but not least, is the main hypothesis. Namely, 'gaps negatively affect the off-axis tows, thus introducing failure/strength knockdown'. The gaps were found to impose increased distortions to some points in the laminate, which was thought to be a synonym for a performance knockdown on a laminate level. The off-axis tows were loaded to microcracks, however, these cracks couldn't be clearly connected to the manufacturing defects. Therefore, the hypothesis was not proven in its (original) form, and further work is required. It is wished to be noted, the hypothesis was not disproven neither.

6.1.5. Answering the main research question

The variable stiffness laminates are thought to be the ultimate method to exploit the admirable performance of fiber-reinforced composites, the state-of-the-art of today. However, it is not a common practice in the industry, and one aspect of it is the lack of knowledge of load-bearing capabilities. The resolution of this issue is deemed to be the final goal of the characterization of manufacturing-induced defects. The resolution is envisioned in the form of strength knockdowns with respect to main variables, which would be a direct tool in the hands of industrial engineers on the application end.

This master's thesis was planned to be a cornerstone, in the vastly unexploited topic of the effects of manufacturing-induced defects, very early on. The literature study chapter pointed out the evident lack of understanding in the field, or in some cases, the misleading characterization processes. It is recommended to deal with gaps/overlaps and fiber waviness topics as one internal package based on the outcome of this work. The element-level characterization in experimental work proved to be very insightful, and it is encouraged in future work.

However, as it was mentioned in the simulation discussion, the number of variables is too large to characterize by experimental methods alone. Therefore, the increasing trend of numerical testing is suggested for the complete characterization work, as per the discussion and similar to the suggestions of Alves et al. [105]. A numerical testing method has been proposed in the previous subsection, see Figure 6.5. This tool, nonetheless needs some supporting research to be able to carry out the sought outcomes. The whole characterization process, including the FEM tool as a core, is proposed on the flowchart of Figure 6.9.

To start an iterative simulation tool, there must be inputs to the model. The primary inputs are the laminate geometry, loading condition, and material inputs. If these are realistic, only then has the

FEM chance to output realistic results. Thus, there is a need for preceding studies in the field - there are two proposed, the material science of post-curing properties of laminates with gaps/overlaps and the other study on VS response behavior. The former is thought to convey an understanding of post-curing ply deformations, possible void formation scenarios, changes in fiber volume content, etc... As an output, there should be a method to generate any arbitrary laminate configuration's cross-section, with respective material data properties. The latter, the laminate behaviour study is a bit less intuitive - it would be connected to the loading mode, and also to the first validation to laminate response of the FEM output. The dire difference between the simulation and reality of the grip section was down to incorrect loading/boundary conditions, and the consequence was obvious. Similar issues could be made at the macro-level simulation of the process, therefore, there must be a way to find the correct boundaries of the model, which gives the correct response based on the initial testing observations. A general example of this is a simple comparison of displacement or force loading - both load up the model, but with differences.

At this point of the whole procedure, there must be an initial method to generate realistic, macro-level geometries, with corresponding material data inputs, and also with loads that create realistic deformations. The main iterative tool could give a first estimation of numerical knockdowns and predicted processes. This being said, the models in general need verification and validation. This is a point where only experimental work is suggested - to describe the actual reality. Discrete sampling points (laminates) are envisioned to be sufficient in this matter, with an experimental setup similar to the one used in this thesis. It must be noted, that the new specimens should advance a step further, correcting the used samples' initial troubles. If an acceptable correlation is found, the failures with respect to the stored variables can be studied, eventually leading to the ultimate conclusions of the effects of manufacturing defects. In case of insufficient correlation, the initial models should be refined until the FEM results agree with the testing data.

To conclude the process, the knockdowns, as a process could be used directly at the industrial front of engineering. This is imagined to happen together with the manufacturing process design. As the AFP robots need trajectory planning - the location of gaps, orientations, and other variables are known. Knowing these defect variables over a product surface, the mechanical performance could be calculated based on the knockdown functions. Ultimately, the effect of gaps, and in general manufacturing defects could be accounted for in structural applications of variable stiffness laminates.

6.2. Future recommendations

The thesis, being a cornerstone of a novel research area, had many recommendations over the main text, especially the discussion part of the thesis. Briefly, the more important are wished to be pointed out, with some prioritizing. Aligned with the characterization proposal, the initial recommendation is to pursue research with respect to the curing process side and the laminate response side. The latter could exploit the used specimen design together with the outcomes. Thus, improved and more efficient characterization samples could be used in the future.

The research into edge location gaps and characterization of such problems could be a rewarding endeavor. However, it is only recommended after the responses of laminates inside structures are understood. This way, the research of free edge location gaps could be built upon solid knowledge. A similar opinion is linked to the other branch of gap defects, the triangular gaps. After sufficient experience in the topic, a deep investigation of the problem is supported.

Lastly, more accurate simulations of frictional loading could be a beneficial study. At coupon-level testing, it is already a problem with high-performance composites, let alone at increased scales. At higher levels, the cost of testing work is exponential, which could be burdened by the inability to test because of such load introduction problems. The accurate prediction of load introduction, together with more efficient design of such areas should erase a major problem in a constant problem of testing work.

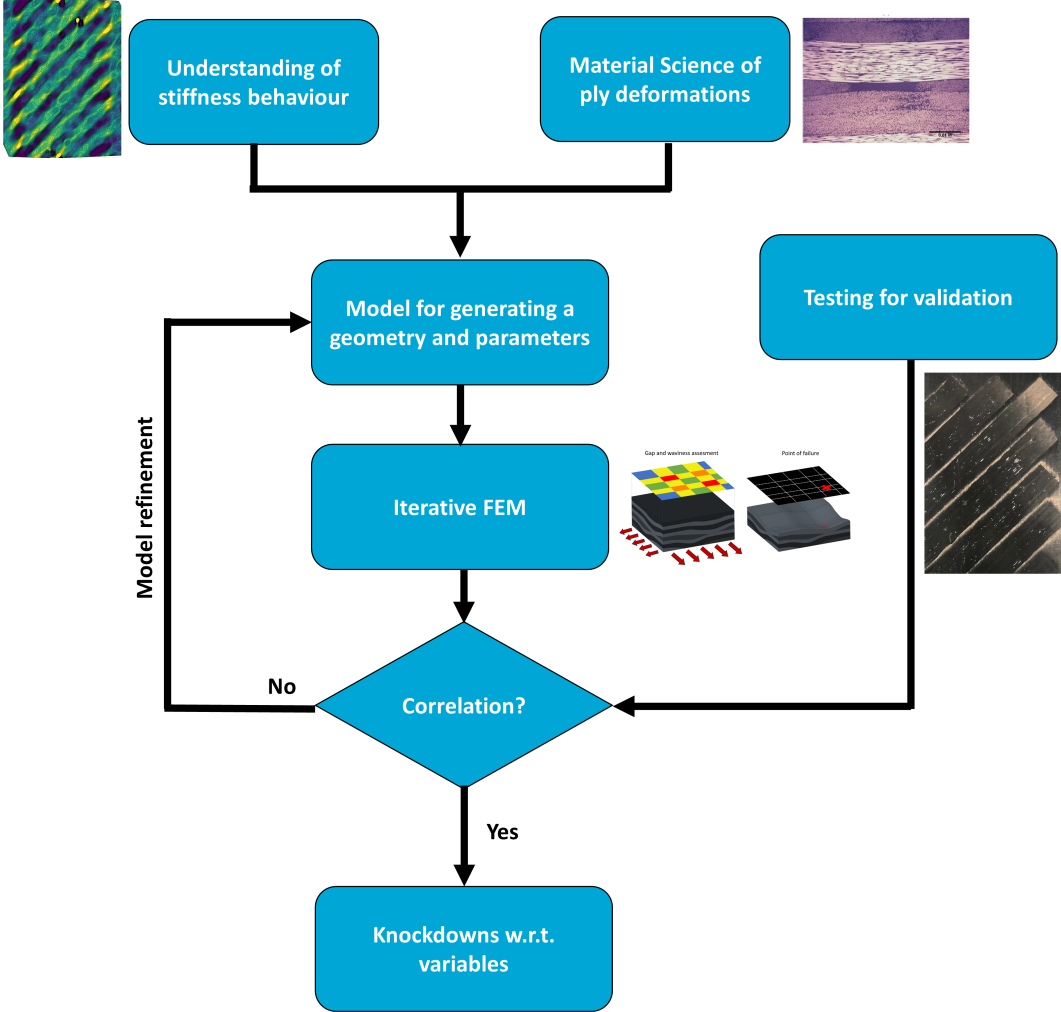


Figure 6.9: Envisioned complete process for mechanical performance characterization of variable stiffness structures.

7

Conclusion

The research objective for the thesis was to find a method to characterize the effects of manufacturing-induced defects, namely gaps in variable stiffness laminates. Early on, this proved to be a great challenge, for which one master's thesis was not enough in terms of both work and time. Therefore, the research was mainly about outlining a promising method that eventually could provide the desired characterization outcomes. Eventually, the work shifted to become a foundation for further work, or a first shot in the dark.

The research focused on providing a specimen that could characterize the effects of gap accurately, and in a well-representative manner. To do so, requirements were set against a feasible concept (chapter 3). Based on these, the design process started with a concept featuring the actual steering of tows. This path ran into problems with manufacturability, machine limits in testing equipment, and the strongest one with the inhomogeneous stress state of tows. As it turned out, the inhomogeneity means the inspected media is masked by one over-stressed point. It can be interpreted as a 'noise' in the observation. Contrary to this, a homogeneous state allows tendencies and affections to be displayed by one problem and in a pure form. Hence, it eventually converged into a second concept, featuring a well-defined controlled gauge zone, where the processes have the preferred homogeneous state. The final design was anticipated to have repetitive failure points, or at least to have onset in the desired location - at gaps.

The research hypothesis was that "gaps negatively affect the off-axis tows, thus introducing failure/strength knockdown". Or in other words, the problem was thought to be a matrix-governed problem. The hypothesis was planned to be validated by the damage onset locations within the specimens. Even though some larger microcracks aligned with the predicted gap locations, there was insufficient evidence to prove the hypothesis true. The problem is thought to be originating from the simulation model used for the predictions.

The simulation model featured simplifications, in order to speed up the design process. However, the geometrical simplifications of post-curing ply geometries were reasoned to be an incorrect move. The comparison of FEM results and DIC strain distributions proved that not only the magnitude, but the tendencies were significantly different also. The former could have been reasoned to be material data property difference, however, general tendency difference points to a fundamental modeling problem. Having no other major simplification, the effect of ply waviness was the one not accounted for. The strong effects of deformed layers, referred to as 'fiber waviness' are documented in the literature, but as a separate topic. If gaps exist in a laminate, so are ply waviness, therefore it is strongly suggested that these problems are dealt with as a package. As finding the correct modeling method was a question, an answer or suggestion for future work was made. The accurate but efficient model is thought to be a macro scale model, with representative cross-sections of a post-cured laminate containing defects. Finding the damage onset in this imperfect unit volume could point to the critical combination of variables.

The experimental work provided many insights, from various sides. It was detected, that gaps imposed deformation peaks to areas of laminates. These deformations were said to be the trace of performance knockdowns - as a local overstressing of media is perceived as a premature failure of the system. Apart from the plots with pronounced trends credited to gaps, microscopical images were

also made from the laminates. A very clear trend was displayed - the gap locations had an increased tendency to form voids. Other observations on ply deformation from curing processes were also discussed. The DIC system also captured out-of-plane tendencies, namely upon loading, frontal gaps were revealed as 'ditches', and backside ones as subtle 'peaks'. This was concluded as a result of plies flattening out during the loading sequence.

Finally, the main research question about the 'how' of characterization was answered through a proposed research process. Since the number of variables is high, automated numerical tools are envisioned to be the core process. The FEM model would be the one mentioned, a macro-scale unit of laminates. As a preliminary step, more understanding is needed to accurately create the ply geometries and to accurately load the unit volume. The former calls for a study in post-curing ply geometries which eventually should provide with a model which can describe the layer deformations accurately, moreover, should account for prediction of defects and other incidents. The latter is expected to provide a deeper understanding of the discussed imperfect laminate responses. It should output a macro-level model with loads and boundary conditions which gives back realistic laminate responses. These information are proposed for further studies. Along the numerical solution, experimental work is required parallel the iterative numerical tool to ensure a correlation between the prediction and reality.

References

- [1] Callister W. D. *Materials science and engineering : an introduction*. 10th edition. Hoboken, NJ: John Wiley & Sons, 2018.
- [2] C. Kassapoglou. *Design and Analysis of Composite Structures - with application to aerospace structures*. Chichester, United Kingdom: John Wiley & Sons, Ltd, 2010.
- [3] P. Boisse. *Advances in Composites Manufacturing and Process Design*. Chichester, England: Woodhead Publishing, 2015.
- [4] DLR German Aerospace Center. *DLR German Aerospace Center*. 2023. URL: <https://www.dlr.de/en/> (visited on 09/22/2023).
- [5] S. Sridhara. *Delamination behaviour of composites*. Cambridge, England: Woodhead Publishing, 2008.
- [6] G. R. Irwin. "Analysis of Stresses and Strains Near the End of a Crack Traversing a Plate". In: *Journal of Applied Mechanics* 24.2 (1957), pp. 361–364.
- [7] E. M. Wu; R.C. Reuter. "Crack extension in fiberglass reinforced plastics". In: *T & AM Report, Department of Theoretical and Applied Mechanics, University of Illinois* 275 (1965).
- [8] M. Kenane M.L. Benzeggagh. "Measurement of Mixed-Mode Delamination Fracture Toughness of Unidirectional Glass/Epoxy Composites with Mixed-Mode Bending Apparatus". In: *Composite Science and Technology* 56 (1996), pp. 439–449.
- [9] J. R. Reeder. "3D Mixed-Mode Delamination Fracture Criteria—An Experimentalist's Perspective". In: *American society for composites 21st annual technical conference* (2006), pp. 1–18.
- [10] M. L. Williams. "The Stresses Around a Fault or Crack in Dissimilar Media". In: *Bulletin of the Seismological Society of America* 49.2 (1959), pp. 199–204.
- [11] E. S. Greenhalgh. "Characterisation of mixed-mode delamination growth in carbon-fibre composites". In: *PhD Thesis, Imperial College of Science, Technology and Medicine* (1998).
- [12] L. F. Varandas; A. Arteiro; G. Catalanotti; B.G. Falzon. "Micromechanical analysis of interlaminar crack propagation between angled plies in mode I tests". In: *Composite Structures* 220 (2019), pp. 827–841.
- [13] E. S. Greenhalgh. *Failure Analysis and Fractography of Polymer Composites*. Oxford, United Kingdom: Woodhead Publishing Limited, 2009.
- [14] J.J. Polaha; B.D. Davidson; R.C. Hudson; A. Pieracci. "Effects of mode ratio, ply orientation and precracking on the delamination toughness of a laminated composite." In: *Journal of Reinforced Plastic Composites* 15 (1996), pp. 141–147.
- [15] J. Schön; T. Nyman; A. Blom; H. Ansell. "A numerical and experimental investigation of delamination behaviour in the DCB specimen." In: *Composite Science and Technology* 60 (2000), pp. 173–184.
- [16] J. Schön J; T. Nyman; A. Blom; H. Ansell. "Numerical and experimental investigation of a composite ENF-specimen." In: *Engineering Fracture Mechanics* 65 (2000), pp. 405–433.
- [17] P. Robinson; D.Q. Song. "A modified DCB specimen for mode I testing of multidirectional laminates." In: *Journal of Composite Materials* 26 (1992), pp. 1554–1577.
- [18] J.C. Fish; S.D. Malaznik. "Fracture of double beam specimens containing 90-degree plies." In: *Key Engineering Materials* 120-121 (1996), pp. 347–360.
- [19] I. Chou; I. Kimpara I; K. Kageyama; I. Ohsawa. "Mode I and mode II fracture toughness measured between differently oriented plies in graphite/epoxy composites." In: *ASTM STP* 1230 (1995), pp. 132–151.

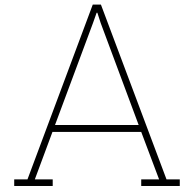
- [20] I. Chou; I. Kimpara I; K. Kageyama; I. Ohsawa. "Effect of fiber orientation on the mode I interlaminar fracture behavior of CF/epoxy laminates." In: *Journal of the Society of Materials Science, Japan* 41 (1992), pp. 1292–1298.
- [21] G. R. Irwin. *Handbuch der Physik*. 1st ed. Springer, 1958.
- [22] D. Broek. *Elementary engineering fracture mechanics*. 3rd ed. Dordrecht, The Netherlands: Martinus Nijhoff Publishers, 1982.
- [23] R. Khan. "Delamination Growth in Composites under Fatigue Loading". In: *PhD Thesis, TU Delft* (2013).
- [24] T. K. Jacobsen B. F. Sørensen. "Large-scale bridging in composites: R-curves and bridging laws". In: *Composites Part A: Applied Science and Manufacturing* 29.11 (1998), pp. 1443–1451.
- [25] J. Andersons; M. König. "Dependence of fracture toughness of composite laminates on interface ply orientations and delamination growth direction". In: *Composites Science and Technology* 64 (2004), pp. 2139–2152.
- [26] American Society for Testing and Materials (ASTM). "Standard Test Method for Mode I Interlaminar Fracture Toughness of Unidirectional Fiber-Reinforced Polymer Matrix Composites", *ASTM D5528/D5528M – 21*. 2022. URL: https://www.astm.org/d5528_d5528m-21.html.
- [27] American Society for Testing and Materials (ASTM). "Standard Test Method for Determination of the Mode II Interlaminar Fracture Toughness of Unidirectional Fiber-Reinforced Polymer Matrix Composites", *ASTM D7905/D7905M-19e1*. 2019. URL: https://www.astm.org/d7905_d7905m-19e01.html.
- [28] A.J. Russell; K.N. Street. "Factors affecting the interlaminar fracture energy of graphite/epoxy laminates." In: *Proceedings of ICCM IV, Tokyo* (1982), pp. 279–300.
- [29] K. Trakas; M.T. Kortschot. "The relationship between critical strain energy release rate and fracture mode in multidirectional carbon-fiber/ epoxy laminates." In: *ASTM STP 1285* (1997), pp. 283–304.
- [30] W. Jordan. "Changing the toughness of graphite fiber/resin based composites by changing their internal structure." In: *Composites: Part B* 42 (2000), pp. 543–562.
- [31] A. Laksimi; A.A. Benyahia; M.L. Benzeggagh; X.L. Gong. "Initiation and bifurcation mechanisms of cracks in multi-directional laminates." In: *Composite Science and Technology* 60 (2000), pp. 597–604.
- [32] J.H. Hwang; C.S. Lee; W. Hwang. "Effect of crack propagation directions on the interlaminar fracture toughness of carbon/epoxy composite materials." In: *Applied Composite Materials* 8 (2001), pp. 411–433.
- [33] A. Laksimi; M.L. Benzeggagh; G. Jing; M. Hecini; J.M. Roelandt. "Mode I interlaminar fracture of symmetrical cross-ply composites." In: *Composite Science and Technology* 41 (1991), pp. 147–164.
- [34] J.P. Lucas. "Delamination fracture: effect of fiber orientation on fracture of a continuous fiber composite laminate." In: *Engineering Fracture Mechanics* 42.3 (1992), pp. 543–561.
- [35] K. Tohgo; Y. Hirako; H. Ishii; K. Sano. "Mode I interlaminar fracture toughness and fracture mechanism of angle-ply carbon–Nylon laminates." In: *Journal of Composite Materials* 30 (1996), pp. 650–661.
- [36] F. Ozdil; L.A. Carlsson. "Beam analysis of angle-ply laminate DCB specimens." In: *Composite Science and Technology* 59 (1999), pp. 305–315.
- [37] F. Ozdil; L.A. Carlsson. "Characterization of mode I delamination growth in glass/epoxy composite cylinders." In: *Journal of Composite Materials* 34 (2000), pp. 398–419.
- [38] F. Lachaud; R. Piquet; L. Michel. "Delamination in mode I and II of carbon fibre composite materials: fibre orientation influence." In: *Proceedings of ICCM-12, Paris, July 5th–9th* (1999).
- [39] O. Allix; D. Leveque; L. Perret. "Identification and forecast of delamination in composite laminates by an interlaminar interface model." In: *Composite Science and Technology* 58 (1998), pp. 671–678.

- [40] D.J. Nicholls; J.P. Gallagher. "Determination of Glc in angle ply composites using a cantilever beam test method". In: *Journal of Reinforced Plastic Composites* 2 (1983), pp. 2–17.
- [41] C. Hwu; C.J. Kao; L.E. Chang. "Delamination fracture criteria for composite laminates." In: *Journal of Composite Materials* 29 (1995), pp. 1962–1987.
- [42] P. Davies; F. Rannou. "The effect of defects in tubes: Part 1. Mode I delamination resistance." In: *Applied Composite Materials* 1 (1995), pp. 333–349.
- [43] A. Laksimi; A. A. Benyahia; X.L. Gong; S. Benmedakhene. "Mode II delamination in +/- theta laminates: analysis and optimisation." In: *Advanced Composite Materials* 9 (2000), pp. 207–221.
- [44] Y.B. Shi; D. Hull; J.N. Price. "Mode II fracture of +/- theta angled laminate interfaces." In: *Composite Science and Technology* 47 (1993), pp. 173–184.
- [45] Ph. Rubbrecht; I. Verpoest. "The development of two new test methods to determine the mode I and mode II fracture toughness for varying fibre orientations at the interface." In: *Proceedings of the 38th International SAMPE Symposium, Anaheim, CA* (1993), pp. 875–887.
- [46] H. Chai. "Interlaminar shear fracture of laminated composites." In: *International Journal of Fracture* 43 (1990), pp. 117–131.
- [47] N.S. Choi; A.J. Kinloch; J.G. Williams. "Delamination fracture of multidirectional carbon-fiber/epoxy composites under mode I, mode II and mixed-mode I/II loading." In: *Journal of Composite Materials* 33 (1999), pp. 73–100.
- [48] F. Ozdil; L.A. Carlsson; P. Davies. "Beam analysis of angle-ply laminate end-notched flexure specimens." In: *Composite Science and Technology* 58 (1998), pp. 1929–1938.
- [49] J. Tao; C.T. Sun. "Influence of ply orientation on delamination in composite laminates." In: *Journal of Composite Materials* 32 (1998), pp. 1933–1947.
- [50] Z. Yang; C.T. Sun. "Interlaminar fracture toughness of a graphite/ epoxy multidirectional composite." In: *Journal Of Engineering Materials And Technology* 122 (2000), pp. 428–433.
- [51] S.L. Donaldson. "Mode III interlaminar fracture characterization of composite materials." In: *Composite Science and Technology* 32 (1988), pp. 225–249.
- [52] W.C. Liao; C.T. Sun. "The determination of mode III fracture toughness in thick composite laminates." In: *Composite Science and Technology* 56 (1996), pp. 489–499.
- [53] S. S. Wang; I. Choi. "Boundary-Layer Effects in Composite Laminates." in: *Journal of Applied Mechanics* 49 (1982), pp. 541–548.
- [54] J. C. Brewer; P. A. Lagace. "Quadratic Stress Criterion for Initiation of Delamination". In: *Journal of Composite Materials* 22 (1988), pp. 1141–1155.
- [55] R. Ganesan C. Zhang; S. V. Hoa. "Experimental Characterization of Interlaminar Shear Strengths of Graphite/Epoxy Laminated Composites". In: *Journal of Composite Materials* 36.13 (2002).
- [56] A. Puck. "Ein Bruchkriterium gibt die Richtung an ("A fracture criteria shows the direction)". In: *Kunststoffe, German Plastics* 82.5 (1992), pp. 207–210.
- [57] C. G. Dávila; P.P. Camanho. "Failure Criteria for FRP Laminates in Plane Stress". In: *Nasa Technical Report* (). NASA/TM-2003-212663.
- [58] C.S. Lopes; P.P. Camanho; Z. Gürdal; B.F. Tatting. "Progressive failure analysis of tow-placed, variable-stiffness composite panels". In: *International Journal of Solids and Structures* 44.25-26 (2007), pp. 8493–8516.
- [59] F. Heinecke; C. Willberg. "Manufacturing-Induced Imperfections in Composite Parts Manufactured via Automated Fiber Placement." In: *Journal of Composites Science* 3 (2).56 (2019).
- [60] C.S. Lopes; Z. Gürdal; P.P. Camanho. "Tailoring for strength of composite steered-fibre panels with cutouts". In: *Composites Part A: Applied Science and Manufacturing* 41.12 (2010).
- [61] K. Fayazbakhsh; M. Arian Nik; D. Pasini; L. Lessard. "The effect of gaps and overlaps on the in-plane stiffness and buckling load of variable stiffness laminates made by automated fiber placement". In: *15th European Conference on Composite Materials, Venice, Italy* (2012).

- [62] K. Croft; L. Lessard; D. Pasini; M. Hojjati; J. Chen; A. Yousefpour. "Experimental study of the effect of automated fiber placement induced defects on performance of composite laminates". In: *Composites Part A: Applied Science and Manufacturing* 42.5 (2011).
- [63] A.W. Blom; C.S. Lopes; P.J. Kromwijk; Z. Gürdal; P.P. Camanho. "A Theoretical Model to Study the Influence of Tow-drop Areas on the Stiffness and Strength of Variable-stiffness Laminates". In: *Journal of Composite Materials* 43.5 (2009).
- [64] O. Falcó; J.A. Mayugo; C.S. Lopes; N. Gascons; J. Costa. "Variable-stiffness composite panels: Defect tolerance under in-plane tensile loading". In: *Composites Part A: Applied Science and Manufacturing* 63 (2014), pp. 21–31.
- [65] M. Lan; D. Cartié; P. Davies; C. Baley. "Microstructure and tensile properties of carbon–epoxy laminates produced by automated fibre placement: Influence of a caul plate on the effects of gap and overlap embedded defects". In: *Composites Part A: Applied Science and Manufacturing* 78 (2015), pp. 124–134.
- [66] M. Lan; D. Cartié; P. Davies; C. Baley. "Influence of embedded gap and overlap fiber placement defects on the microstructure and shear and compression properties of carbon–epoxy laminates". In: *Composites Part A: Applied Science and Manufacturing* 82 (2016), pp. 198–207.
- [67] F. Heinecke; W. van den Brink; T. Wille. "Assessing the structural response of automated fibre placement composite structures with gaps and overlaps by means of numerical approaches". In: *20th International Conference on Composite Materials, Copenhagen* (2015).
- [68] O. Falcó; C.S. Lopes; F. Naya; F. Sket; P. Maimí; J.A. Mayugo. "Modelling and simulation of tow-drop effects arising from the manufacturing of steered-fibre composites". In: *Composites Part A: Applied Science and Manufacturing* 93 (2017), pp. 59–71.
- [69] D. Lucas; M. J. Van Tooren; A. Elham. "Stiffness Corrections for Overlaps and Gaps in Steered Composite Panel optimization". In: *58th AIAA/ASCE/AHS/ASC Structures, Structural Dynamics, and Materials Conference, Grapevine, Texas* (2017).
- [70] A. Hornig; M. Gude W. Woigk; S. R. Hallett; M. I. Jones; M. Kutz; "Experimental investigation of the effect of defects in Automated Fibre Placement produced composite laminates". In: *Composite Structures* 201 (2018), pp. 1004–1017.
- [71] W.E. Guin; J.R. Jackson; C.M. Bosley. "Effects of tow-to-tow gaps in composite laminates fabricated via automated fiber placement". In: *Composites Part A: Applied Science and Manufacturing* 115 (2018), pp. 66–75.
- [72] D. De Rossi. "Effect of Half Gap/Overlap Defects on the Strength of Composite Structures Fabricated with Automated Fiber Placement Methods". In: *Master's Thesis, McGill University, Montreal* (2018).
- [73] V. Cadran. "Effects of Defects Made by Automated Fibre Placement Process on Carbon/Epoxy Composite Structures." In: *Master's Thesis, McGill University, Montreal* (2019).
- [74] T. Zenker; F. Bruckner; K. Drechsler. "Effects of defects on laminate quality and mechanical performance in thermoplastic Automated Fiber Placement-based process chains". In: *Advanced Manufacturing: Polymer & Composites Science* 5.4 (2019), pp. 184–205.
- [75] M. H. Nguyen; A. A. Vijayachandran; P. Davidson; D. Call; D. Lee; A. M. Waas. "Effect of automated fiber placement (AFP) manufacturing signature on mechanical performance of composite structures". In: *Composite Structures* 228 (2019).
- [76] M. H. Nguyen; P. Davidson; A. M. Waas. "Experimental and numerical study on the tensile failure behavior of toughened-interlayer composite laminates with automated fiber placement (AFP) induced gap and overlap defects". In: *International Journal of Material Forming* 14 (2021), pp. 105–119.
- [77] B. Böckl; A. Wedel; A. Misik; and K. Drechsler. "Effects of defects in automated fiber placement laminates and its correlation to automated optical inspection results". In: *Journal of Reinforced Plastics and Composites* 42 (2022), pp. 3–16.
- [78] H. Suemasu; Y. Aoki; S. Sugimoto; T. Nakamura. "Effect of interaction of gaps on compressive strength of automated-fiber-placement-manufactured laminates". In: *Composite Structures* 306 (2023).

- [79] J. Rouchon. "Certification of large airplane composite structures, recent progress and new trends in compliance philosophy". In: *17th ICAS Congress, Stockholm 2* (1990), pp. 1439–1447.
- [80] M. Ghayour; M. Hojjati; R.n Ganesan. "Effect of tow gaps on impact strength of thin composite laminates made by Automated Fiber Placement: Experimental and semi-analytical approaches". In: *Composite Structures* 248 (2020).
- [81] S. T. IJsselmuiden. "Optimal Design of Variable Stiffness Composite Structures using Lamination Parameters". In: *PhD thesis, TU Delft* (2011).
- [82] K. Fayazbakhsh; M.A. Nik; D. Pasini; L. Lessard. "Defect layer method to capture effect of gaps and overlaps in variable stiffness laminates made by Automated Fiber Placement". In: *Composite Structures* 97 (2013), pp. 245–251.
- [83] M. Ghayour; M. Hojjati; R. Ganesan. "Induced defect layer method to characterize the effect of fiber tow gaps for the laminates manufactured by automated fiber placement technique". In: *Journal of Composite Materials* 55.27 (2021), pp. 4011–4027.
- [84] T. Laux. "Experimental and computational characterisation of composite laminates subjected to multiaxial loading". In: *PhD Thesis, University of Southampton* (2020).
- [85] L. Werfelman. "Thin skinned". In: *Aerosafety world* (2011), pp. 18–20.
- [86] International Organization for Standardization. "*Determination of tensile properties - Part 5: Test conditions for unidirectional fibre-reinforced plastic composites*", ISO 527-5:1997. 1997. URL: <https://www.iso.org/standard/80370.html>.
- [87] A. Khani; S.T. IJsselmuiden; M.M. Abdalla; Z. Gürdal. "Design of variable stiffness panels for maximum strength using lamination parameters". In: *Composites Part B: Engineering* 42.3 (2011), pp. 546–552.
- [88] L. F. Sánchez-Heres. "Comparison of operational limit estimations for FRP laminates – effects of material modelling and stochastic behaviour". In: *Master's Thesis, Chalmers University of Technology, Gothenburg* (2012).
- [89] B. Seers; R. Tomlinson; P. Fairclough. "Residual stress in fiber reinforced thermosetting composites: A review of measurement techniques". In: *Polymer composites* 42.4 (2021), pp. 1631–1647.
- [90] G. Clancy; D. Peeters; V. Oliveri; D. Jones; R. M. O'Higgins; P. M. Weaver. "A study of the influence of processing parameters on steering of carbon Fibre/PEEK tapes using laser-assisted tape placement". In: *Composites Part B: Engineering* 163 (2019), pp. 243–251.
- [91] American Society for Testing and Materials (ASTM). "*Standard Test Method for Compressive Properties of Polymer Matrix Composite Materials Using a Combined Loading Compression (CLC) Test Fixture*", ASTM D6641/D6641M. 2019. URL: https://www.astm.org/d6641_d6641m-16e02.html.
- [92] F. Hild; S. Roux. "Digital Image Correlation: From Displacement Measurement to Identification of Elastic Properties - A Review". In: *Strain* 42.2 (2005).
- [93] M. Kersemans; E. Verboven; J. Segers; S. Hedaytrasa; W. Van Paepegem. "Non-Destructive Testing of Composites by Ultrasound, Local Defect Resonance and Thermography". In: *18th International Conference on Experimental Mechanics (ICEM18), Brussels, Belgium* (2018).
- [94] Sonatest website. *How to Analyse C-scan Mapping?* 2023. URL: <https://sonatest.com/resources/educational-notes/how-analyse-c-scan-mapping> (visited on 12/13/2023).
- [95] S.T. Pinho; R. Darvizeh; P. Robinson; C. Schuecker; P.P. Camanho. "Material and structural response of polymer-matrix fibre-reinforced composites". In: *Journal of Composite Materials* 46 (2012), pp. 2313–2341.
- [96] A.S. Kaddour; M.J. Hinton. "Maturity of 3D failure criteria for fibre-reinforced composites: Comparison between theories and experiments: Part B of WWFE-II". In: *Journal of Composite Materials* 47.6-7 (2013).
- [97] D. Gouskos; L. Iannucci. "Finite Element Analysis of Non-crimp Fabric Laminates Under Compact Tension". In: *ECCM18 - 18th European Conference on Composite Materials, Athens, Greece* (2018).

- [98] Toray Advanced Composites. "Toray TC250 product datasheet". In: *The Title of the Journal* (2020).
- [99] A. Ramji; Y. Xu; M. Yasae; M. Grasso; P. Webb. "Delamination migration in CFRP laminates under mode I loading". In: *Composites Science and Technology* 190 (2020).
- [100] American Society for Testing and Materials (ASTM). "*Standard Test Method for Tensile Properties of Polymer Matrix Composite Materials*", ASTM D3039/D3039M. 2017. URL: https://www.astm.org/d3039_d3039m-00.html.
- [101] D. O. Adams; D. F. Adams. "Tabbing Guide for Composite Test Specimens". In: *Final Report for Federal Aviation Administration* (2002).
- [102] N. B. Ravi; N. Chakraborty; M. Steckel; P. Betagiri; P. Raghuraman; R. Shivamurty; R. Sridaran Venkat; D. R. Mahapatra; C. Boller. "A Study on Effectiveness of an SHM Sensor System for Fatigue Damage Inspection". In: *8th European Workshop on SHM (EWSHM), Bilbao, Spain* (2016).
- [103] SHD Composites. *MTC510 Epoxy Component Prepreg technical data sheet*. 2024. URL: <https://shdcomposites.com/assets/prepregs/mtc510-tds-1.pdf> (visited on 03/14/2024).
- [104] Toray Composite Materials America Inc. *T300 Standard modulus carbon fiber Prepreg technical data sheet*. 2024. URL: <https://www.toraycma.com/wp-content/uploads/T300-Technical-Data-Sheet-1.pdf> (visited on 03/16/2024).
- [105] M.P. Alves; C.A. Cimini Junior; S.K. Ha. "iber waviness and its effect on the mechanical performance of fiber reinforced polymer composites: An enhanced review". In: *Composites Part A: Applied Science and Manufacturing* 149 (2021).
- [106] Y. Naito; M. Nishikawa; C. Mobuchon; A. Poursartip; N. Matsuda; M. Hojo. "Effect of rheological transitions in matrix resin on flow mechanism of carbon Fiber/Epoxy prepreg". In: *Composites Part A: Applied Science and Manufacturing* 151 (2021).
- [107] 3M adhesives. *Scotch-Weld™ EC-9323 B/A structural adhesive technical data sheet*. 2024. URL: https://multimedia.3m.com/mws/media/21579210/3m-ec-9323-ba-structural-epoxy-paste-adhesive-tds.pdf&fn=EC-9323%20BA%20Structural%20Epoxy%20Paste%20Adhesive_TDS_Apr%2022_ref260_R1.pdf (visited on 02/26/2024).
- [108] TSF global fastening solutions. *Table of preloads and tightening approximate values*. 2024. URL: <https://www.tsftsh.com/docs/documentation/Precargas%20Web.pdf> (visited on 02/26/2024).
- [109] The Engineering ToolBox. *Friction coefficients and calculator*. 2024. URL: https://www.engineeringtoolbox.com/friction-coefficients-d_778.html (visited on 02/26/2024).



Mesh convergence study

After running the model with several mesh sizes, the convergence plot presented on Figure A.1 was the resultant. The plotted value is the failure index in the central 'surface tows', and at locations of stress peaks. From a coarse mesh to a finer one, the failure index reduces by about 5% and converges to a value close to 1. Apart from this numerical value convergence, in the spatial field, the distribution of the raw output goes through a significant change. The software, by default, plots the results with a 75% spatial averaging. This averaging smoothens out the distributions and contours, working as a low-pass filter essentially. The global tendencies are still kept this way, but the numerical high-frequency noise is negated. Figure A.2 and Figure A.3 present the coarsest and finest mesh results with no averaging respectively. As one can see, the coarse mesh has significant numerical issues, however, the fine mesh shows a converged solution even without any filtering. Thus, in the tows, an average mesh size of 0.25 millimeters was used, whereas in the supporting plies, this value was 1 millimeter. Note, through the thickness the tows featured 2 elements, as it results in 3 integration points, a rather minimum value for thin parts.

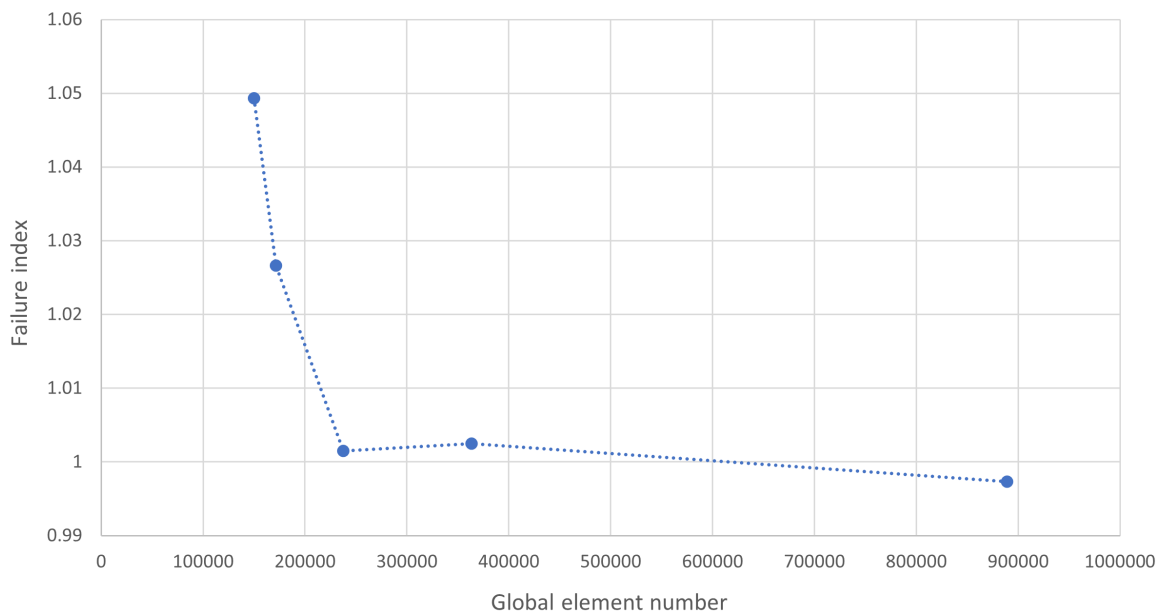


Figure A.1: Failure criteria convergence plot for the central tow's failure peak

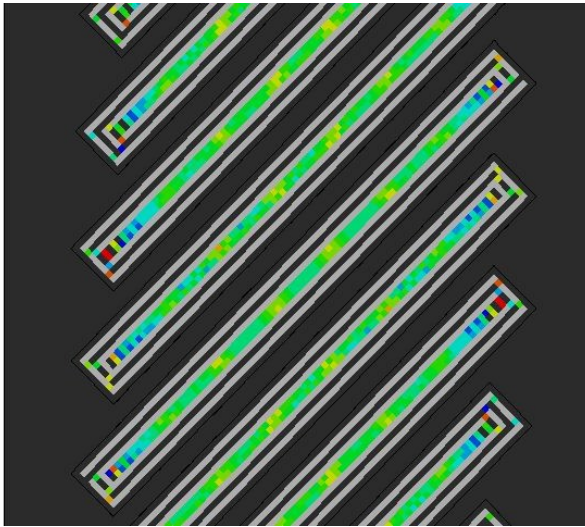


Figure A.2: Coarse mesh failure index plot with no spatial averaging.

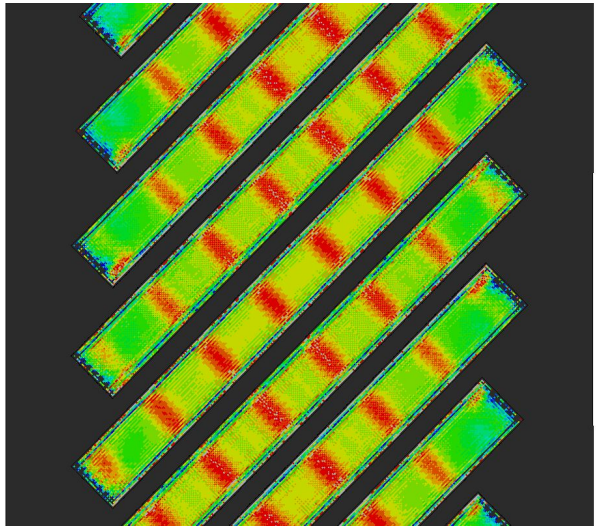


Figure A.3: Fine mesh failure index plot with no spatial averaging.

B

Adhesive failure calculation

The total tabbing surface was calculated in CAD, which resulted in 9359 mm² (Figure B.1). It must be noted, on one end of the specimen there are two tabs on each side, therefore the total sheared surface is double this area.

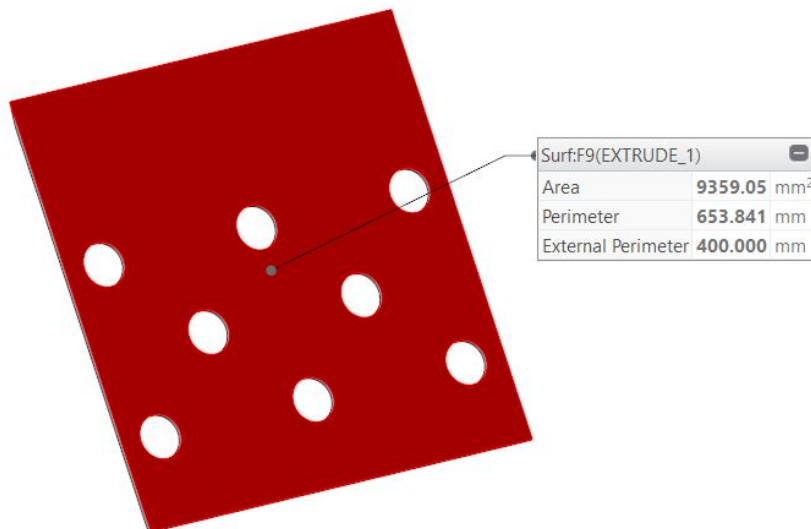
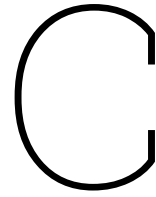


Figure B.1: Adhesive surface of the tabbing plate.

The maximum load of the testing machine is 250 kN, which will be used for checking for failure of adhesion. The used Scotch-Weld EC-9323 B/A adhesive product has an overlap shear strength on CFRP composites (epoxy matrix) of 28 MPa [107], for aluminium this value is higher. The shear stress for the maximum machine load and the factor of safety therefore becomes:

$$\tau_{applied} = \frac{F_{max}}{2A_{tab}} = \frac{250000}{2 \cdot 9359} = 13.36 [MPa] \quad (B.1)$$

$$FoS = \frac{\tau_{ultimate}}{\tau_{applied}} = \frac{28}{13.36} = 2.096 [-] \quad (B.2)$$



Frictional force calculation for clamping plates

A 12.9 coarse thread, M10 bolt has a preload of 44 kN (with a friction coefficient of 0.14) [108]. The 8 bolts altogether make up 352 kN of clamping force. The static friction coefficient for the aluminum-steel material pair is 0.61 (clean and dry condition) [109]. There are two frictional surface pairs in contact, or in other words, both sides of the specimen are loaded with friction. A schematic, simplified example of the problem is presented on Figure C.1.

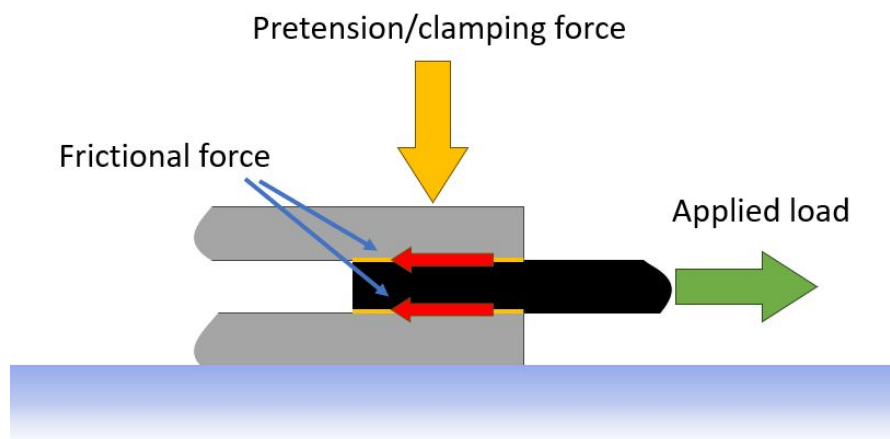


Figure C.1: Simplified example for the frictional loading.

Therefore the maximum non-slip condition force and the safety factor for the maximum machine load is:

$$F_{max} = 2 \cdot (\mu_{Al-Fe} \cdot 8 \cdot F_{bolt}) = 2 \cdot (0.61 \cdot 8 \cdot 44000) = 429.4 [kN] \quad (C.1)$$

$$FoS = \frac{F_{max}}{F_{machine}} = \frac{429.4}{250} = 1.72 [-] \quad (C.2)$$

It is noteworthy that, in case of a slip, bearing force should help the loading above the friction, therefore the clamping case should be able to load up the specimen. This being said, the sliding frictional coefficient for the same material pair is 0.47 according to [109], which is still sufficient to load up the specimen by a safety factor of 1.3.

D

DIC plots not discussed in main text

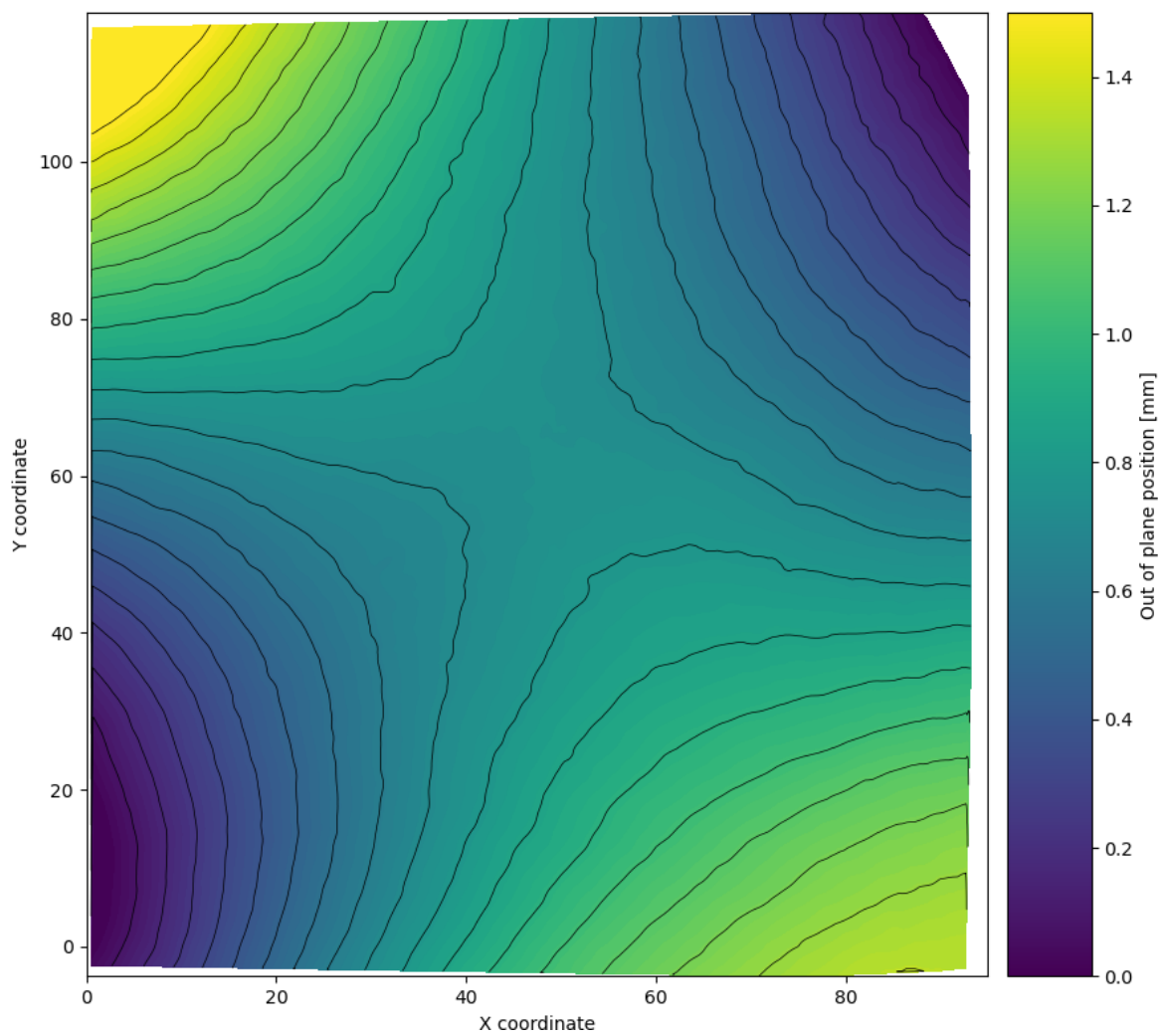


Figure D.1: Initial warp of specimen at the beginning of the test.

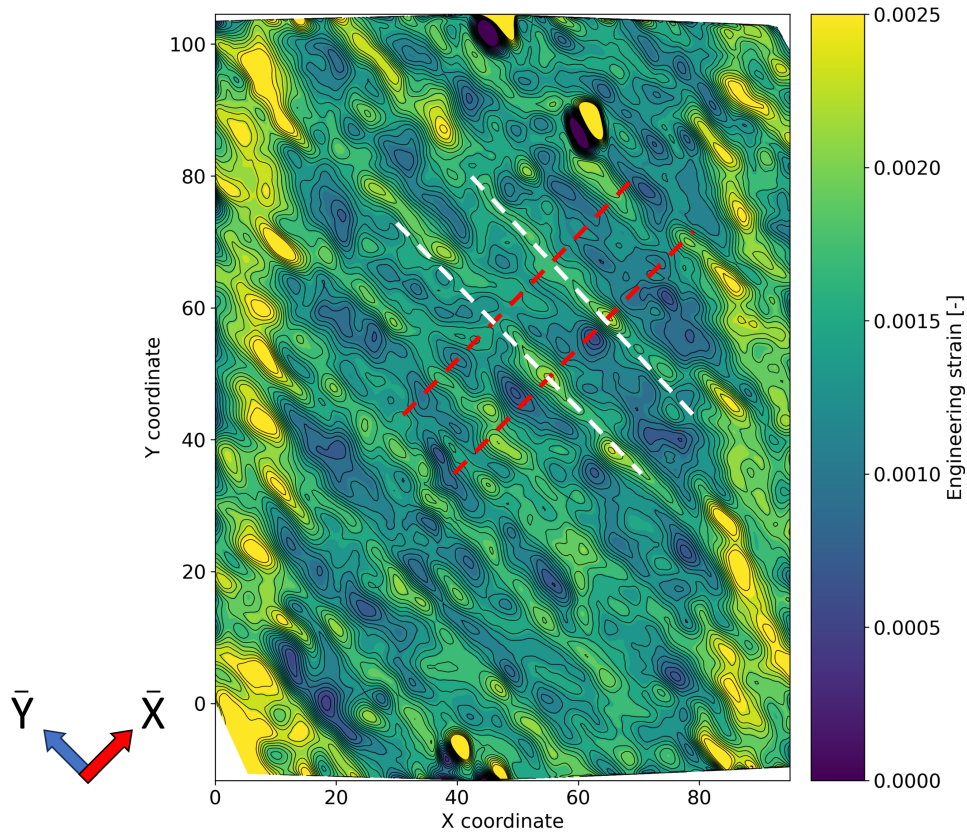


Figure D.2: Strain component in the rotated coordinate system. The direction is aligned with the frontal surface tow orientation.

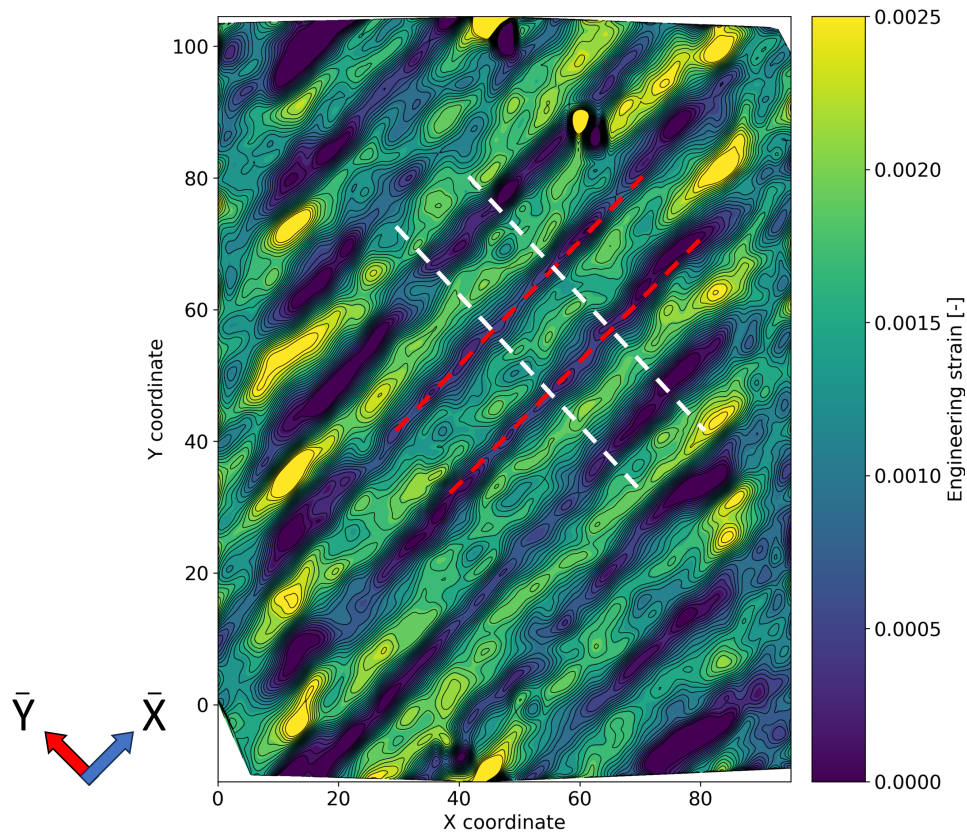
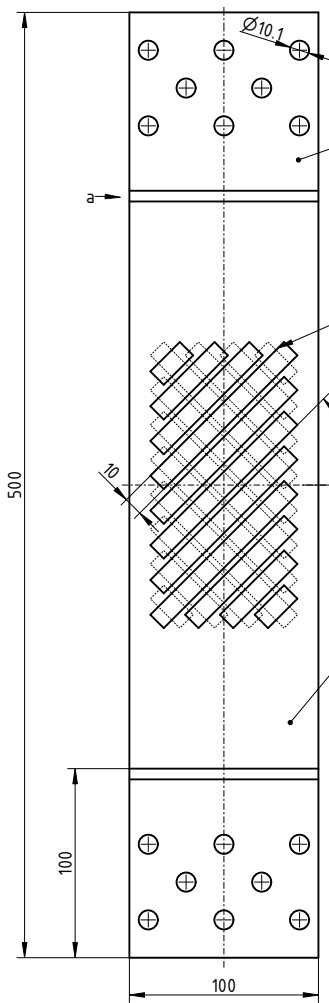


Figure D.3: Strain component in the rotated coordinate system. The direction is perpendicular to the frontal surface tow orientation.

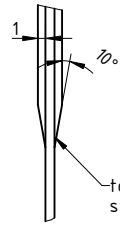


aluminium tabbing

tows placed in 45° with respect to loading direction on one side, backside has -45° tows

- 8 backing plies in total, thus the layup from bottom to top:
- (-45°) tows placed by hand
 - (0°) without gaps
 - (-15°) w.g.
 - (+15°) w.g.
 - (0°) w.g.
 - (0°) w.g.
 - (+15°) w.g.
 - (-15°) w.g.
 - (0°) w.g.
 - (+45°) tows placed by hand

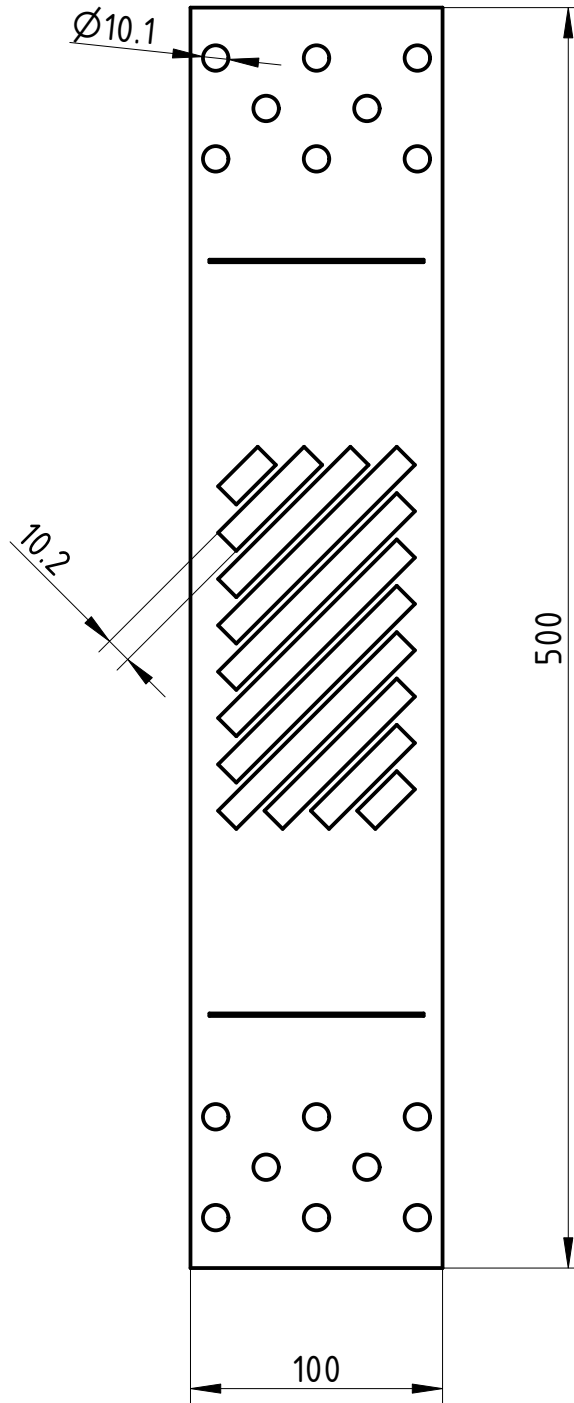
$[(-45)/(0)/(-15)/(+15)/(0)/(0)/(+15)/(-15)/(0)/(+45)]_t$

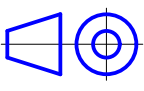


A
2:1

to be joined with 3M Scotch-Weld 9323 structural adhesive

Designer: László Czél	Product: AFP specimen	Scale: 1:2	
Date: 2023.12.05.	Description:	Projection: 	
Approver:	Material:	Mass [kg]:	Page / Total pages: 1 / 1



Designer: László Czél	Product: Jig plate	Scale: 1:3	
Date: 2023.12.04.	Description:	Projection: 	
Approver:	Material: Steel	Mass [kg]: 0.086	Page / Total pages: 1 / 1